NASA TECHNICAL REPORT

NASA TR R-337

c.1

NASA TR R-337

TECHNIQUES FOR ELIMINATING BASEBAND VOICE INTERFERENCE WITH TELEMETRY FOR THE APOLLO COMMUNICATION SYSTEM

by G. Dickey Arndt, Sidney W. Novosad, and Robert J. Panneton

Manned Spacecraft Center
Houston, Texas

NATIONAL AERONAUTICS AND SPACE ADMINISTRATION • WASHINGTON, D. C. • APRIL 1970

1. REPORT NO.	2. GOVERNMENT ACCESSION NO.	3. RECIPIENT'S CATALOG NO.
NASA TR R-337		

4. TITLE AND SUBTITLE	5. REPORT DATE
TECHNIQUES FOR ELIMINATING BASEBAND VOICE INTERFERENCE WITH TELEMETRY FOR THE APOLLO COMMUNICATION SYSTEM	April 1970
	6. PERFORMING ORGANIZATION CODE

7. AUTHOR(S)	8. PERFORMING ORGANIZATION REPORT NO.
G. Dickey Arndt, Sidney W. Novosad, MSC; and Robert J. Panneton, TRW	S-228

9. PERFORMING ORGANIZATION NAME AND ADDRESS	10. WORK UNIT NO.
Manned Spacecraft Center Houston, Texas 77058	914-50-40-06-72
	11. CONTRACT OR GRANT NO.

12. SPONSORING AGENCY NAME AND ADDRESS	13. REPORT TYPE AND PERIOD COVERED
National Aeronautics and Space Administration Washington, D.C. 20546	Technical Report
	14. SPONSORING AGENCY CODE

15. SUPPLEMENTARY NOTES

16. ABSTRACT

Excessive telemetry error rates caused by baseband voice interference occur in several modes of the Apollo communication system. Demodulation, using essentially nonlinear quadrature phase detection, causes voice terms to appear in the telemetry spectrum. In this report, two methods which effectively linearize the demodulation process are used to reduce the voice interference. One method uses a negative feedback loop incorporated around the present nonlinear phase detector. The other method uses a frequency-modulation demodulator preceded by a composite filter containing three band-pass filters in parallel. The theoretical development, construction, and testing of both methods are presented. Significant improvement in telemetry performance is obtained. Results show that voice interference to both the 1.6- and 51.2-kbps telemetry data is negligible for all spacecraft/ground-station conditions when using either of the two methods. It is recommended that the negative-feedback-loop method be implemented in the Manned Space Flight Network ground stations as a result of its relative simplicity and superior performance.

17. KEY WORDS (SUPPLIED BY AUTHOR)	18. DISTRIBUTION STATEMENT
* Apollo Communication System * Voice/Telemetry Interference * Linear Phase-Detection Techniques	Unclassified - Unlimited

19. SECURITY CLASSIFICATION (THIS REPORT)	20. SECURITY CLASSIFICATION (THIS PAGE)	21. NO. OF PAGES	22. PRICE*
None	None	96	$3.00

*For sale by the Clearinghouse for Federal Scientific and Technical Information
Springfield, Virginia 32151

CONTENTS

FIGURES

TECHNIQUES FOR ELIMINATING BASEBAND VOICE INTERFERENCE WITH TELEMETRY FOR THE APOLLO COMMUNICATION SYSTEM

By G. Dickey Arndt, Sidney W. Novosad, and Robert J. Panneton*
Manned Spacecraft Center

SUMMARY

The Apollo unified S-band communication system has several phase-modulation modes containing baseband voice and a 1.024-megahertz telemetry subcarrier. It was noted early in the Apollo Program that the present demodulation process, which uses nonlinear quadrature phase detection, can produce severe telemetry degradations caused by voice interference.

This report presents the results of investigations into possible demodulation techniques for eliminating the telemetry data degradations caused by baseband voice. Emphasis is placed upon developing techniques which use present Manned Space Flight Network equipment and, consequently, require only small modifications to the ground stations.

Two methods, which effectively linearize the demodulation process by reducing the voice modulation index, can be used to reduce the nonlinear demodulation terms causing telemetry interference. The methods use (1) a negative feedback loop (consisting of a loop filter, amplifier, and phase modulator) which is incorporated around the existing Manned Space Flight Network wideband phase detector or (2) a frequency-modulation demodulator (with subsequent integration) preceded by a composite filter which consists of three high-Q band-pass filters in parallel. These methods can produce significant improvements in telemetry performance in the presence of excessive voice interference.

The negative feedback loop allows the voice frequency components appearing at the phase-detector output to phase-modulate the phase-detector reference signal. This negative feedback action compresses the voice modulation index and effectively eliminates degradations in telemetry data in lunar module modes 4 and 8 and command and service module mode 8. In addition, the feedback action eliminates degradations in the biomedical-subcarrier data in lunar module mode 8.

*TRW Systems Group, Houston, Texas.

The frequency demodulation technique uses either high-Q helical resonators or crystal filters for predetection filtering. A 15-decibel reduction in the required input signal power of the frequency demodulator obtained with the filtering technique enables the telemetry signal to be detected "linearly" with minimal degradation below the frequency-modulation threshold. The frequency demodulation technique reduces voice interference for 1.6- and 51.2-kbps telemetry data. However, biomedical data cannot be detected using this scheme.

The negative-feedback-loop technique is recommended for implementation into the Manned Space Flight Network receiving equipment. The telemetry bit-error-rate performance (when using this method) is superior to that obtained from the frequency-modulation detection scheme. Low cost, ease of implementation, and lack of operational switching requirements are especially desirable features of this technique.

INTRODUCTION

The Apollo unified S-band (USB) communication system has several down-link phase-modulation (PM) modes containing a 1.024-megahertz telemetry subcarrier and backup (baseband) voice. These modes have low-bit-rate telemetry (1.6 kbps) biphase-modulating the 1.024-megahertz subcarrier, which is summed with the baseband voice to phase-modulate the down-link S-band carrier. Serious degradations occur in the performance of the telemetry channel of the lunar module (LM) down-link PM modes 4 and 8 and the command and service module (CSM) down-link PM mode 8 during periods of speech transmission. The information channels of the LM and CSM modes under consideration are given in the following section. The telemetry degradation is caused by incompatibility between the spacecraft signal design and the demodulation characteristics of the ground-station receiver.

Tests conducted at the Manned Spacecraft Center (MSC) Electronic Systems Compatibility Laboratory (ESCL) indicate that high telemetry bit error rates occur because of backup-voice interference with the 1.024-megahertz subcarrier data. The bit error rate (BER) is a function of the backup-voice modulation index and the ground-receiver carrier-tracking-loop (CTL) bandwidth. The interference problem is severe when the wide-loop bandwidth (700 hertz) is used; however, lower voice indices will reduce or eliminate the interference problem, regardless of the CTL bandwidth selected. The modulation index for the backup-voice channel in the CSM communication system is low enough to prevent 1.6-kbps telemetry interference, provided the ground receiver uses the proper CTL bandwidth (50 hertz). However, the voice modulation indices for LM modes 4 and 8 are high (above 1.3 radians) for most of the production LM vehicles. Severe telemetry degradation can be expected during voice transmission with these high indices.

The most straightforward solution for improving the telemetry performance of LM modes 4 and 8 is to modify the spacecraft to reduce the voice modulation index. However, the cost and schedule impacts associated with the required spacecraft modifications were deemed too severe by the MSC LM Configuration Control Board (CCB) in June 1968. At that time, it was decided that telemetry degradations would have to be tolerated during speech transmission because no practical solution for eliminating the interference was known to MSC or to Goddard Space Flight Center (GSFC).

The purpose of this report is to present the results of further investigations conducted by the MSC Information Systems Division (ISD) into possible demodulation techniques for eliminating the data degradations. Two methods, involving relatively minor modifications to the ground-station receivers, have been tested successfully in the ESCL. These methods use linear phase-detection schemes, which include (1) an external negative feedback loop (consisting of a loop filter, amplifier, and phase modulator) incorporated around the existing Manned Space Flight Network (MSFN) wideband phase detector and (2) a frequency-modulation (FM) demodulator preceded by a parallel bank of narrowband band-pass filters. Both techniques eliminate telemetry interference by effectively reducing the voice modulation index in the demodulation process. Theoretical analyses and experimental verification of the two methods are presented in this report. The advantages and disadvantages of each technique are discussed, considering ease of implementation into existing MSFN equipment and possible operational constraints. It is recommended that one of the two techniques be implemented in the MSFN stations in time to support the later lunar-landing missions.

A list of the symbols used in this report is given in appendix A.

The authors wish to express their appreciation to W. B. Warren of TRW Systems Group, Houston, Texas, for the design of the phase modulator in the negative feedback loop; to B. H. Batson of MSC for helpful discussions on the voice interference; to P. L. Harton, J. A. Webb, and M. W. Jones of Lockheed Electronics Company, Houston, Texas, for the design and fabrication of the crystal filters; to C. V. Hill of Lockheed Electronics Company, Houston, Texas, for his suggestions on the simplified phase-cancellation technique; to W. L. Snyder and G. C. Fajardo of Lockheed Electronics Company, Houston, Texas, for the fabrication and tuning of the helical resonators; and to J. W. Seyl and B. G. Smith of MSC for their contributions in the ESCL tests.

INFORMATION CHANNELS OF SELECTED LUNAR MODULE AND COMMAND AND SERVICE MODULE DOWN-LINK PHASE-MODULATION MODES

Carrier combination	Service or information	Modulation technique	Subcarrier frequency, kHz
LM to MSFN down-link PM combinations			
4	Carrier:		
	Backup voice	PM on carrier	
	1.6-kbps telemetry	Pulse code modulation (PCM)/PM/PM	1024
8	Carrier:		
	Backup voice	PM on carrier	
	Hard line biomed	PM on carrier	14.5
	Extravehicular communications system (EVCS)	PM on carrier	3.9 5.4 7.35 10.5
	1.6-kbps telemetry	PCM/PM/PM	1024
CSM to MSFN S-band down-link PM combination			
8	Carrier:		
	Backup voice	PM on carrier	
	1.6-kbps telemetry	PCM/PM/PM	1024

PRESENT MANNED SPACE FLIGHT NETWORK DEMODULATION SCHEME

The MSFN stations use a phase-lock, double superheterodyne receiver for detecting the S-band signals (fig. 1). A long phase-lock-loop (PLL) configuration is used in the receiver to provide coherent detection; that is, the coherent reference (as derived in a narrowband CTL) is applied as the local oscillator signal into the first mixer rather than into the wideband phase detector. The 10-megahertz reference for the wideband phase detector is derived from a crystal oscillator which also provides the reference for the CTL phase detector.

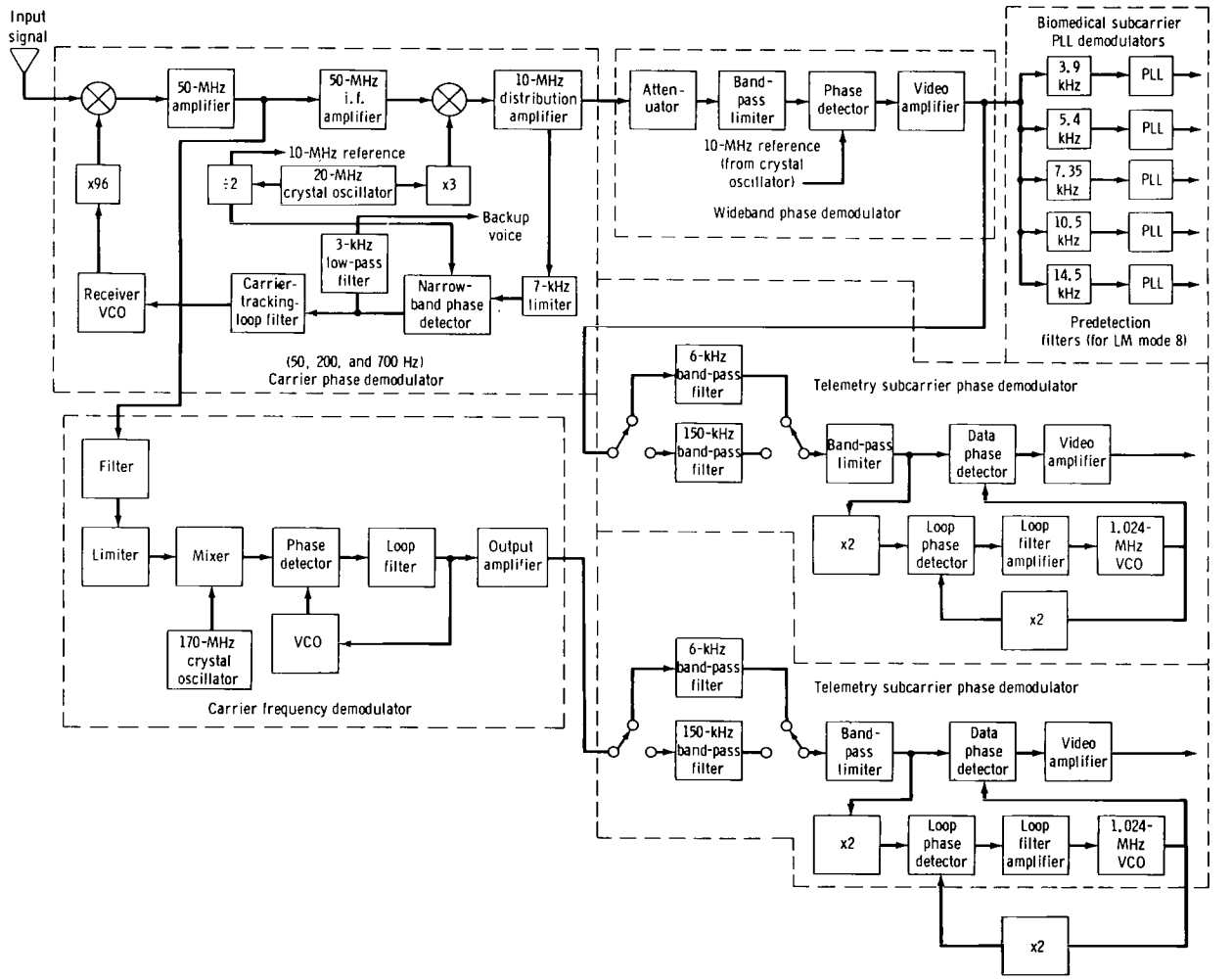

Figure 1. - Block diagram of the phase-modulation and the frequency-modulation channels in the Manned Space Flight Network ground-station receiver.

The narrowband phase detector within the CTL demodulates the baseband voice signal, and the voice is taken out through a low-pass filter prior to the loop filter. The CTL has three possible filter bandwidths: 50, 200, or 700 hertz. The 50-hertz loop bandwidth position is the normal operational configuration when the spacecraft is at lunar distance, and the 700-hertz loop bandwidth position is designed for use during earth orbit.

The biphase-modulated 1.024-megahertz telemetry subcarrier (after removal from the 10-megahertz intermediate frequency (i.f.) by the wideband phase detector) is demodulated in a PLL demodulator. The phase reference for demodulating the subcarrier is derived in a squaring loop. The reference signal and the telemetry subcarrier are routed into a balanced detector, with the resultant PCM bit-stream output being routed to a bit synchronizer and matched filter.

It has been shown mathematically that a linear phase-detection scheme should be used instead of the nonlinear quadrature product detector for the Apollo signal combinations containing baseband voice and telemetry (ref. 1). The deficiencies in such a product detector can be seen from the following development. The MSFN phase-detection scheme can be represented as shown in figure 2. The input signal $\sin [\omega_c t + \phi_v(t) + \phi_{TM}(t)]$ has phase modulation caused by the baseband voice $\phi_v(t)$ and the telemetry subcarrier $\phi_{TM}(t)$. The quadrature reference $\cos \omega_c t$ is derived from a crystal oscillator in the receiver. The phase detector has a sensitivity of K_m V/rad.

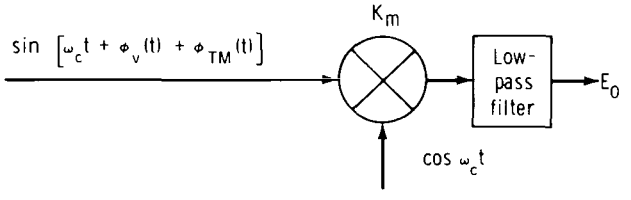

Figure 2. - Functional representation of the Manned Space Flight Network wideband phase detector.

The output voltage E_0, after filtering by a low-pass filter, may be written as follows.

$$E_0 = \frac{1}{2} K_m \sin \left[\phi_v(t) + \phi_{TM}(t)\right] \tag{1}$$

The baseband voice modulation $\phi_v(t)$ can be represented as

$$\phi_v(t) = \beta_v f_v(t) \tag{2}$$

where β_v is the peak phase deviation of the voice signal and $f_v(t)$ is the time waveform of the voice signal. (The backup voice is clipped 24 decibels for LM mode 4 and CSM mode 8, resulting in a near square-wave waveform with random transitions. The

speech information is preserved in the zero crossings of the waveform.) The telemetry-subcarrier phase modulation $\phi_{TM}(t)$ may be written as follows.

$$\phi_{TM}(t) = \beta_{TM} \sin\left(\omega_{TM}t \pm \frac{\pi}{2}\right) \tag{3}$$

where β_{TM} is the telemetry-subcarrier modulation index, ω_{TM} is the telemetry-subcarrier frequency, and $\pm\pi/2$ represents the biphase modulation on the subcarrier. By substituting equations (2) and (3) into equation (1) and expanding the resultant with Bessel functions and trigonometric identities, the output voltage may be rewritten as follows.

$$E_0(t) = \frac{1}{2} K_m \sin\left[\beta_v f_v(t)\right] \left\{J_0(\beta_{TM}) + 2\sum_{n=1}^{n=\infty} J_{2n}(\beta_{TM})\cos\left[2n\left(\omega_{TM}t \pm \frac{\pi}{2}\right)\right]\right\}$$

$$+ \frac{1}{2} K_m \cos\left[\beta_v f_v(t)\right] \left\{2\sum_{n=1}^{n=\infty} J_{2n-1}(\beta_{TM}) \cdot \sin\left[(2n-1)\left(\omega_{TM}t \pm \frac{\pi}{2}\right)\right]\right\} \tag{4}$$

By considering only the signal components passed by the band-pass predetection filter in the telemetry-subcarrier demodulator, the telemetry voltage at the output of the wideband phase detector is

$$E_{0_{TM}}(t) = K_m \cos\left[\beta_v f_v(t)\right] J_1(\beta_{TM}) \sin\left(\omega_{TM}t \pm \frac{\pi}{2}\right) \tag{5}$$

If $f_v(t)$ is a square wave, that is, the voice signal is infinitely clipped, then

$$f_v(t) = \pm 1 \tag{6}$$

Equation (5) can be rewritten as follows.

$$E_{0_{TM}} = K_m \cos(\beta_v) J_1(\beta_{TM}) \sin\left(\omega_{TM}t \pm \frac{\pi}{2}\right) \tag{7}$$

which indicates that the backup-voice signal attenuates the telemetry subcarrier out of the phase detector. The amount of attenuation is dependent upon the modulation index of the voice. As the voice index increases toward $\pi/2$ radians, the amplitude of the telemetry subcarrier is reduced, thereby increasing the effects of noise. Thus, a square wave will reduce the 1.024-megahertz subcarrier amplitude by a constant factor but will not produce any direct voice interference in the telemetry spectrum. However, under actual operating conditions, the 24-decibel clipped voice will not be a square wave. Thus, there will be intermodulation products between the baseband voice signal and the 1.024-megahertz subcarrier which cause direct telemetry interference. From a power series expansion of the voice signal, $\cos[\beta_v f_v(t)]$ can be written as follows.

$$\cos\left[\beta_v f_v(t)\right] = 1 - \frac{\beta_v^2 f_v^2(t)}{2!} + \frac{\beta_v^4 f_v^4(t)}{4!} - \cdots \tag{8}$$

Substitute equation (8) into equation (5) to obtain the output telemetry signal as follows.

$$E_{0_{TM}}(t) = K_m J_1(\beta_{TM}) \sin\left(\omega_{TM} t \pm \frac{\pi}{2}\right)\left[1 - \frac{\beta_v^2 f_v^2(t)}{2!} + \frac{\beta_v^4 f_v^4(t)}{4!} - \cdots\right] \tag{9}$$

The telemetry interference terms are dependent upon the even-ordered powers of the voice signal. Any reduction in the voice modulation index results in a reduction in voice interference with the telemetry signal, as seen from equation (9).

Previous experimental results for LM mode 4 (fig. 3) indicate that a voice index of less than 0.9 radian is needed to limit telemetry channel interference to a level that would enable the 10^{-4} BER requirement to be met at the expected lunar-distance radio-frequency (rf) level. The voice modulation index of 1.3 radians (representing the expected value for the LM lunar-mission spacecraft) yields totally unacceptable telemetry performance. The voice interference is increased drastically for LM mode 8 (fig. 4).

The present MSFN product phase detector does not perform satisfactorily with the high voice modulation indices (figs. 3 and 4). The total effective phase deviation (which, for LM mode 8, includes contributions from the biomedical subcarriers, in addition to those from the baseband voice and the telemetry subcarrier) exceeds the linear range of the phase detector. However, the linear range of the detection scheme can be improved by using negative feedback to track out the voice modulation. Negative feedback, which effectively reduces the voice modulation index, forms the basis for the two solutions proposed in the following discussion.

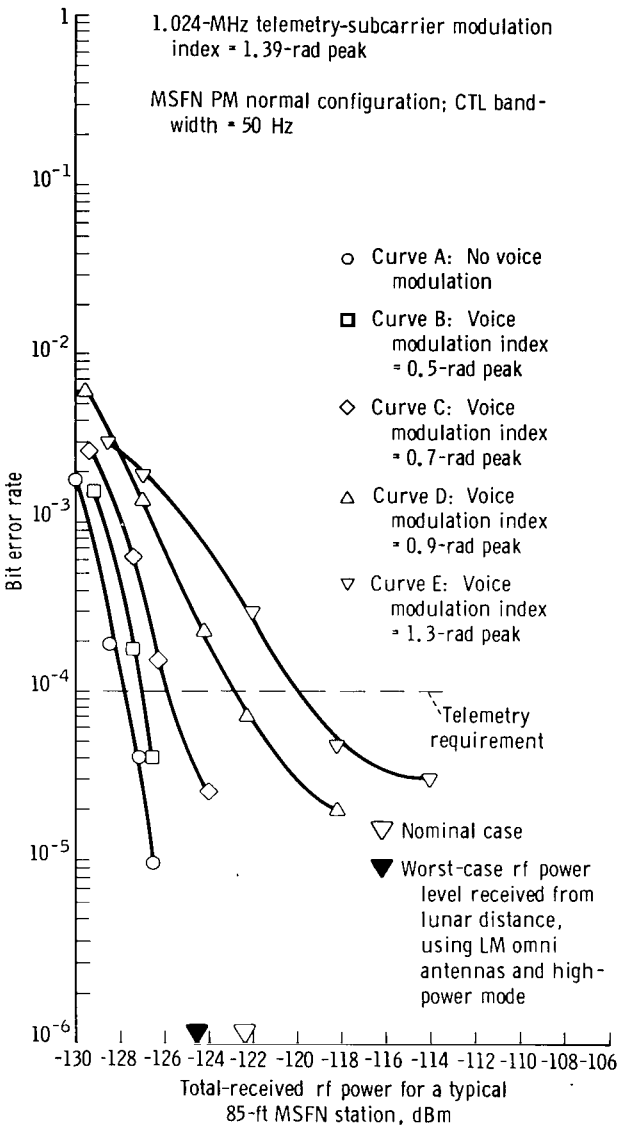

Figure 3. - Lunar module mode 4: bit error rate for 1.6-kbps telemetry — preflight spacecraft equipment (test numbers TPET-050268-5, TPET-050268-6, TPET-050368-2, TPET-050368-3, and TPET-050368-4).

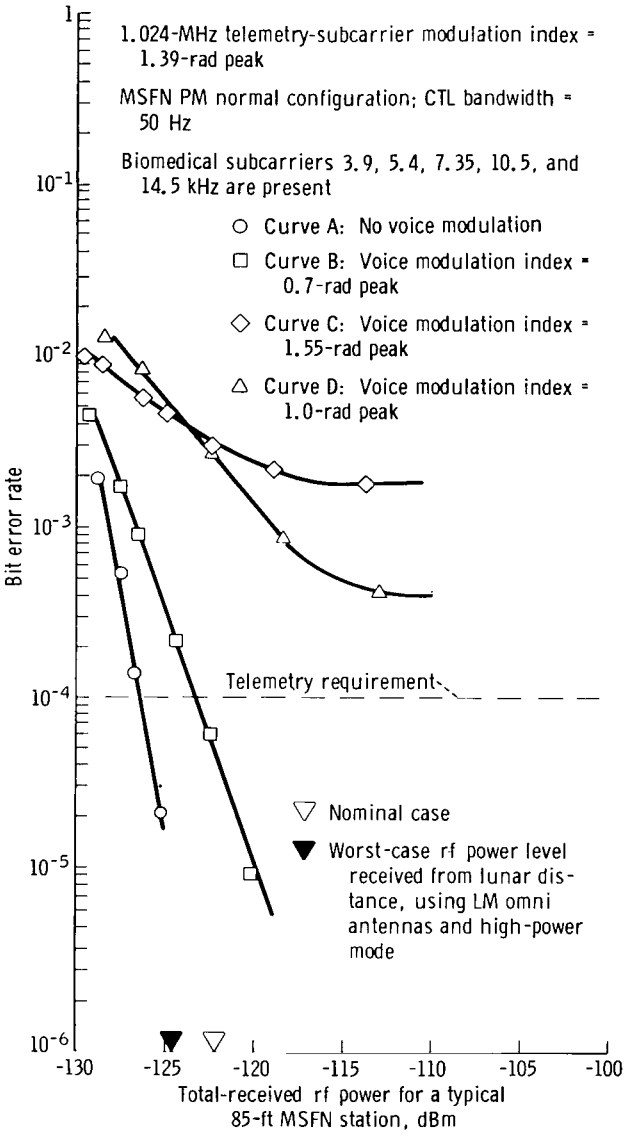

Figure 4. - Lunar module mode 8: bit error rate for 1.6-kbps telemetry (test numbers TPET-050768-1 and TPET-050768-2).

LINEAR DETECTION USING PHASE-MODULATION DEMODULATION WITH NEGATIVE FEEDBACK

In the previous section, it was shown that if a composite modulated signal

$$E_{RF} = A \sin\left[\omega_c t + \beta_v f_v(t) + \beta_{TM} \sin\left(\omega_{TM} t \pm \frac{\pi}{2}\right)\right] \tag{10}$$

is demodulated by using a quadrature product detector, sidebands caused by the baseband voice signal $f_v(t)$ will appear about the telemetry-subcarrier frequency ω_{TM}. The voice sidebands about the ω_{TM} term cause degradation in the telemetry BER performance.

If a linear phase detector were used, the detected output signal would be

$$E_0 = \beta_v f_v(t) + \beta_{TM} \sin\left(\omega_{TM} t \pm \frac{\pi}{2}\right) \tag{11}$$

where the output telemetry spectrum contains no sidebands caused by backup voice. Thus, a linear detection scheme is required to eliminate the possibilities of telemetry BER degradation caused by backup-voice interference. However, preliminary investigations of a linear (zero crossing) phase detector indicated that poor demodulation performance could be expected at the low-input signal levels in the MSFN receiver. Also, it is preferable to use existing MSFN demodulation equipment rather than to develop new equipment at this late stage in the Apollo Program. Therefore, it is desirable to consider a technique whereby the nonlinear product detector presently used in the MSFN ground-station receiver can be linearized effectively. The application of negative feedback is such a technique. One of the results of negative feedback is a reduction in the effective modulation index of the received input signal. Because the input-voice-signal phase deviation is compressed, the phase detector will operate over only a fraction of its original dynamic range, which means that a quadrature phase detector will tend to approximate a linear detector.

A feedback loop is used in the negative feedback technique. The feedback loop consists of a loop filter, amplifier, and phase modulator; and it encloses the wideband quadrature phase detector of the MSFN receiver. The method involves controlled phase subtraction in the path of the reference signal to the phase detector. The overall effect of the feedback loop is the compression of the backup-voice phase deviation or modulation index and the linearization of the wideband phase detector.

A linear model for the MSFN carrier phase demodulator with and without the negative feedback loop is shown in figure 5. When the feedback loop is used, the amplified output of the phase detector is filtered by the loop filter which passes only the backup-voice signal. Then, the voice signal is amplified and used to phase-modulate the reference signal to the wideband phase detector. The phase-shift network following

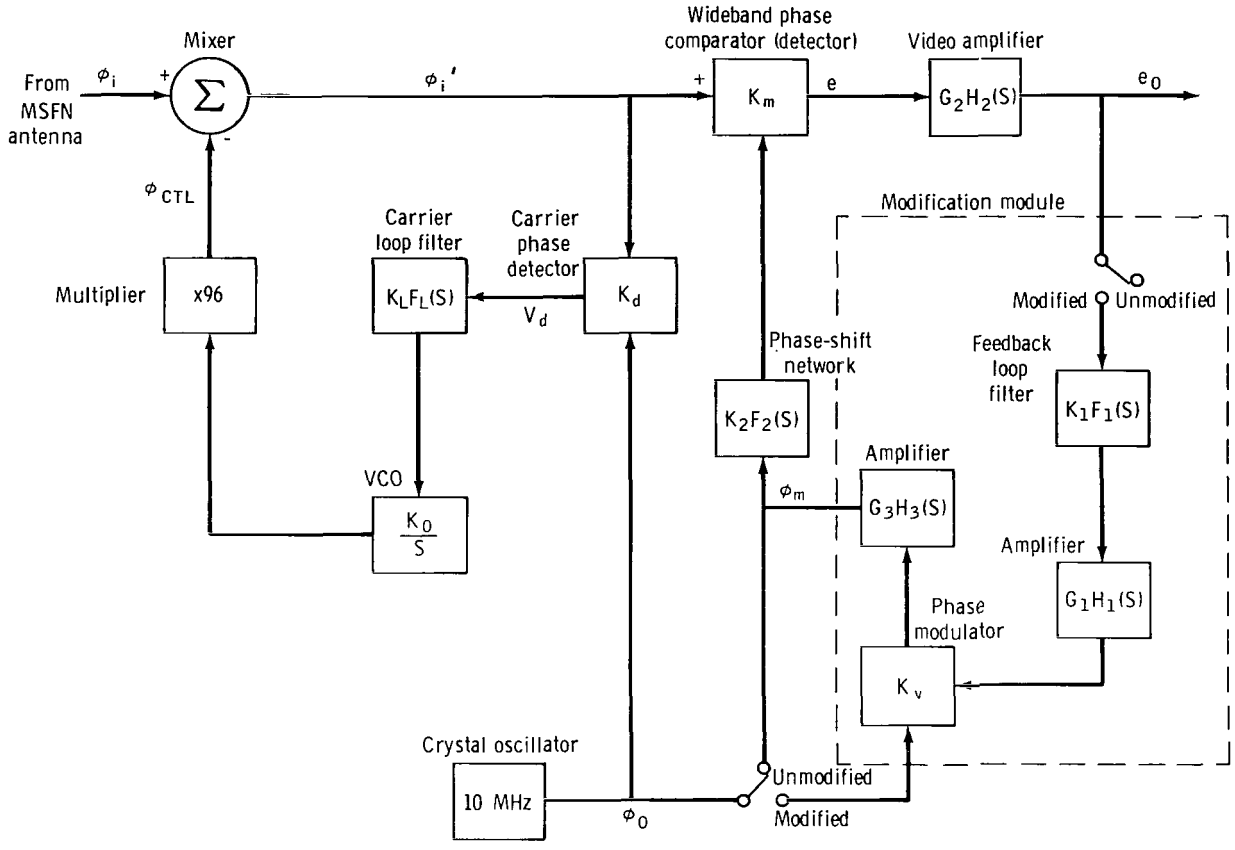

Figure 5. - Linear model of the Manned Space Flight Network carrier phase demodulator with and without the negative feedback loop.

the phase modulator provides the 90° phase shift required for the quadrature condition between the reference and the input i.f. signals to the wideband phase detector. Because the reference signal is modulated in the same manner as the wideband-detector input signal, phase cancellation occurs in the detection process for the low audio frequencies passed by the loop filter. The result is a reduction in the backup-voice phase deviation or modulation index and a reduction in the amplitude of the voice signal at the detector output.

The dynamic response of the carrier phase demodulator, both modified (with the negative feedback loop) and unmodified, is discussed in the following section. The transfer function of each element given in figure 5 is considered. Linearity implies that the phase comparator (detector) and phase modulator can be represented by linear summers, which is valid for small signals. The blocks are identified as follows.

1. The wideband phase comparator (detector) is represented as a summer with a sensitivity of K_m V/rad and with an output voltage of e.

2. The video amplifier following the phase comparator has a frequency response $H_2(S)$ with a constant gain G_2.

3. The negative-feedback-loop filter, which has a transfer function $F_1(S)$, has a gain constant K_1.

4. The amplifier driving the phase modulator has a frequency response $H_1(S)$ with a constant gain G_1.

5. The phase modulator is represented as a summer with a sensitivity of K_v rad/V.

6. The amplifier following the phase modulator has a frequency response $H_3(S)$ with a constant gain G_3.

7. The phase-shift network at the output of the modification module has a transfer function $F_2(S)$ and a gain constant K_2.

8. The CTL phase comparator (detector) is represented as a summer with a sensitivity of K_d V/rad and an output voltage V_d.

9. The CTL filter has a transfer function $F_L(S)$ and a gain constant K_L.

10. The CTL voltage-controlled oscillator is represented as an integrator. It has a sensitivity of K_0 (rad/sec)/V.

Consideration of the linearized model for the unmodified carrier phase demodulator (without the feedback loop) leads to the closed-loop transfer response for the system (fig. 5). From equation (B19) (appendix B)

$$\left(\frac{e_0}{\phi_i}\right)_{UNMOD} = K_m G_2 H_2(S)\left[\frac{S}{S + KF_L(S)} + \frac{KF_L(S)}{S + KF_L(S)}\frac{\phi_0}{\phi_i} - K_2 F_2(S)\frac{\phi_0}{\phi_i}\right] \tag{12}$$

where $K = 96K_0K_LK_d$. Consideration of the linearized model for the modified carrier phase demodulator (fig. 5) leads to the closed-loop transfer response for the system with the phase-modulator loop. From equation (B18) (appendix B)

$$\left(\frac{e_0}{\phi_i}\right)_{MOD} = \frac{K_m G_2 H_2(S)}{1 + K_m A(S)B(S)}\left[\frac{S}{S + KF_L(S)} + \frac{KF_L(S)}{S + KF_L(S)}\frac{\phi_0}{\phi_i} - \frac{A(S)\phi_0}{\phi_i}\right] \tag{13}$$

where

$$A(S) = K_2F_2(S)G_3H_3(S) \tag{14}$$

$$B(S) = G_2H_2(S)K_1F_1(S)G_1H_1(S)K_v \tag{15}$$

and

$$K = 96K_0K_LK_d \tag{16}$$

By comparing equations (12) and (13), it is evident that equation (13) has the additional factor $\frac{1}{1 + K_mA(S)B(S)}$ which includes the feedback factor $K_mA(S)B(S)$. Thus

$$\frac{\left(\frac{e_0}{\phi_i}\right)_{MOD}}{\left(\frac{e_0}{\phi_i}\right)_{UNMOD}} = 1 + K_mK_2F_2(S)G_1H_1(S)G_2H_2(S)K_1F_1(S)K_v \tag{17}$$

when it is assumed that $G_3H_3(S) = 1$.

Further insight into the action of the phase detector with and without the feedback loop may be obtained by assuming that the video and i.f. amplifiers following the wideband phase detector and phase modulator, respectively, are sufficiently wideband to pass all signals without distortion and have unity gain. These restrictions are such that $G_2H_2(S) = 1$ and $G_3H_3(S) = 1$. Also, it can be assumed that the phase error ϕ_0 from the crystal oscillator reference into the phase detectors will approach zero. The MSFN receivers have static phase-shift networks which are manually adjusted to enable $\phi_0 \rightarrow 0$. Thus, from equations (12) and (13), the responses for the baseband voice signal and the 1.024-megahertz telemetry subcarrier are as follows.

1. Phase detector with the feedback loop — equation (13)

   a. Backup voice (voice spectrum is 300 to 3000 hertz)

$$\frac{e_0}{\phi_i} = \frac{K_m}{1 + K_m K_2 F_2(S) G_1 H_1(S) K_v} \left[\frac{j\omega_v}{KF_L(S)} \right] \tag{18}$$

where $K_1 F_1(S) \approx 1$ and $j\omega_v << KF_L(S)$ because K, the loop gain of the CTL, is nominally greater than 10^6 (ref. 2).

   b. 1.024-megahertz telemetry subcarrier

$$\frac{e_0}{\phi_i} = K_m \tag{19}$$

where $K_m K_2 F_2(S) G_1 H_1(S) K_v K_1 F_1(S) << 1$ and $j\omega_{TM} >> KF_L(S)$.

2. Phase detector without the feedback loop — equation (12)

   a. Backup voice (voice spectrum is 300 to 3000 hertz)

$$\frac{e_0}{\phi_i} = K_m \frac{j\omega_v}{KF_L(S)} \tag{20}$$

where $j\omega_v << KF_L(S)$.

   b. 1.024-megahertz telemetry subcarrier

$$\frac{e_0}{\phi_i} = K_m \tag{21}$$

where $j\omega_{TM} >> KF_L(S)$. A comparison of equations (19) and (21) indicates that the telemetry subcarrier is unaffected by the feedback loop. However, the backup-voice signal is reduced by one plus the feedback factor or $1 + K_m K_2 F_2(S) G_1 H_1(S) K_v$ when the feedback loop is used, as seen by comparing equations (18) and (20).

The feedback factor for the particular loop described in this report is approximately 12.7 decibels for the backup-voice frequency range (appendix B).

$$\frac{\left(\frac{e_0}{\phi_i}\right)_{MOD}}{\left(\frac{e_0}{\phi_i}\right)_{UNMOD}} = \frac{1}{1 + K_m K_2 F_2(S) G_1 H_1(S) K_v} \tag{22}$$

where the feedback factor $K_m K_2 F_2(S) G_1 H_1(S) K_v = 4.3$ (12.7 decibels) for the frequency range occupied by the backup-voice spectrum. The feedback factor can be varied by adjusting the gain G_1 of the loop amplifier in the modification module.

Modification Module (Negative Feedback Loop)

As discussed in the previous section, a practical technique by which the MSFN wideband phase detector may be linearized is to use a negative feedback loop containing a phase modulator around the quadrature phase detector. This section describes the modification module or negative feedback loop and its interface with the MSFN receiver.

A block diagram of the MSFN carrier phase demodulator implemented with the modification module is shown in figure 6. The module is a self-contained unit which may be inserted directly into the existing system with no changes required. The detailed schematic diagram of the modification module is shown in figure 7.

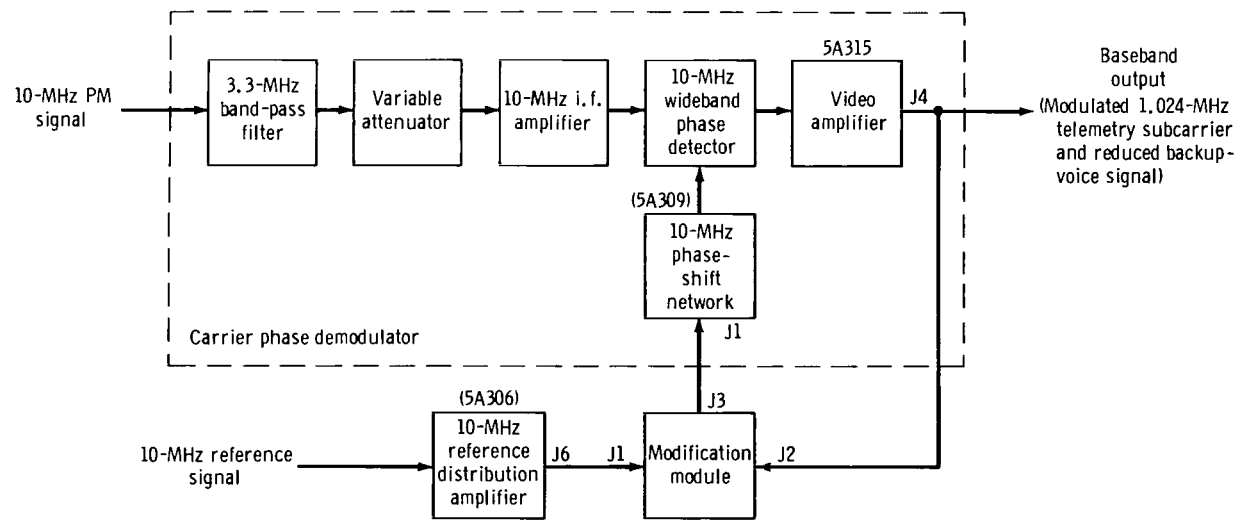

Figure 6.- Block diagram of the Manned Space Flight Network carrier phase demodulator implemented with the modification module (negative feedback loop).

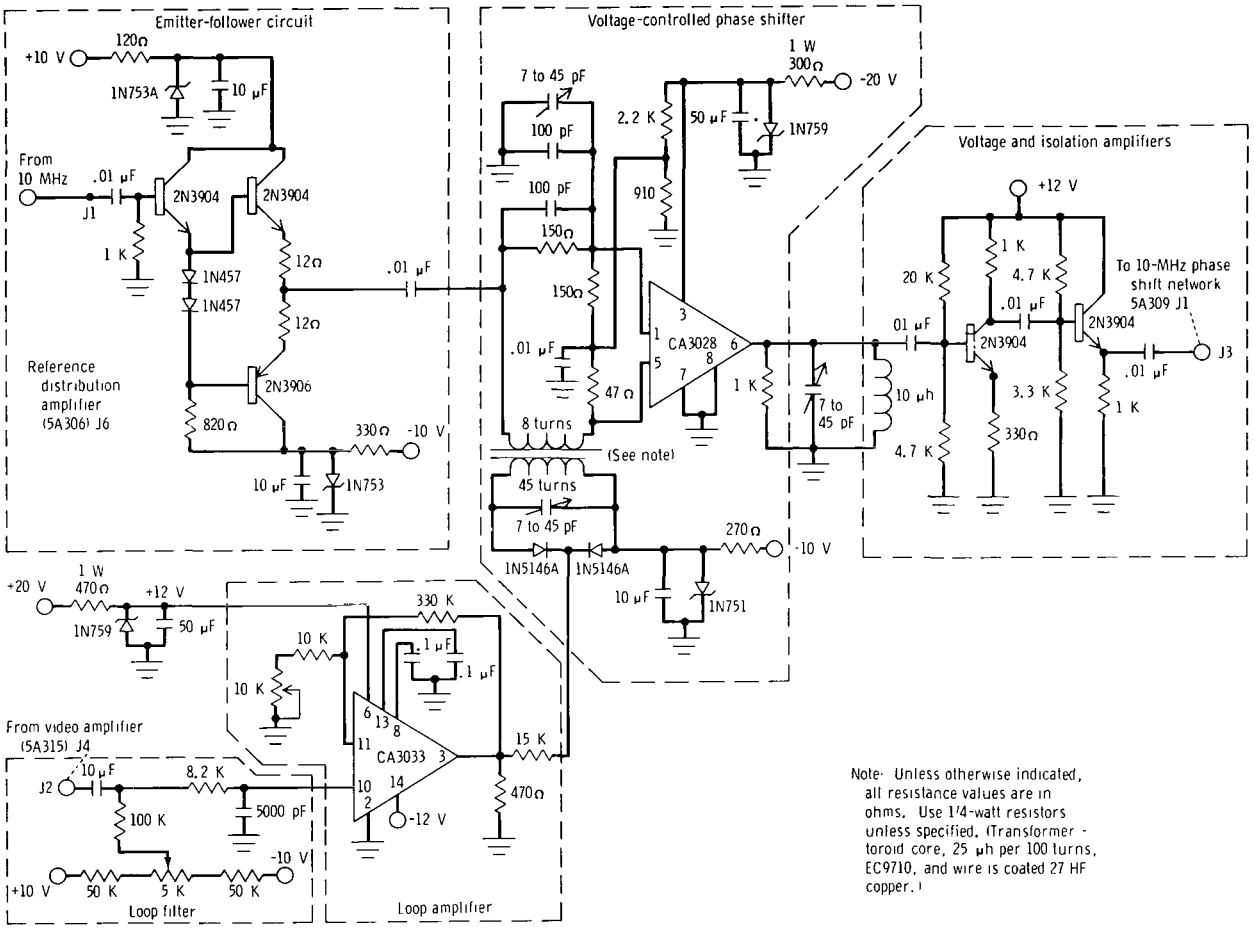

Figure 7. - Modification module (negative feedback loop).

The modification module is comprised basically of a loop filter, a voltage amplifier, and a 10-megahertz voltage-controlled phase shifter. The loop filter and the loop amplifier condition the output signal of the wideband phase detector. Only the backup voice is allowed to pass through the loop filter. Then, the filtered signal is amplified and inserted into the phase shifter as the control voltage. A 10-megahertz reference signal serves as the input to the 10-megahertz phase shifter. The phase shifter varies the phase of the input reference signal in accordance with the amplitude and frequency of the backup-voice control signal. Then, the phase-shifter output is amplified and routed through a single-stage isolation amplifier. The output of the module is a 10-megahertz signal phase-modulated by the conditioned backup-voice signal. Then, this PM signal is used as the reference for the wideband phase detector.

The modification module (fig. 7) consists of the following four electronic circuits.

1. Isolation amplifier (emitter follower)

2. Loop filter and amplifier

3. Voltage-controlled phase shifter

4. Voltage and isolation amplifiers

Isolation amplifier (emitter follower). - The purpose of this circuit is to isolate the 10-megahertz voltage-controlled phase shifter from the 10-megahertz voltage reference source. The circuit is called a single-ended complimentary-emitter follower.

Loop filter and amplifier. - The loop filter consists of two resistive-capacitive (RC) filter sections in cascade. The first RC combination is a dc blocking section, and the second RC combination is a low-pass section. Together, they form a band-pass filter with the 3-decibel cut-off points at 0.03 hertz and at 3.9 kilohertz.

The loop amplifier is an integrated-circuit operational amplifier with negative feedback and a variable voltage gain from 16.5 to 33. The amplifier frequency response is flat to 200 kilohertz.

Voltage-controlled phase shifter. - The central part of the modification module is the phase modulator which can provide a phase shift of approximately $\pm 140^\circ$ with a low level of incidental amplitude modulation (appendix C). In this phase modulator, the signal to be modulated is split into two paths. The upper path has a voltage gain of one-half and has no phase shift; the lower path has a voltage gain and phase shift which depend on the reactance of the tuned circuit. The outputs of the two paths are combined in a difference amplifier in which the output is the desired phase-shifted signal. The amplitude of the difference amplifier output is independent of the reactance of the tuned circuit (appendix C). Ideally, the phase of the output signal can vary from -180° to $+180^\circ$ as the reactance of the tuned circuit varies from highly capacitive to highly inductive. Consequently, varying the resonant frequency of the tuned circuit with the modulating signal, by means of a voltage variable capacitor, produces a corresponding phase modulation of the output of the difference amplifier. The phase modulator has a symmetrical phase-shift characteristic which provides a linear phase shift of $\pm 40^\circ$ and a total phase swing of $\pm 140^\circ$.

Voltage and isolation amplifiers. - A single-stage common-emitter voltage amplifier with current feedback follows the voltage-controlled phase shifter (modulator). The amplifier has a voltage gain of 3. In cascade with the voltage amplifier is a single-stage emitter follower which isolates the phase modulator from the phase-shift network preceding the wideband phase detector.

Experimental Results with the Negative Feedback Loop

This section presents experimental data taken in the MSC ESCL. Tests were performed to determine the effectiveness of the feedback loop in eliminating telemetry degradation caused by backup-voice interference. Production LM and CSM spacecraft equipment, together with an MSFN ground-station receiver and associated demodulation equipment, was used in the tests. The spacecraft-to-ground link was simulated with a calibrated rf attenuator.

Most of the tests were conducted with the modification module (negative feedback loop (fig. 7)) connected to an engineering model of the MSFN carrier phase demodulator.

The engineering model had been built previously to simulate the operation of the MSFN carrier phase demodulator. The engineering model, which was used because of its availability for laboratory developmental experimentation, was connected to the limited 10-megahertz output in the MSFN receiver. Comparison tests made with the modification module connected to the engineering model phase detector and then connected to the MSFN wideband phase detector were identical, as indicated by the BER curves shown in figure 8.

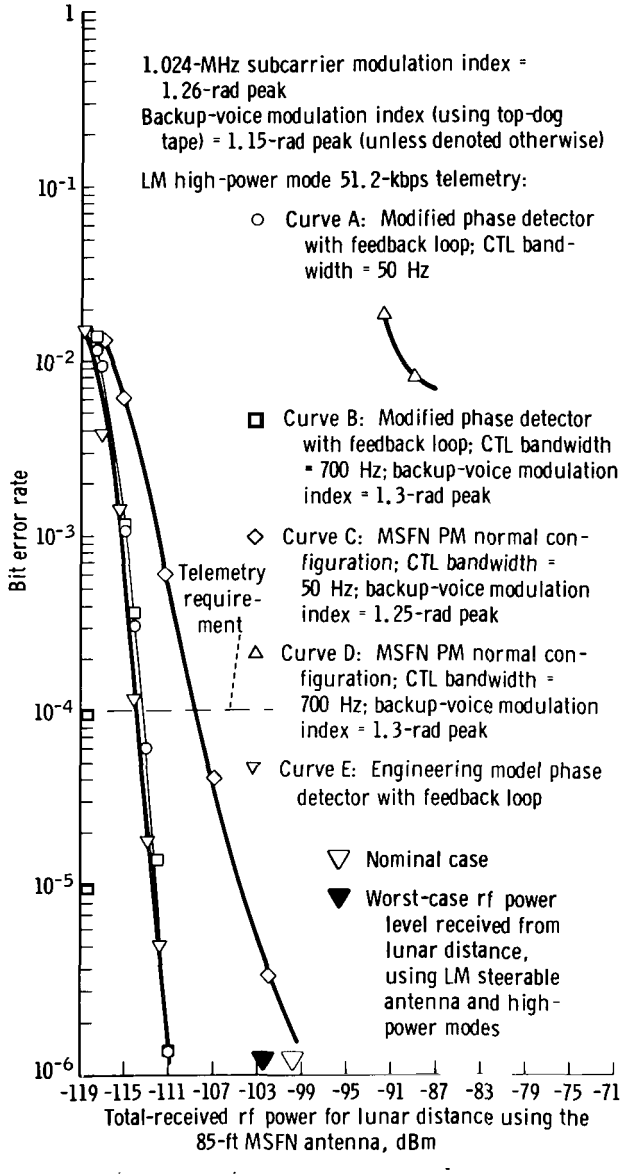

Figure 8. - Lunar module mode 4: bit error rate for 51.2-kbps telemetry (test numbers TPET-021269-10 (curve A), TPET-021269-6 (curve B), TPET-021369-4 (curve C), TPET-021069-4 (curve D), and TPET-031269-2 (curve E)).

The BER and signal-to-noise ratio (SNR) tests were conducted for LM down-link PM modes 4 (backup voice and 1.6-kbps telemetry) and 8 (baseband voice, biomedical information, and 1.6-kbps telemetry) and CSM PM mode 8 (backup voice and 1.6-kbps telemetry). The three modes are the only signal combinations whereby down-link telemetry data and backup voice are transmitted simultaneously on the S-band carrier. It will be shown that telemetry degradation occurs only when the voice signal is present. The amount of telemetry degradation experienced is dependent upon the modulation index of the backup voice. The greater the voice modulation index, the greater the degradation in telemetry performance, as indicated by an increase in the number of telemetry bit errors for a given S-band rf power level.

Lunar module system tests. - This section presents the data results for the BER and SNR tests conducted for the LM PM down-link modes 4 and 8. Tests were conducted for the CTL 50- and 700-hertz noise bandwidths of the MSFN receiver. The 50-hertz loop noise bandwidth normally will be used when communicating with the LM spacecraft at lunar distances. However, near-earth transmissions from the LM (for example, during the spacecraft transposition and docking maneuvers) may necessitate use of the 700-hertz loop bandwidth. Two values for the backup-voice modulation index were tested for LM mode 4 (1.15- and 1.3-radian peak deviations), and one value was tested for LM mode 8 (1.1-radian peak). The nominal voice index for the particular LM transceiver being tested was 1.15-radian peak. However, the exact value for the voice modulation index varied slightly during day-to-day testing.

The BER tests were conducted for 51.2-kbps telemetry, as well as for the 1.6-kbps data rate. The 51.2-kbps telemetry tests were performed because a hybrid communication mode was used often during the Apollo 8 mission. The spacecraft crewmembers found that it was advantageous to use a mode consisting of backup voice and 51.2-kbps telemetry during certain portions of the mission. These two services minimize the manual switching required in the spacecraft when it is slowly rolling.

The test configuration for obtaining BER curves for the LM communication system is given in figure 9. Tests were made with the modification module (negative

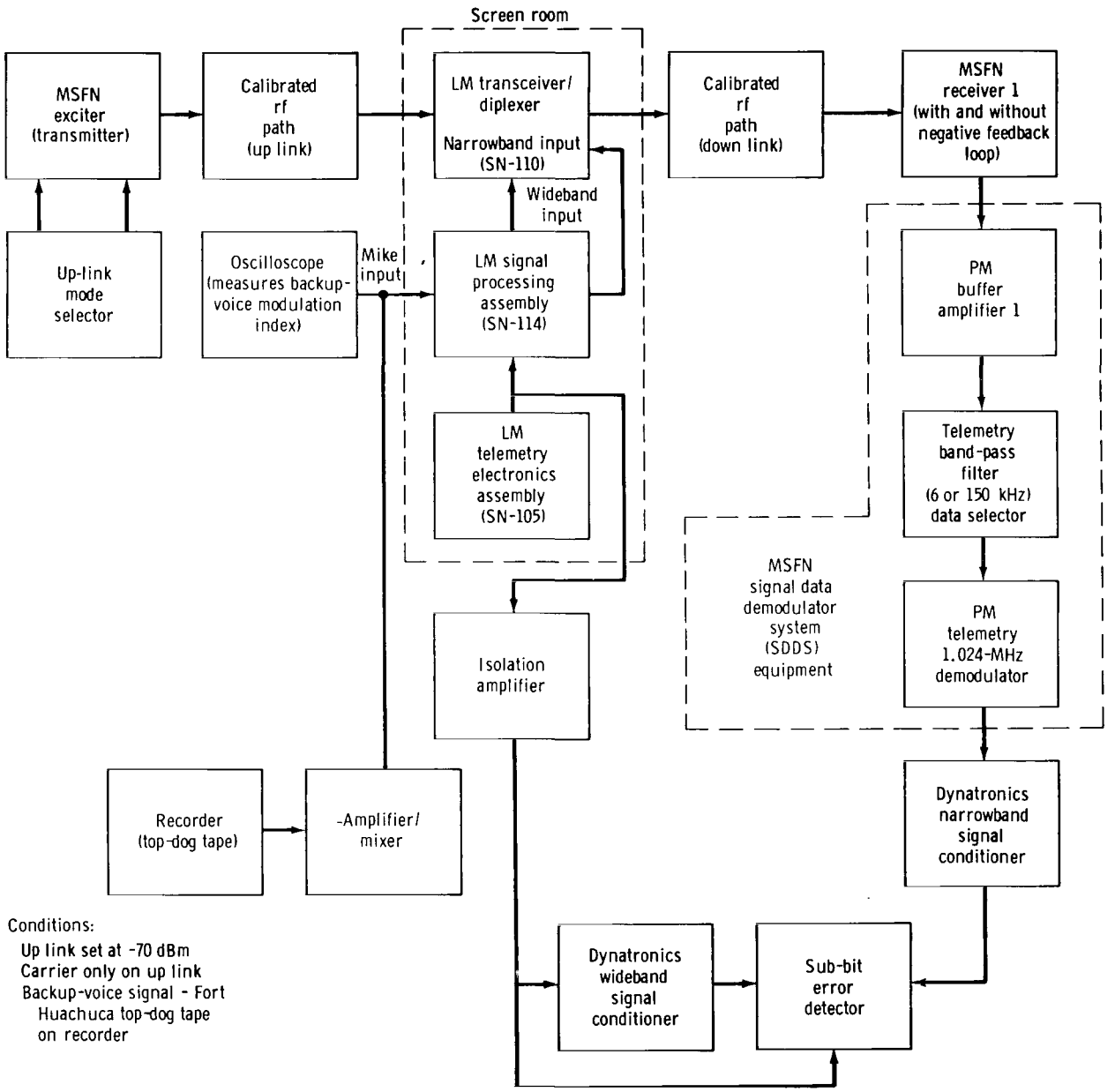

Figure 9.- Lunar module S-band bit-error-rate configuration with and without the negative feedback loop.

feedback loop) connected (1) directly to the MSFN wideband phase detector and (2) to the engineering model phase detector. For the latter condition, the signal input to the phase detector was taken from the limited output connector of the MSFN receiver 10-megahertz i.f. amplifier. The output of the engineering model phase detector was connected to the PM buffer amplifier, as shown in figure 9 for the MSFN phase detector.

Lunar module mode 4 test results: Lunar module mode 4 BER curves for 1.6-kbps telemetry are shown in figure 10 with and without the modification module. The curves (fig. 10), taken with the receiver in the 50-hertz carrier loop bandwidth, are essentially the same with the modification module (curve B) and without the modification module (curve A). These two curves, when compared to the theoretical data represented by curve C, indicate that little or no backup-voice interference is present because no noticeable degradation exists in the BER performance. (See appendix D for the theoretical BER calculations.) The 700-hertz carrier bandwidth configuration (fig. 10) shows severe telemetry degradation without the feedback loop (curve E); however, little or no degradation exists when the feedback loop is used (curve D).

In these tests, the MSFN phase detector without the negative feedback loop showed little BER degradation when the 50-hertz loop filter was used (fig. 10). Essentially the same demodulation configuration using preflight equipment was used for the data given in figure 3, where poor BER performance was obtained. The only significant difference in the two test setups for generating the data in figures 3 and 10 is in the voice processing in the LM spacecraft. The LM signal processor assembly (SPA), used in the second series of tests (fig. 10), had different automatic gain-control (AGC) time constants in the audio amplifiers. Because the telemetry interference is dependent upon $f_v(t)$ (the voice signal as given in eq. (9)), it is possible that the voice signal from the reconfigured LM spacecraft more nearly approaches a square wave. (It may be recalled that no voice interference exists if

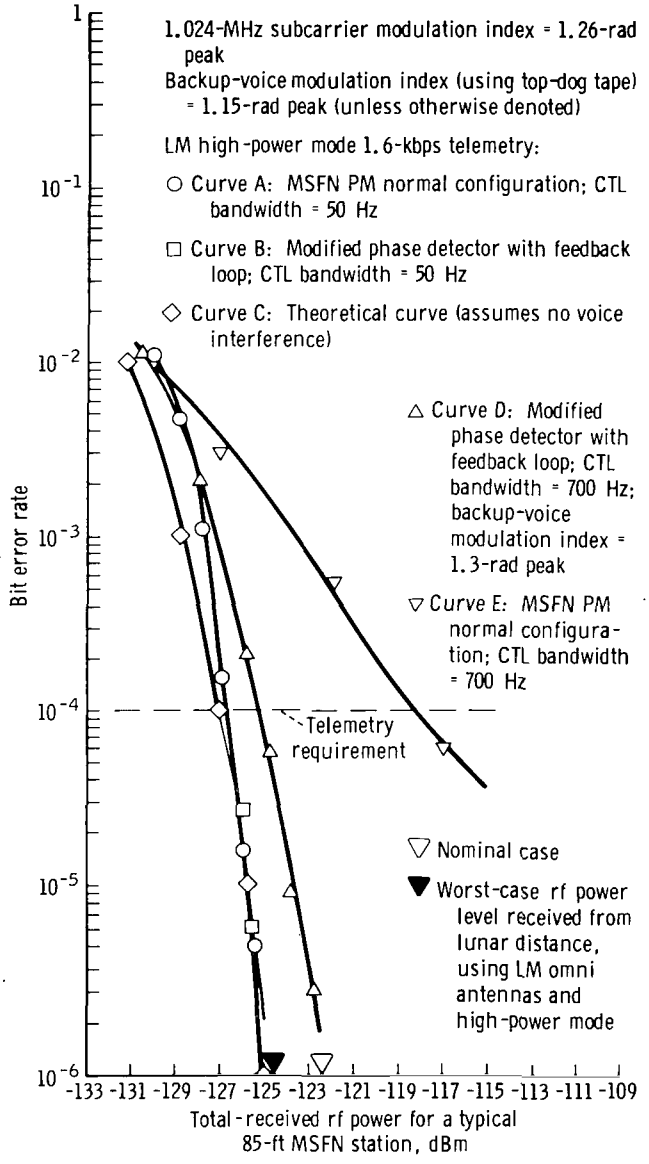

Figure 10. - Lunar module mode 4: bit error rate for 1.6-kbps telemetry (test numbers TPET-021269-7 (curve D), TPET-021269-8 (curve B), TPET-020869-3 (curve A), and TPET-021069-3 (curve E)).

$f_v(t)$ is a square wave.) However, the voice signal will never be a pure square wave; and at some higher value of voice modulation index, severe telemetry degradation will result if a feedback loop is not used.

The most significant improvement in BER performance with the feedback loop is obtained when 51.2-kbps telemetry is transmitted. From observation of the curves plotted in figure 8, it is evident that the choice of a receiver loop bandwidth (50 or 700 hertz) or a backup-voice modulation index (β_v = 1.15- or 1.3-radian peak) does not significantly affect the results of telemetry performance when using the feedback loop at the 51.2-kbps data rate (curves A and B). The normal configuration without the feedback loop shows degraded performance with the 50-hertz loop filter and shows completely unusable data with the 700-hertz loop filter. Because the performance of the MSFN wideband phase detector and the engineering model phase detector is equivalent when using the negative feedback loop, no distinction will be made henceforth between the two detectors.

The destructive effect of backup voice on a received telemetry waveform is shown in figures 11 and 12. Backup-voice interference with the 800-hertz fundamental of a 1.6-kbps alternating 101010 PCM/nonreturn-to-zero (NRZ) code format was investigated. A 1-kilohertz low-pass filter was used to filter out the higher order frequency components of the demodulated code format, leaving only the 800-hertz fundamental. With no backup voice present, a clean 800-hertz sinusoid was received. The modulation indices used for these tests were β_{TM} = 1.3-radian peak and β_v = 1.0-radian peak for the telemetry and backup-voice signals, respectively. The S-band rf power

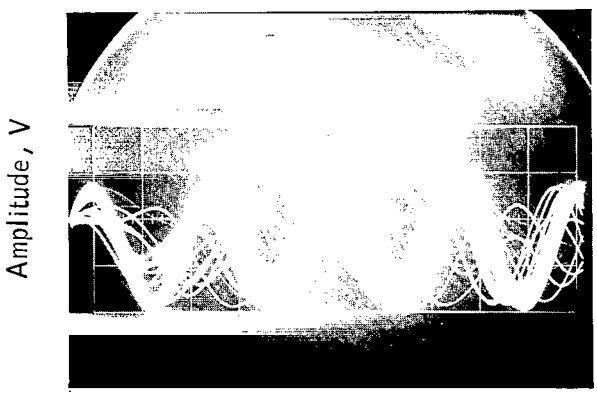

Figure 11. - Fundamental component of a 1.6-kbps PCM 101010 code demodulated with the unmodified Manned Space Flight Network wideband phase detector (the backup-voice modulation index is 1.0-rad peak, and the radio-frequency level is -124.5 dBm).

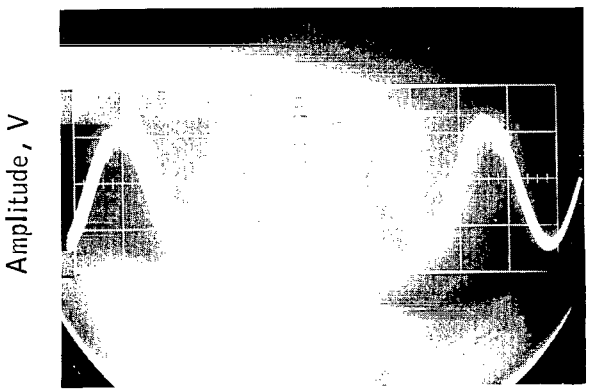

Figure 12. - Fundamental component of a 1.6-kbps PCM 101010 code demodulated with the modified Manned Space Flight Network phase detector with the feedback loop (the backup-voice modulation index is 1.0-rad peak, and the radio-frequency level is -124.5 dBm).

level was -124.5 dBm, which corresponds to the worst-case expected rf power level into the MSFN ground receiver. The voice interference to the fundamental of the PCM code when the composite signal is demodulated by the unmodified MSFN phase detector in the 50-hertz loop bandwidth configuration is illustrated in figure 11. The elimination of the backup-voice signal interference through the use of the feedback loop is shown in figure 12. Excellent improvement in telemetry-signal quality is obtained when the negative feedback loop is used with the phase detector.

An illustration of the effect of the negative feedback loop in reducing the amplitude of the detected backup voice at the output of the carrier phase demodulator (using the 50-hertz loop bandwidth) is shown in figures 13 and 14. A low-pass filter was added to the output of the carrier phase demodulator to filter out the telemetry data, thus passing only the backup voice. The filtered output of the unmodified wideband phase detector is shown in figure 13. The voice signal is reduced by approximately 14 decibels (fig. 14) when the feedback loop is used with the phase detector. Thus, the backup-voice modulation index has been reduced by 14 decibels through the wideband phase detector; therefore, a large improvement in telemetry performance should result.

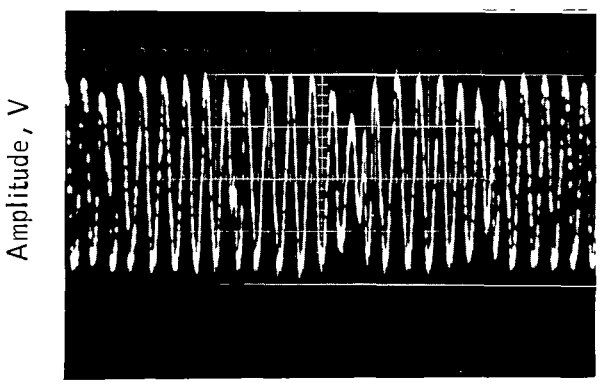

Figure 13. - Backup-voice signal at output of unmodified Manned Space Flight Network wideband phase detector (the backup-voice modulation index is 1.0-rad peak, the radio-frequency level is -100 dBm, and the scale sensitivities are 0.5 V/cm and 20 msec/cm).

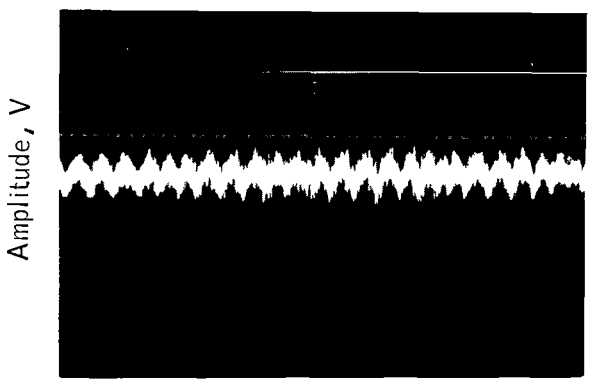

Figure 14. - Backup-voice signal at output of modified Manned Space Flight Network phase detector with the feedback loop (the backup-voice modulation index is 1.0-rad peak, the radio-frequency level is -100 dBm, and the scale sensitivities are 0.5 V/cm and 20 msec/cm).

Lunar module mode 8 test results: The LM down-link PM mode 8 with the baseband voice, the biomedical information subcarriers (3.9, 5.4, 7.35, 10.5, and 14.5 kilohertz), and the 1.024-megahertz telemetry subcarrier (biphase modulated with 1.6-kbps telemetry) was tested. This mode is designed for use if the 1.25-megahertz subcarrier oscillator in the LM spacecraft fails. (The voice and biomedical subcarriers

are normally frequency modulated onto the 1.25-megahertz subcarrier.) The baseband voice signal for LM mode 8 is unclipped and consequently will have different characteristics than the 24-decibel clipped backup-voice signal in LM mode 4. The unclipped baseband voice should produce more interference components (but of lower amplitude) in the telemetry spectrum than the heavily clipped backup-voice signal.

The 1.6-kbps telemetry BER curves for LM mode 8, using both the unmodified and the modified phase detectors, are shown in figure 15. For a receiver loop bandwidth of 700 hertz, the improvement in telemetry performance can be seen by comparing curves C and D (fig. 15). Use of the negative feedback loop with the phase detector enables very low BER to be attained; whereas, leveling off occurs at a BER of 2×10^{-5} for the normal (unmodified) configuration.

The BER measurements (fig. 15) were made without the four biomedical subcarriers because the EVCS backpack equipment from which these subcarriers are generated was not available. However, the 14.5-kilohertz subcarrier is generated within the spacecraft equipment and is always present in the LM mode 8 modulation spectrum. An oscillator was used to simulate the 3.9-kilohertz biomedical subcarrier for the SNR tests in this channel. If the four subcarriers had been modulated onto the S-band down-link carrier, additional telemetry degradations would have been expected when the unmodified phase detector was used. The sum and difference frequencies of the baseband voice and the biomedical subcarriers would produce additional interference components in the telemetry spectrum.

While LM mode 8 normally has low-bit-rate telemetry, the feasibility of using high-bit-rate telemetry was examined (fig. 16). Curve A (fig. 16) was obtained by using the modified phase detector. Although a BER test was made for each receiver loop bandwidth (50 and 700 hertz), the resultant curves were coincident and both are represented by curve A. A marked improvement in telemetry

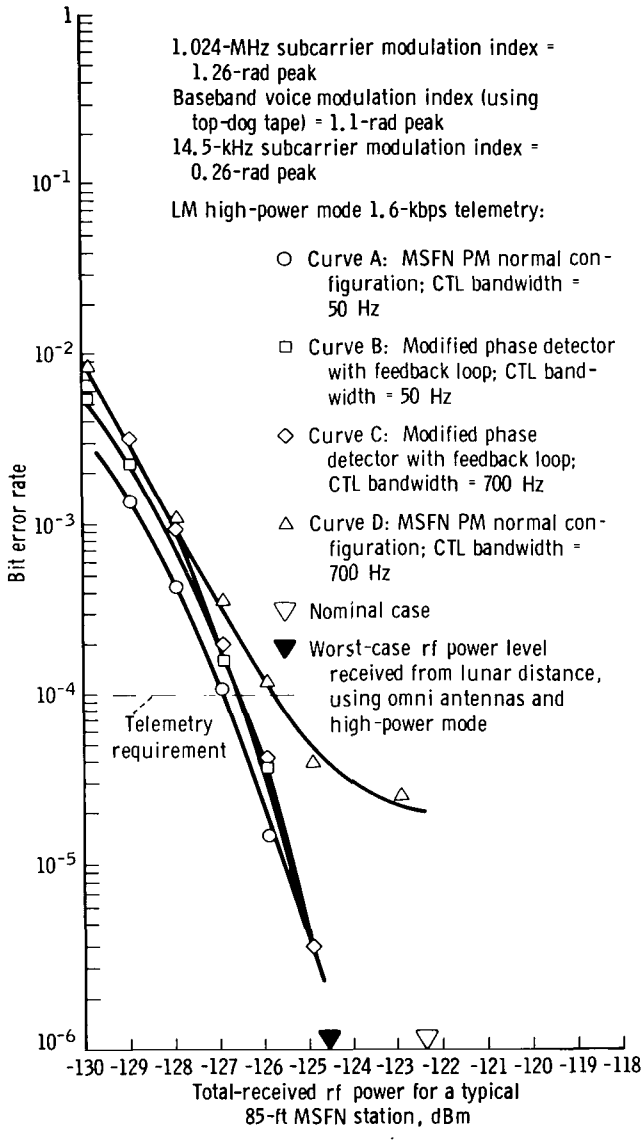

Figure 15.- Lunar module mode 8: bit error rate for 1.6-kbps telemetry (test numbers TPET-021769-2 (curve A), TPET-021469-1 (curve B), TPET-021469-2 (curve C), and TPET-021769-3 (curve D)).

performance can be obtained with the negative-feedback-loop configuration, as seen by comparing curve A with curves B and C (taken with the unmodified phase detector). For the 700-hertz loop bandwidth, the modified phase detector eliminates the "flaring out" effect caused by excessive bit errors due to baseband voice interference. Without modification, the best possible BER is 10^{-4}, as illustrated by curve C.

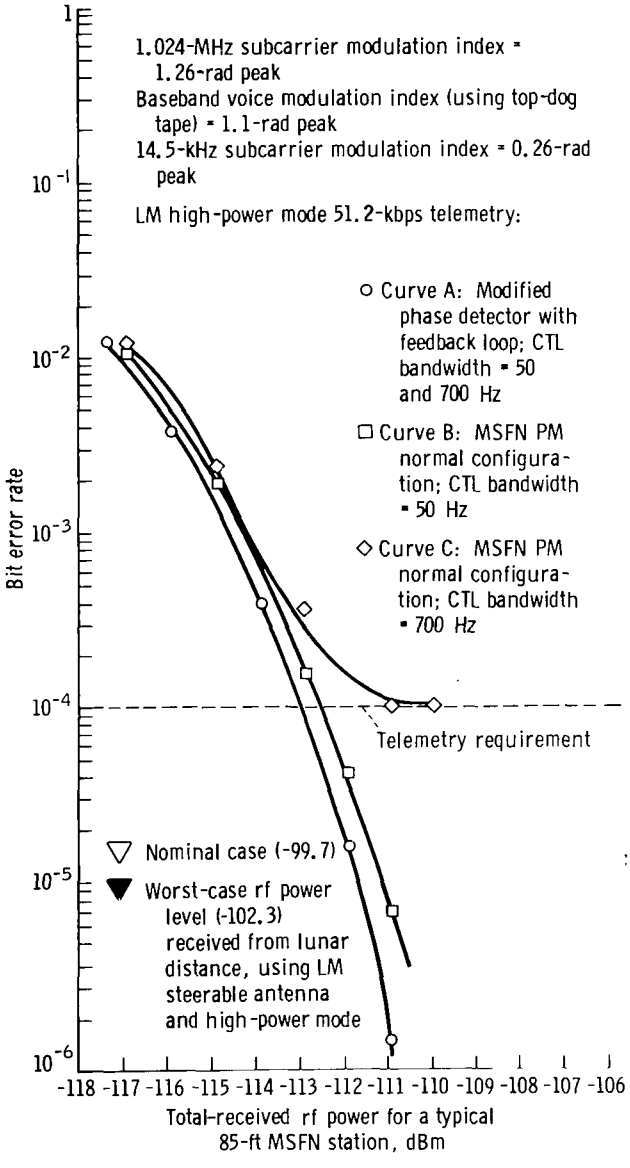

Figure 16. - Lunar module mode 8: bit error rate for 51.2-kbps telemetry (test numbers TPET-021369-5 (curve A), TPET-021369-6 (curve A), TPET-021569-8 (curve B), and TPET-021569-9 (curve C)).

The SNR measurements were made in the predetection bandwidths of the 14.5- and 3.9-kilohertz biomedical-subcarrier demodulators (fig. 1) with and without the modification module implemented in the MSFN receiver. The purpose of the tests was to make a qualitative evaluation of the effects of the negative feedback on the performance of the biomedical subcarriers. The 14.5-kilohertz subcarrier is outside the passband of the feedback-loop filter and should not be affected by the loop. The SNR test results for the 3200-hertz band-pass filter of the 14.5-kilohertz subcarrier (fig. 17) agree with this conclusion. No change occurs in the SNR data when the phase detector is modified.

The 3.9-kilohertz biomedical subcarrier is within the passband of the feedback-loop filter. The filter cannot distinguish between the 3.9-kilohertz subcarrier signal and the narrowband noise around the subcarrier and therefore reduces both signal and noise. Thus, the predetection SNR for the 3.9-kilohertz channel should remain unchanged when the phase detector is modified. However, the SNR in the 800-hertz band-pass filter of the 3.9-kilohertz subcarrier channel is reduced by approximately 12.5 decibels at the higher total-received rf power levels (fig. 18). As the rf level is decreased, the SNR curves with and without the modification module gradually converge at an rf level of -120 dBm. Further tests indicate a possible explanation for the significant SNR reduction at strong rf levels. The modified phase detector reduces the baseband signal and only the quadrature noise component of the input i.f. noise. The in-phase noise component which would appear as incidental amplitude modulation (AM) at the input to the phase detector is not

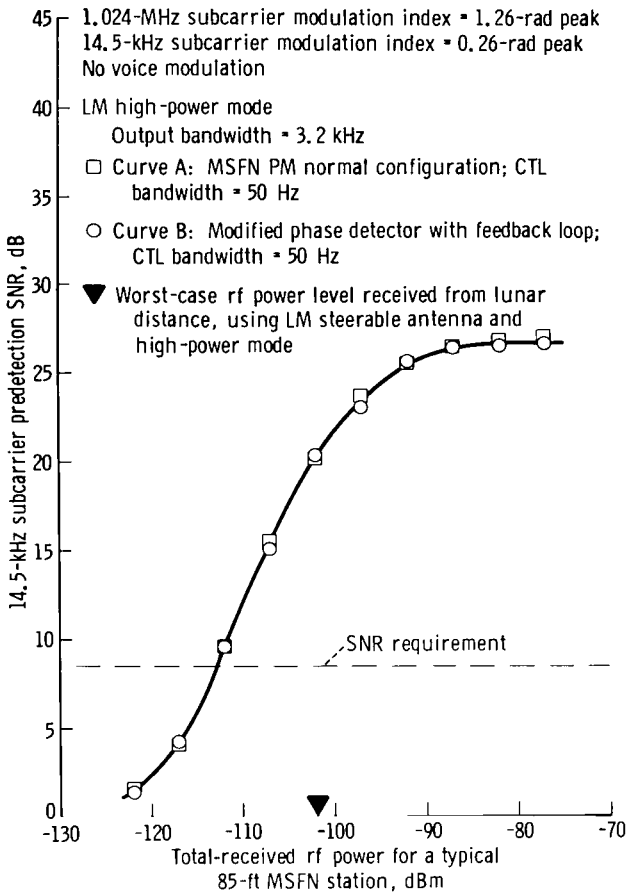

Figure 17.- Lunar module mode 8: 14.5-kilohertz biomedical-subcarrier predetection SNR test results (test numbers TPET-021469-4 (curve B) and TPET-021569-6 (curve A)).

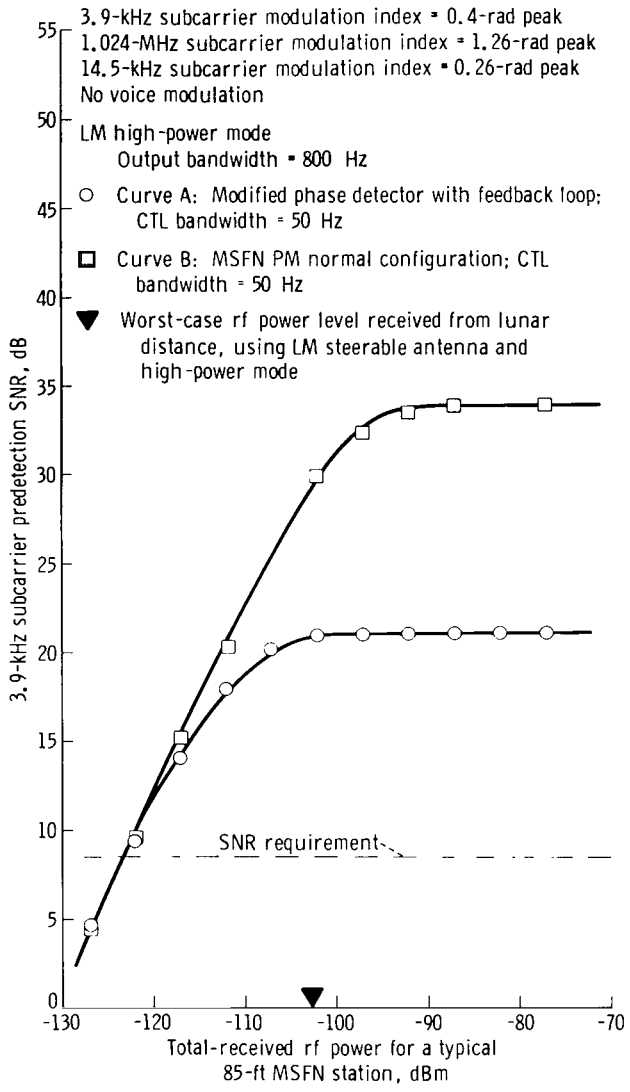

Figure 18.- Lunar module mode 8: 3.9-kilohertz biomedical-subcarrier predetection filter SNR test results (test numbers TPET-021569-3 (curve B) and TPET-021569-4 (curve A)).

affected by the quadrature detection process. Normally, the quadrature noise predominates. However, with the reduction in quadrature noise because of the action of the negative feedback loop within the phase detector, the in-phase noise generated by the nonperfect limiter preceding the phase detector could determine the minimum possible noise power at strong rf levels. Because the feedback-loop gain is directly dependent upon the amplitude of the 10-megahertz signal entering the phase detector, the loop gain decreases with decreasing received rf signal levels. As the rf signal level is reduced, the noise component at the output of the phase detector, caused by the quadrature noise component (PM noise) of the i.f. noise, increases. This increase is caused by the decreasing loop gain of the feedback loop which provides the reduction of

the input quadrature noise component. Therefore, the reduction in the biomedical-subcarrier signal (and the quadrature noise component) is less at lower rf levels. The quadrature noise should become the dominant noise component at lower rf levels; and the SNR curves, with and without the negative feedback loop, should be identical (fig. 18).

The reduction in the SNR data for the 3.9-kilohertz biomedical subcarrier at strong rf levels does not affect the overall performance of the channel. The predetection SNR requirement is listed as 8.5 decibels for satisfactory output biomedical data in the LM-MSFN S-band System Signal Performance and Interface Specification (ref. 3). At the 8.5-decibel SNR requirement, the data curves for the modified and unmodified phase detectors coincide.

Command and service module mode 8 test results. - This section presents the data for the BER tests conducted for CSM PM down-link mode 8. Mode 8 has backup voice at baseband and 1.6-kbps telemetry on a 1.024-megahertz subcarrier. This mode was used often on the Apollo 8 mission with 51.2-kbps telemetry rather than with 1.6-kbps telemetry. Severe telemetry degradations were experienced frequently during the Apollo 8 mission when backup voice was present on the downlink.

In the following section, it will be shown that the feedback loop provides the most significant BER improvements of the current test program for CSM mode 8. Two values of voice modulation index are used: 0.85- and 1.47-radian peak deviations when transmitting 1.6- and 51.2-kbps telemetry, respectively. The test configuration is the same as that shown in figure 9 except that the LM spacecraft equipment has been replaced by a CSM transponder (Q3-SN-67603), a premodulation processor (Q2-SN-1224B), and a PCM assembly (Q3-SN-68186).

The results of the CSM BER tests for 1.6-kbps telemetry are plotted in figure 19. Tests were conducted for both receiver CTL noise bandwidths (50 and 700 hertz). As was seen for the LM modes, the 50-hertz loop bandwidth provides satisfactory 1.6-kbps telemetry performance with the unmodified phase detector. However, the 700-hertz bandwidth produces an unsatisfactory BER curve which levels off at approximately 10^{-4} BER. The modified phase detector produces satisfactory results with both the 50- and 700-hertz loop bandwidths. No backup-voice degradations are observed with either bandwidth configuration.

The BER curves for the 51.2-kbps telemetry are shown in figure 20. The unmodified phase detector is unable to detect the PCM data at 51.2-kbps telemetry with simultaneous transmission of the backup-voice signal. This is shown by the upper BER curve which levels off at 10^{-2} BER. However, the modified phase detector allows excellent BER results with no backup-voice interference noted. The theoretical curve, which does not include any voice interference, is very close to the measured results.

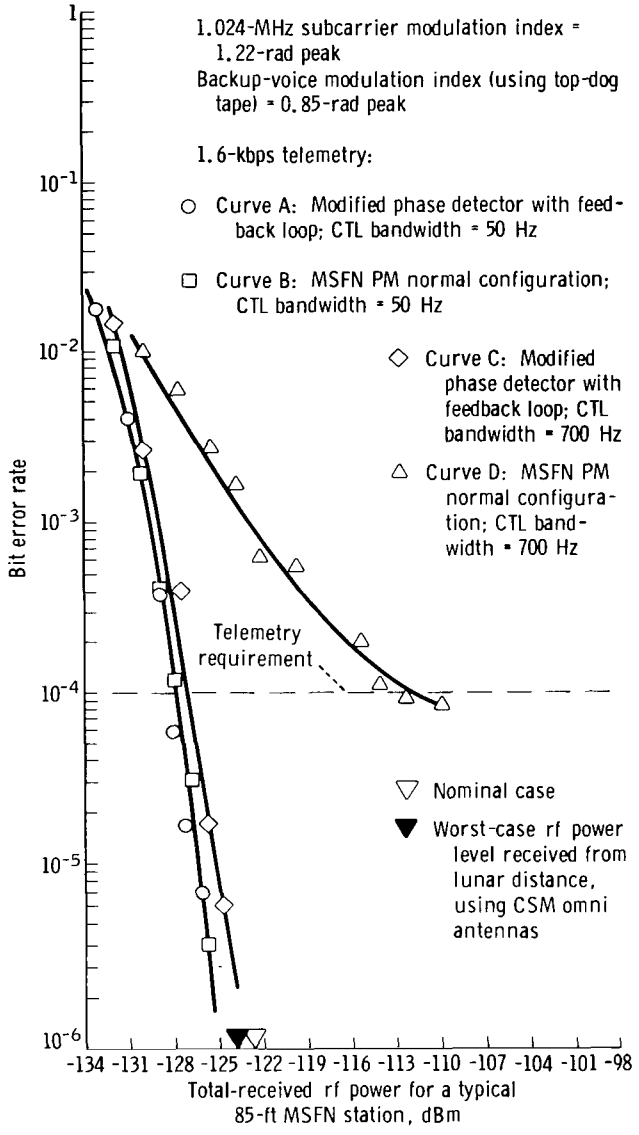

Figure 19. - Command and service module mode 8: bit error rate for 1.6-kbps telemetry (test numbers TPET-022069-1 (curve A), TPET-021969-7 (curve B), TPET-022069-2 (curve C), and TPET-021969-8 (curve D)).

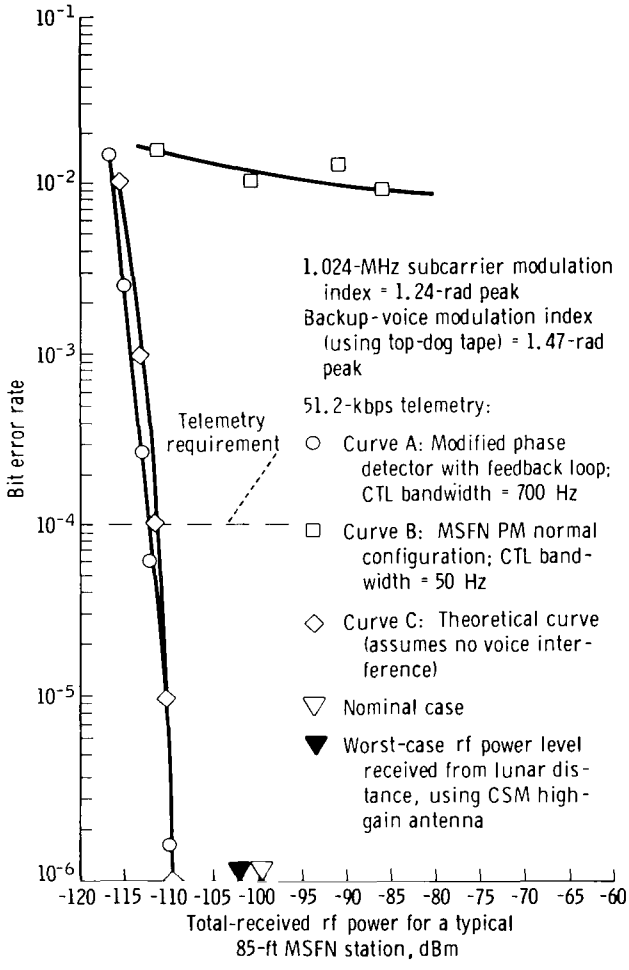

Figure 20. - Command and service module mode 8: bit error rate for 51.2-kbps telemetry (test numbers TPET-021969-9 (curve B) and TPET-022069-4 (curve A)).

Results of Using a Simplified Method of Phase Cancellation

A simplified method of reducing the backup-voice modulation index by phase cancellation in the MSFN wideband phase detector has been suggested. This method

operates on the same basic principle as the previously discussed technique which used the modification module, where modulation cancellation occurred in the detection process. However, instead of using the modification module with the low-pass feedback loop and the 10-megahertz phase modulator, the wideband phase-detector reference is taken directly from the 10-megahertz amplifier preceding the narrowband phase detector in the CTL. An external cable connects the output of the 10-megahertz amplifier to the static phase shifter in the reference channel of the wideband detector. Partial phase cancellation of the backup-voice modulation occurs in the wideband phase detector. However, since the simplified method uses no feedback process, close tracking of the baseband voice signal or controlled reduction to its modulation index by adjustment of loop gain is impossible. The test configuration for this method is shown in figure 21.

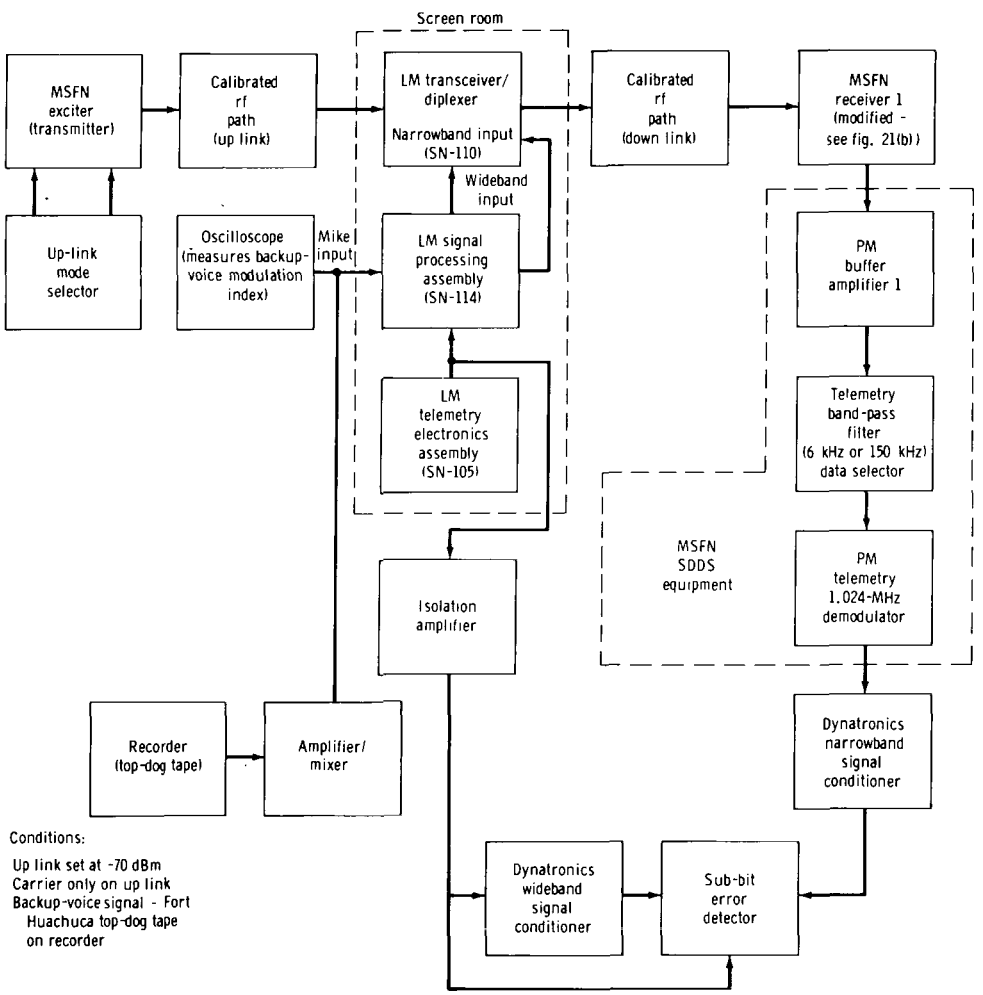

(a) Block diagram of test configuration.

Figure 21. - Bit-error-rate test configuration for simplified phase-cancellation detection scheme.

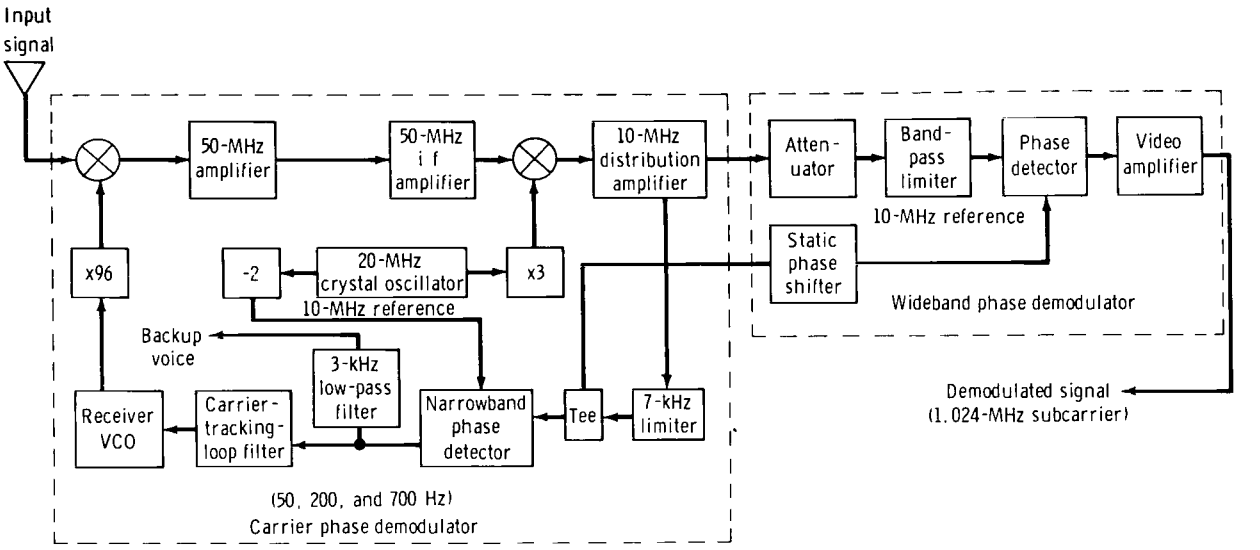

(b) Insert for receiver modifications for phase-cancellation method.

Figure 21. - Concluded.

The BER results for LM mode 4 with 1.6- and 51.2-kbps telemetry, using the simplified method of phase cancellation, are shown in figures 22 and 23, respectively. The simplified method of phase cancellation can produce significant improvement for 1.6-kbps telemetry BER performance, as shown by curves B and C in figure 22. However, this method does not eliminate the voice interference with 51.2-kbps telemetry (fig. 23). The BER performance is degraded and is limited to a minimum of 3×10^{-5} BER at strong rf levels. Thus, the simplified method will provide some improvement over the present MSFN PM demodulation scheme. However, for a high voice modulation index, the voice interference degrades BER performance for 51.2-kbps telemetry.

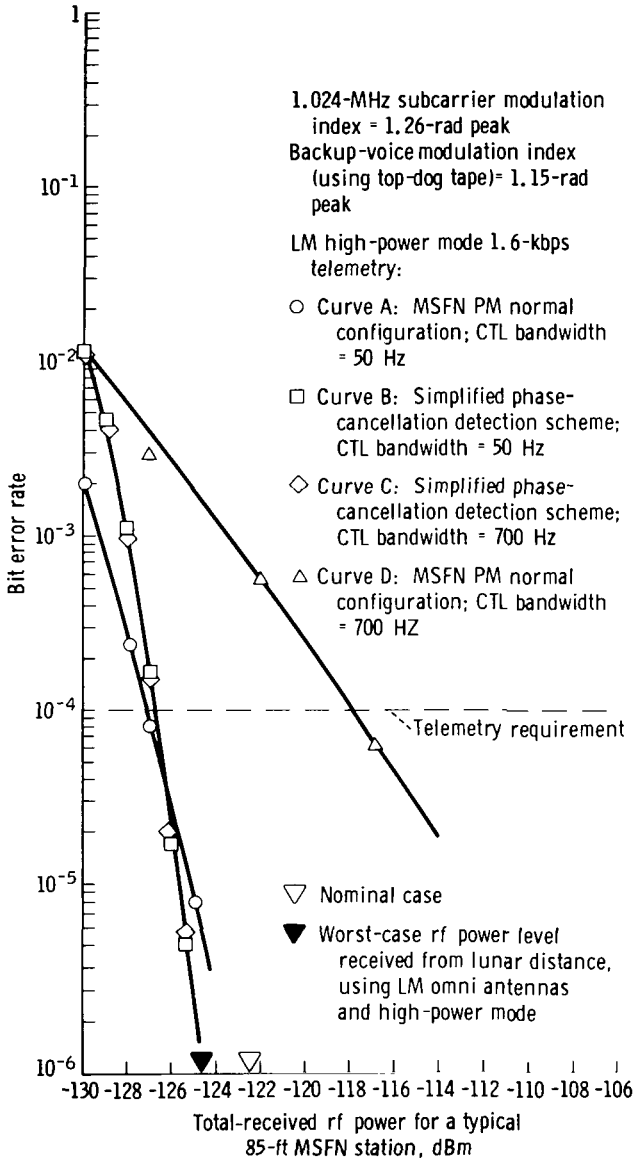

Figure 22. - Lunar module mode 4: bit error rate for 1.6-kbps telemetry (test numbers TPET-020869-3 (curve A), TPET-021269-2 (curve B), TPET-021269-1 (curve C), and TPET-021069-3 (curve D)).

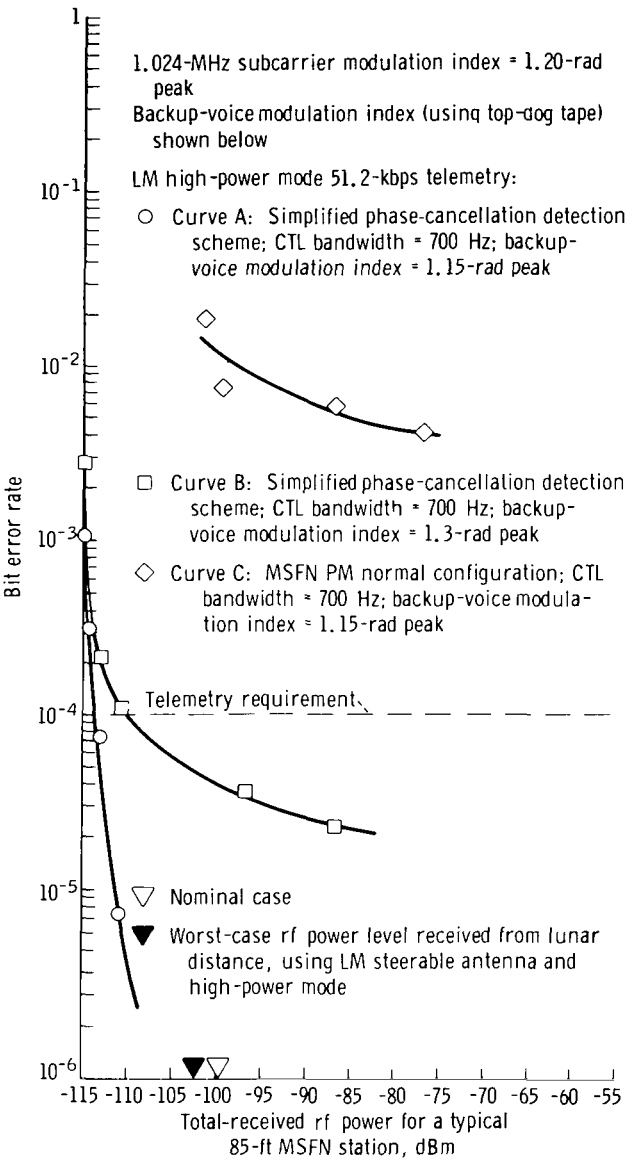

Figure 23. - Lunar module mode 4: bit error rate for 51.2-kbps telemetry (test numbers TPET-021269-3 (curve A), TPET-021269-4 (curve B), and TPET-021069-4 (curve C)).

LINEAR DETECTION USING FREQUENCY-MODULATION DEMODULATION TECHNIQUES

It has been shown previously that a linear demodulation technique is necessary to recover adequately the down-link telemetry information when the modulated telemetry subcarrier and baseband voice are phase-modulated onto a carrier. However,

linear phase detectors are difficult to construct and inherently have a threshold associated with them which can severely degrade demodulation performance at a low-input SNR.

The second demodulation technique investigated uses the FM demodulator as the linear detector. Because frequency discriminators respond linearly to frequency changes, the integrated outputs should respond linearly to phase changes. It is more desirable to use FM detectors (although threshold problems also exist when using this technique) rather than linear phase detectors because the MSFN receivers have FM demodulators available. The feasibility of using the existing carrier frequency demodulator in the MSFN receiver as the FM detector will be determined.

The mathematical representation of a basic PLL FM demodulator (assuming linear operation of the phase detector) may be expressed in terms of the input signal phase θ_i, the voltage-controlled oscillator (VCO) output signal phase θ_0, the phase error θ_e, the phase-detector gain constant K_d, the loop-filter-response function F(S), the phase-detector output voltage V_d, the loop-filter output voltage V_{FO}, and the VCO gain constant K_v (fig. 24).

The phase-detector output voltage is proportional to the difference in phase between the quadrature reference and the input signal.

$$V_d = K_d(\theta_i - \theta_0) \qquad (23)$$

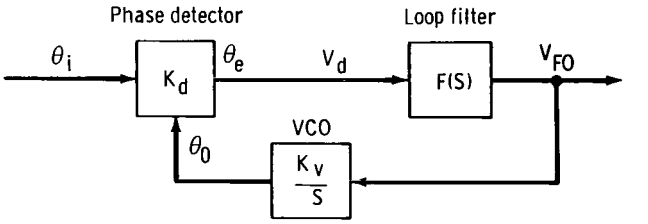

Figure 24. - Linear representation of a phase-lock-loop frequency-modulation demodulator.

Because

$$\theta_0 = F(S)\frac{K_v}{S}V_d \qquad (24)$$

the phase error response θ_e/θ_i can be written as

$$\frac{\theta_e}{\theta_i} = \frac{\theta_i - \theta_0}{\theta_i} = \frac{S}{S + K_v K_d F(S)} \qquad (25)$$

by combining equations (23) and (24).

For a second-order, passive RC loop filter, the loop-filter output voltage V_{FO} is given by

$$V_{FO} = S\theta_i\left(\frac{1}{K_v}\right)\left(\frac{\omega_n^2}{S^2 + 2\zeta\omega_n S + \omega_n^2}\right) \tag{26}$$

where the loop damping constant ζ and the loop natural frequency ω_n are defined by Gardner (ref. 4).

By considering the PLL demodulator to be used as an FM discriminator, the first term $S\theta_i$ of V_{FO} (eq. (26)) represents the frequency modulation; the terms in parentheses represent a gain constant and the low-pass filter-response function, respectively. This model is valid provided the phase error θ_e is small, thereby allowing linear operation of the phase detector.

By considering a simple RC integrator at the output of the loop filter, the integrator response may be written as

$$F_I(S) \cong \omega_I\left(\frac{1}{S}\right) \tag{27}$$

where $F_I(S)$ is the integrator transfer function and ω_I is the integrator cut-off frequency. Then, the voltage expression of an integrated FM demodulator output is

$$V_{FO_{int}} = V_{FO}(S)F_I(S) = \frac{\theta_i}{K_v}\left(\frac{\omega_I\omega_n^2}{S^2 + 2\zeta\omega_n S + \omega_n^2}\right) \tag{28}$$

which signifies "linear" detection of the telemetry subcarrier and baseband voice signals (appendix E).

A PLL FM demodulator may be categorized as a modulation tracking loop, whereby the modulation spectrum is within the loop bandwidth. The loop "tracks" the modulation, thereby allowing a large modulation index with the constraint that the loop bandwidth be wide enough so that the phase error is less than 90°. The MSFN FM demodulator considered in this study has selectable loop bandwidths of 4 and 11 megahertz, both of which are wide enough to provide a linear response to the phase-modulated input signal.

A significant constraint is imposed upon this demodulation scheme when the effects of noise on PLL operation are considered. At a sufficiently low input SNR, the

loop will not track the modulation, and the VCO will begin to skip cycles (drop out of lock). The MSFN FM demodulator used in the tests has an input noise bandwidth of 4.4 megahertz when configured in the wide predetection filter-switch position. The MSFN demodulator has three switch-selectable prefilter positions: unfiltered (14 megahertz), wide (4.4 megahertz), and narrow (1 megahertz). Previous laboratory tests, using the Apollo FM telemetry channels, have indicated that an input SNR of approximately zero decibel is required in the 4.4-megahertz filter to achieve satisfactory demodulation performance for the 1.024-megahertz telemetry subcarrier. However, to meet the specified telemetry performance for 10^{-4} BER, under worst-case specified conditions from lunar distance over the spacecraft omni antennas to an 85-foot MSFN ground station, the PLL demodulator would have to operate at an input predetection SNR of approximately -15 decibels. The -15-decibel value is based upon a received MSFN rf level of -124.5 dBm and a system noise temperature of 209° Kelvin.

To achieve satisfactory operating performance for the FM demodulator, a 15-decibel SNR improvement is required at the input. For this study, the SNR improvement was obtained by installing a high-Q band-pass filtering network at the FM demodulator input to reduce effectively the input noise bandwidth by 15 decibels. This bandwidth reduction is equivalent to increasing the input SNR by 15 decibels, provided there is no loss of signal power. The improvement is evident by examining the following demodulator input SNR equation.

$$(\mathrm{SNR})_{IN} = \frac{P_{tr}}{P_N} = \frac{P_{tr}}{kT_S B_{IN}} \tag{29}$$

where P_{tr} is the total-received power at the receiver input, P_N is the noise power in the demodulator input noise bandwidth, k is the Boltzmann constant, T_S is the system temperature, and B_{IN} is the demodulator input noise bandwidth. Reducing B_{IN} to achieve a significant SNR improvement is practical only because of the particular signal-modulation design for the telemetry/baseband voice modes (figs. 25 and 26). The signal power spectrum (neglecting cross-modulation terms) of LM mode 4 and CSM mode 8 in the predetection bandwidth of the MSFN FM demodulator is shown in figure 25. The signal power spectrum of LM mode 8 at the same point in the demodulator is shown in figure 26. In both figures, the band of frequencies enclosed by the rectangle between frequencies $f_c - (1/2)B_{IN}$ and $f_c + (1/2)B_{IN}$ represents the signal and noise passband preceding the present receiver carrier demodulator. Since the telemetry-subcarrier sidebands are removed relatively far from the carrier and its baseband modulation (voice modulation for LM mode 4 and CSM mode 8 and voice and biomedical subcarriers for LM mode 8), a significant portion of the passband essentially passes only white Gaussian noise. Therefore, by installing a composite filter network which consists of three high-Q band-pass filters in parallel (centered at the carrier frequency and the two telemetry-subcarrier sideband frequencies, respectively) and which precedes the demodulator (illustrated by the dotted lines in figs. 25 and 26),

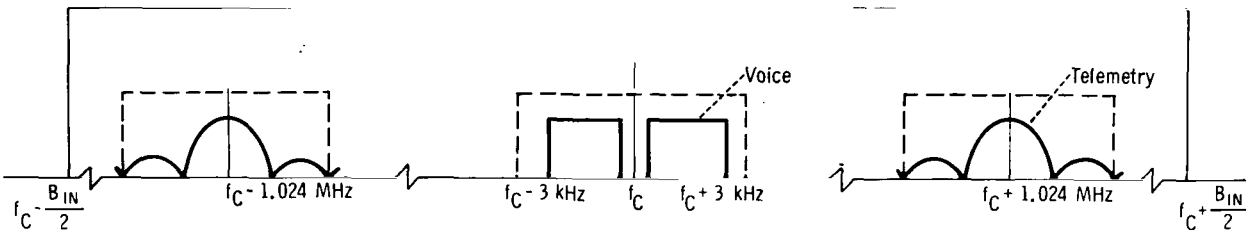

Figure 25. - Signal spectrum for lunar module mode 4 and command and service for module mode 8.

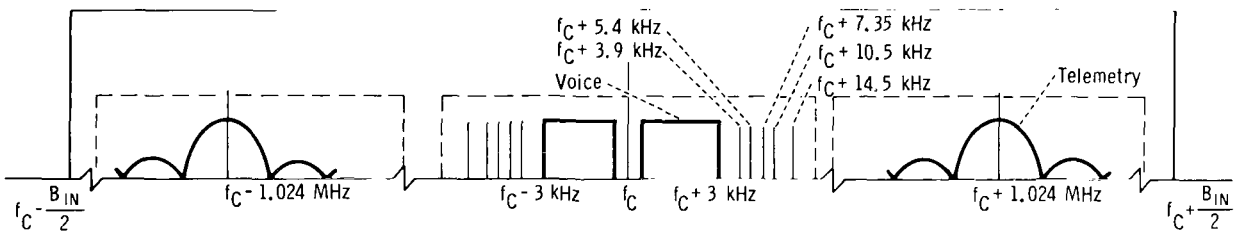

Figure 26. - Signal spectrum for lunar module mode 8.

a significant amount of noise will be attenuated. These filters will pass only the first-order sidebands of the telemetry subcarrier. However, since a radio-frequency interference (RFI) filter at the front end of the MSFN receiving equipment already passes only the first-order sidebands of the 1.024-megahertz subcarrier, little additional distortion should be introduced by the composite band-pass filters.

Narrowband Filtering Techniques

The narrowband filter/FM demodulator technique for linear demodulation may be configured as shown in figure 27. The input modulation is "notch filtered" by the three high-Q band-pass filters and then is recombined by a linear summer. Appropriate isolation between each of the filters is necessary at both the input and output of the filter network. Hybrid transformers are used to provide isolation. To preserve the original phase information of the input modulation, the phase slope of each filter must be identical and linear throughout each passband (appendix E). Also, each of the telemetry-subcarrier sidebands should be attenuated equally in the sideband filters. After the filtered, recombined signal is demodulated in the FM discriminator, it can be integrated to obtain the original phase information. A mathematical justification of the composite filter configuration is presented in appendix E. (Also, appendix E shows that an integrator is unnecessary at the FM discriminator output if only telemetry information is desired.)

It has been stated in the previous section that a 15-decibel SNR improvement in the form of a noise bandwidth reduction is required in the predetection filter of the MSFN FM demodulator. This improvement is necessary to maintain loop lock for the low-received signal levels expected for the telemetry and baseband voice modes at

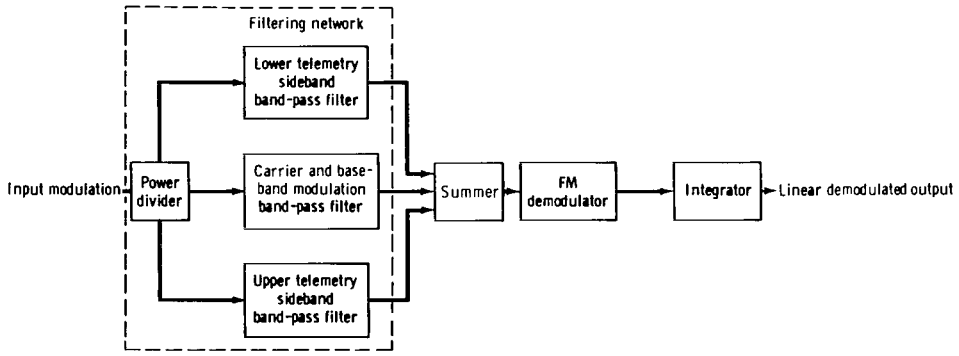

Figure 27. - Composite filter and frequency demodulator detection scheme.

lunar distance. The combined noise bandwidth of the narrowband filter bank should be approximately 140 kilohertz, based upon a 15-decibel reduction in the 4.4-megahertz bandwidth. Therefore, the noise bandwidth of each filter in the filter bank should be approximately 47 kilohertz or less. A 47-kilohertz band-pass filter would pass the 1.6-kbps telemetry data satisfactorily but would degrade the 51.2-kbps telemetry data.

Two types of narrowband filters — the helical resonators and the crystal filters — were fabricated and tested. The three helical resonators (centered at 48.976, 50, and 51.024 megahertz) are designed for use with the MSFN 50-megahertz PLL FM demodulator. The crystal filters (centered at 8.976, 10, and 11.024 megahertz) can be used with either a 10-megahertz frequency-modulation feedback (FMFB) discriminator or with the MSFN 50-megahertz PLL FM demodulator by mixing the signal after filtering. Since the FMFB discriminator has better FM threshold performance than the MSFN PLL demodulator, one objective of the crystal filter tests was to determine the advantages of using an improved FM demodulator. The helical resonators were designed for LM modes 4 and 8 and CSM mode 8. The crystal filters were designed for LM mode 4 and CSM mode 8. (The response of the crystal filters is too narrow to pass the LM mode 8 biomedical subcarriers.) Design and fabrication details for the resonators and the crystals are given in appendix F.

The amplitude- and phase-response curves of the helical resonators and the crystal filters are presented in figures 28 and 29, respectively. The 3-decibel bandwidth of each resonator is approximately 85 kilohertz, which corresponds to a Q of 590. The desired noise bandwidth of 47 kilohertz (Q = 1180) could not be attained before the scheduled testing began. It is doubtful that any improvements in the cavity resonator (such as soldering of the helix and end caps and silver plating of the device) would have made a significant reduction in the bandwidth of the resonator (ref. 5). The noise bandwidth of each crystal filter is approximately 7.5 kilohertz, thus corresponding to a Q of 1340 which should provide satisfactory FM demodulation threshold performance. With the frequency responses as shown in figure 28, the helical resonators should pass either 51.2- or 1.6-kbps telemetry data, as well as the biomedical subcarriers. However, the 51.2-kbps telemetry data will be degraded by the resonators because of the relatively narrow bandwidths. The crystal filters will pass only 1.6-kbps telemetry data. However, the bandwidth of each crystal filter is determined by external load resistance (appendix F). Increasing the load resistance will degrade the Q of the filter and will increase the bandwidth, if so desired.

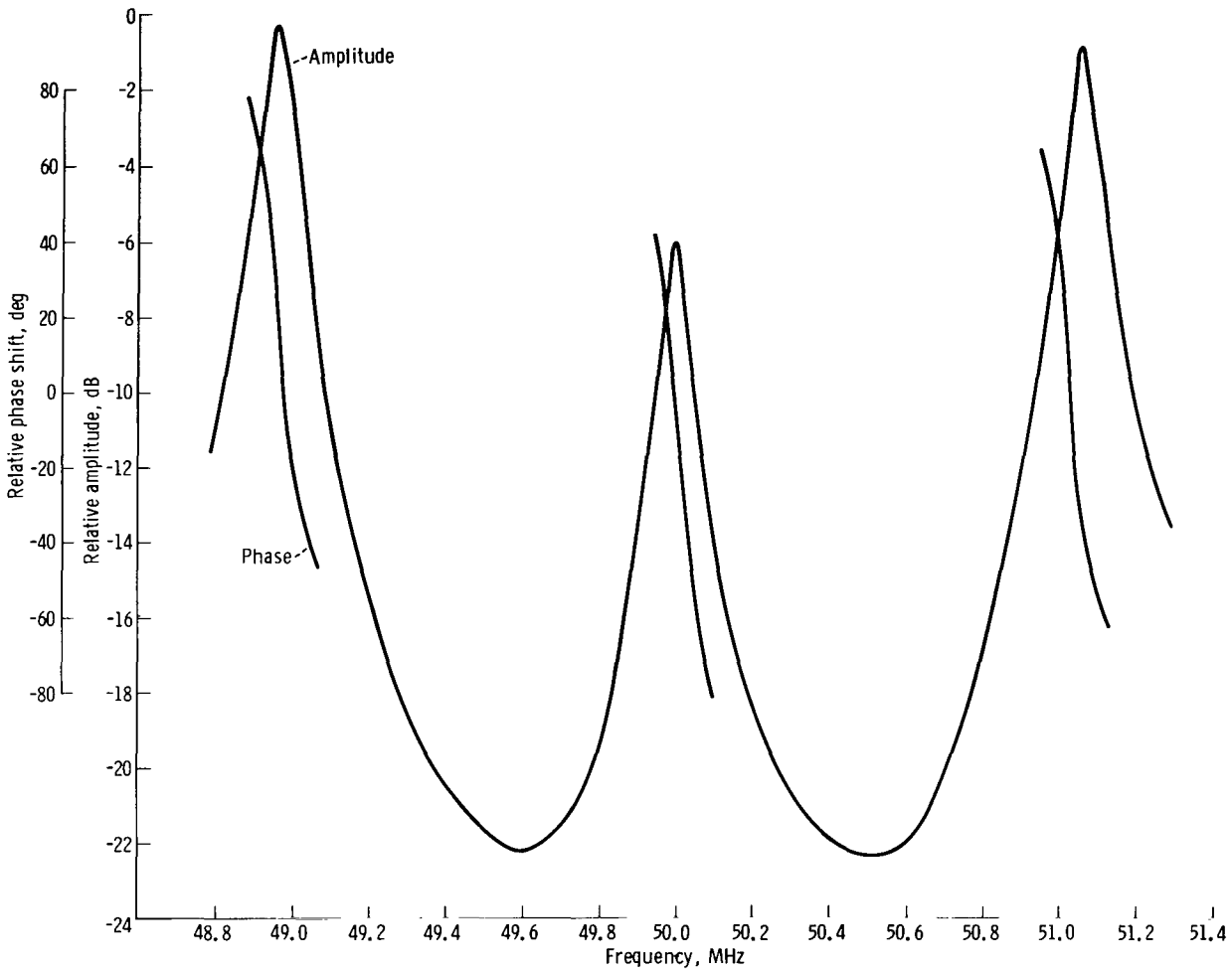

Figure 28. - Amplitude- and phase-response curves for the helical resonators.

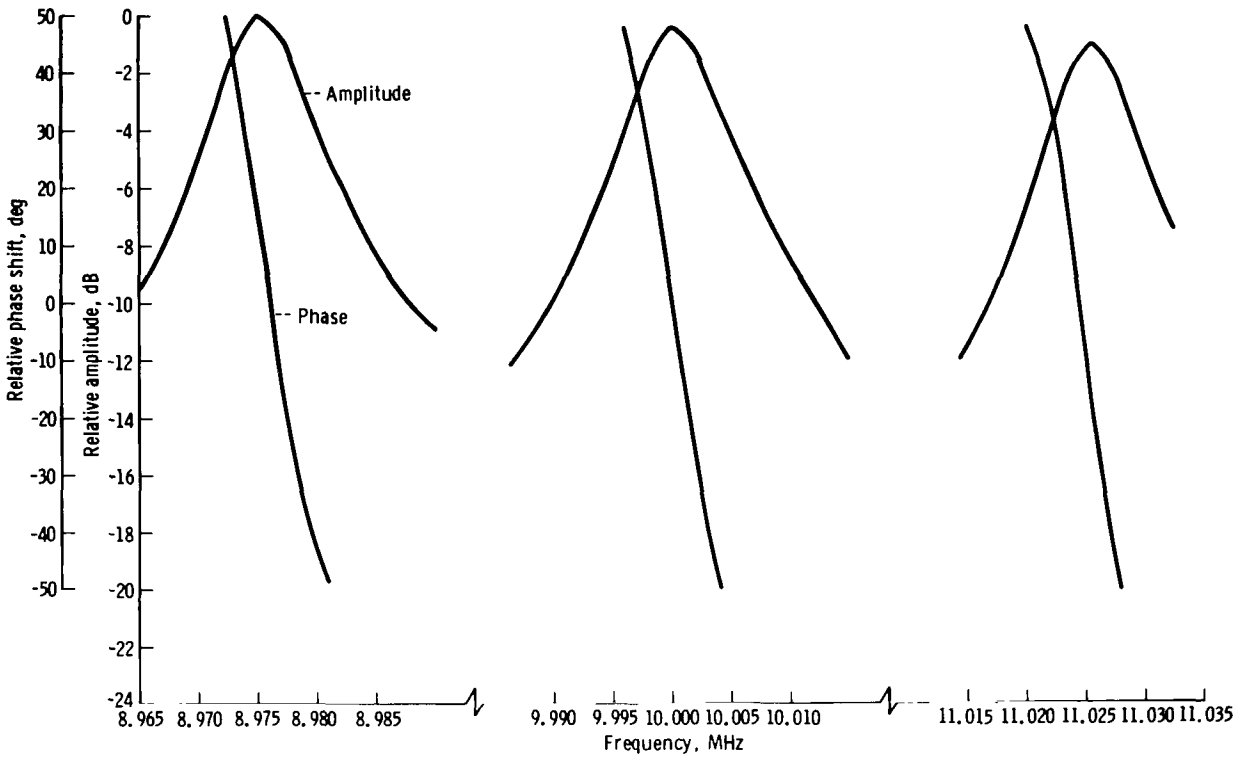

Figure 29. - Amplitude- and phase-response curves for the crystal filters.

Experimental Results with Frequency-Modulation Demodulation

System tests were conducted in the ESCL to determine the effectiveness of using FM demodulation techniques to eliminate telemetry degradation caused by backup-voice interference. Engineering models of the high-Q helical resonators and crystal filters were constructed and tested to determine the effective FM threshold extension obtainable by using narrowband filtering techniques. (The FM threshold is defined as the input rf level at which the output SNR is 1 decibel below an extension of the linear portion of the output SNR curve.) Two FM demodulators, the MSFN 50-megahertz PLL demodulator and a 10-megahertz FMFB discriminator, were implemented at the output of the MSFN receiver for the ESCL tests. The production LM and CSM spacecraft equipment was used to generate the S-band signals, and a calibrated rf attenuator simulated the spacecraft-to-ground link.

The experimental results included SNR tests for the 1.024-megahertz subcarrier with and without the helical resonators and crystal filters for LM modes 4 and 8 and CSM mode 8. The BER curves were made for 1.6- and 51.2-kbps telemetry for LM modes 4 and 8. The SNR tests were not conducted for the biomedical subcarriers of LM mode 8 because the FM demodulators would not properly detect these subcarriers; that is, the MSFN FM demodulator, which has a sensitivity of 1 V/MHz, will not respond to the small phase deviations of the biomedical subcarriers. (The worst-case

specified phase deviations of the biomedical subcarriers range from a low of 0.07 radian for the 3.9-kilohertz subcarrier to a high of 0.17 radian for the 10.5-kilohertz subcarrier.)

The test configurations for the filters and the FM demodulators are shown in figures 30 and 31. No special modifications to the MSFN equipment are necessary because the external composite filters are self-contained. The 10-megahertz crystal

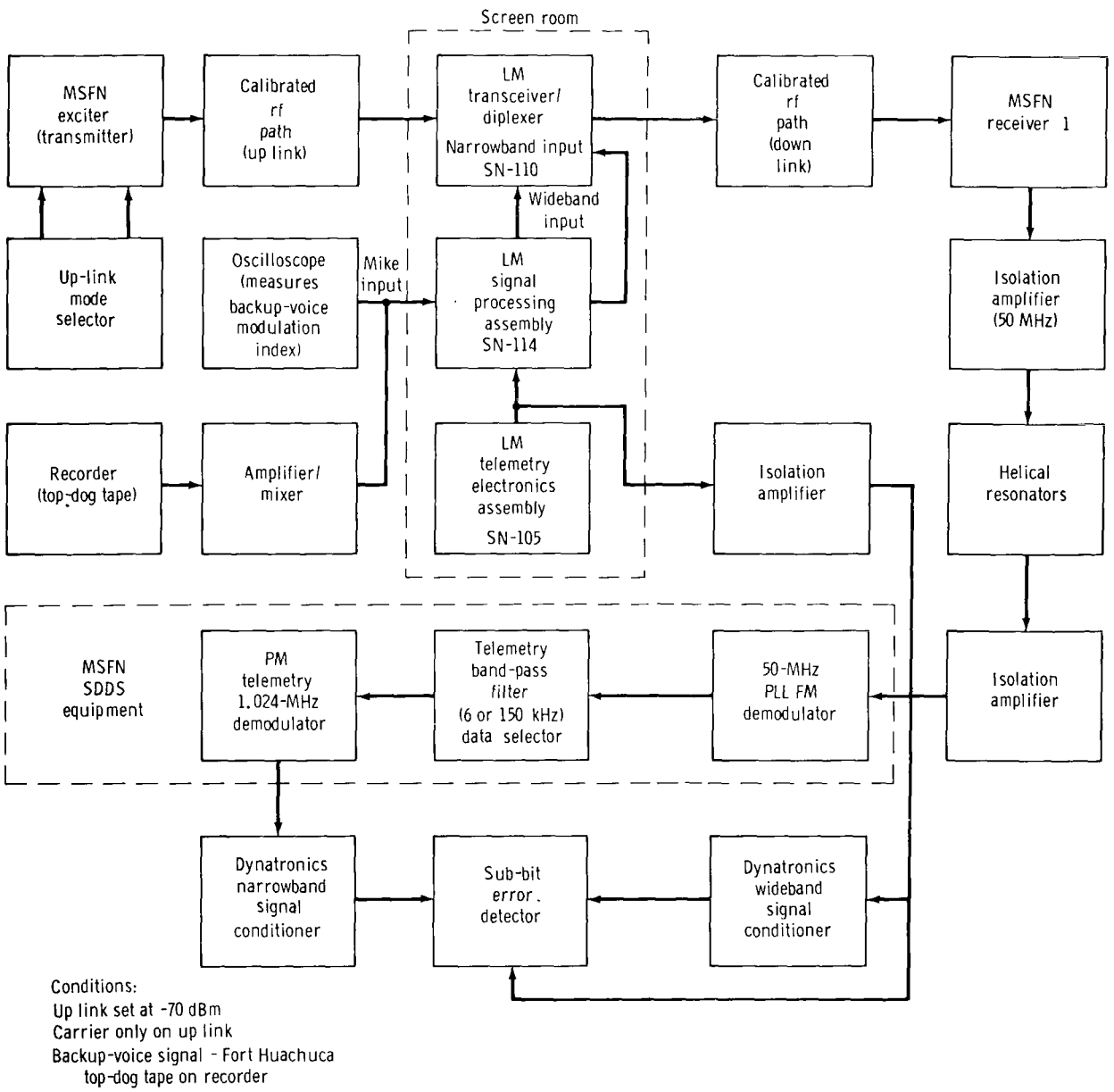

Figure 30. - Test configuration for frequency-modulation detection, using helical resonator prefilters.

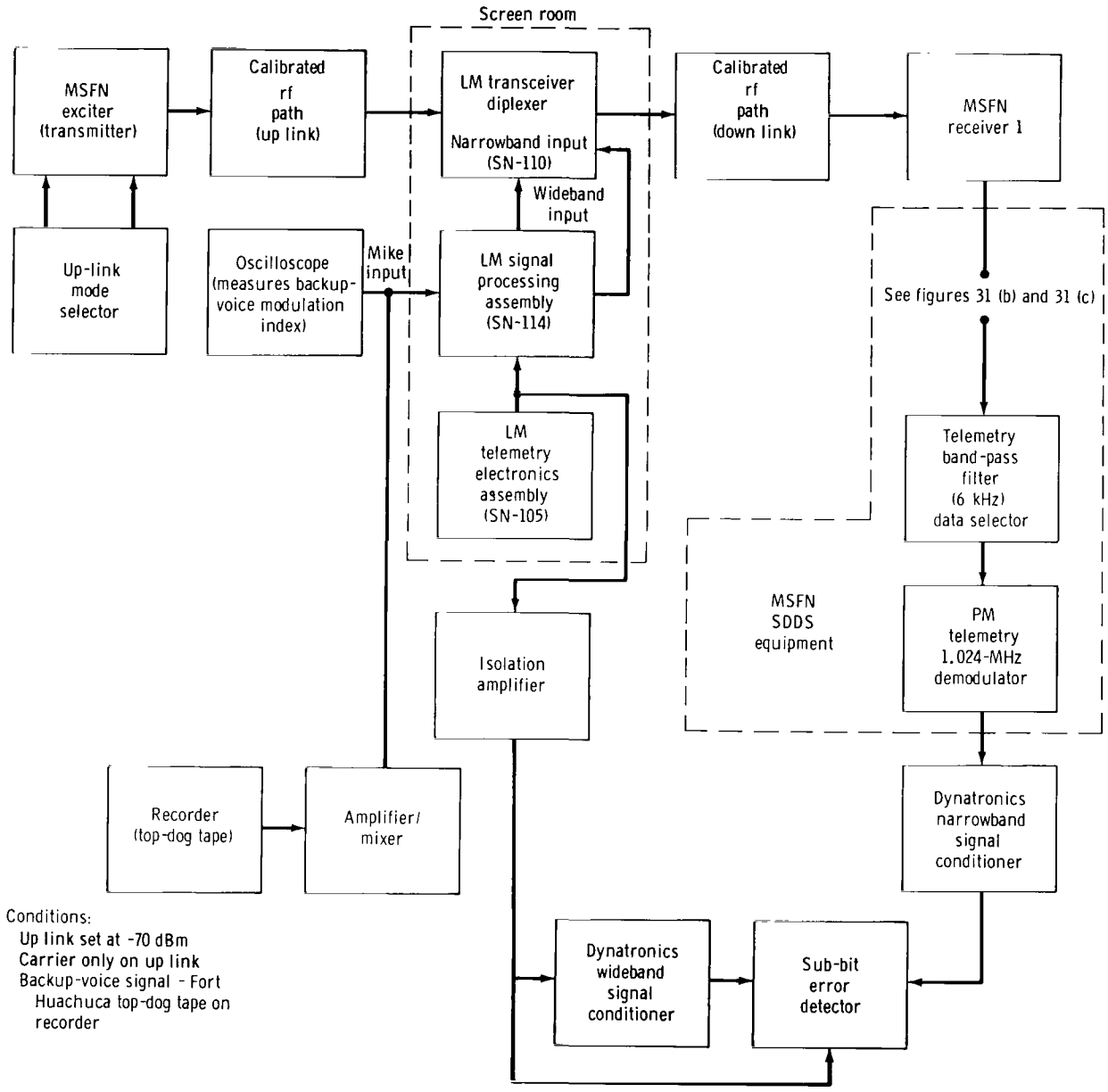

(a) Block diagram of test configuration.

Figure 31. - Lunar module test configurations for frequency-modulation detection, using crystal filters.

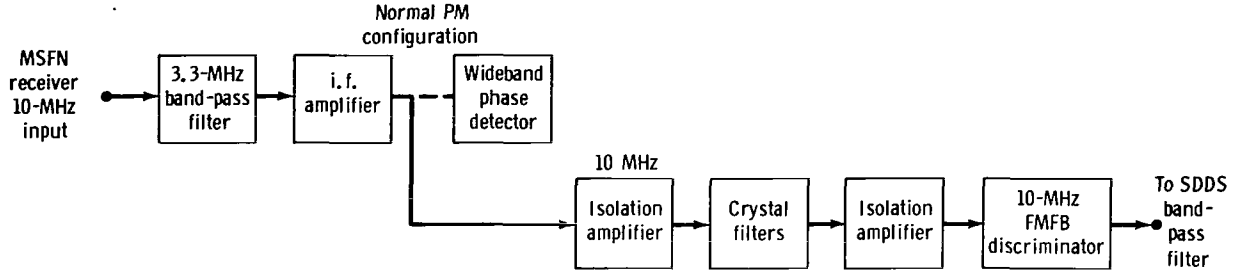

(b) Crystal filters with 10-megahertz frequency-modulation feedback discriminator.

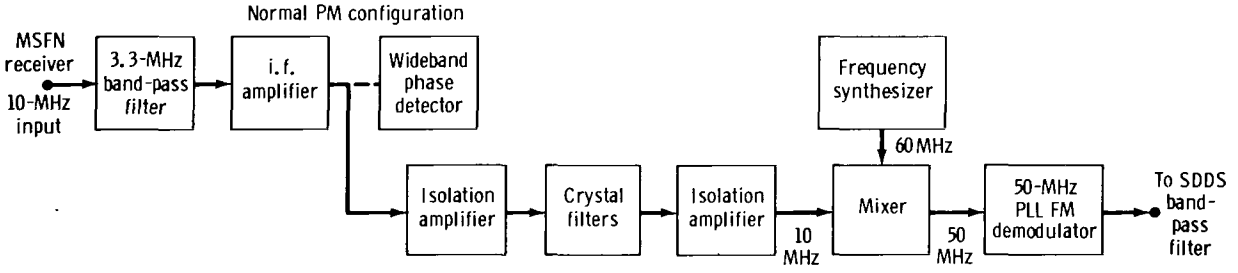

(c) Crystal filters with 50-megahertz PLL frequency-modulation demodulator.

Figure 31. - Concluded.

filters are connected between the output of the MSFN receiver and the input to the filter data selector (1.024-megahertz band-pass filter) preceding the telemetry-subcarrier demodulator. The 50-megahertz resonators are inserted in front of the MSFN FM demodulator. It was necessary to use wideband amplifiers to compensate for the insertion losses in the helical resonators and crystal filters. Although the insertion losses are excessive (a maximum of 45 decibels for the crystal filters), it is possible to reduce these losses to less than 10 decibels by modifying the filter design.

To determine the effects of the narrowband filtering and FM demodulation on the telemetry information, an 800-hertz square wave (corresponding to a periodic 101010 telemetry wave train at a bit rate of 1.6 kbps) was used to biphase-modulate the 1.024-megahertz telemetry subcarrier. Photographs of the demodulated telemetry waveform were taken at the output of a low-pass filter following the 1.024-megahertz subcarrier demodulator. The modulation indices used for these tests were 1.3- and 1.0-radian peaks for the telemetry and backup-voice signals, respectively. The fundamental frequency of the 800-hertz square wave (with backup voice present), when the signal is processed through the helical resonators and the crystal filters, is shown in figures 32 and 33. The degraded 800-hertz signal, using the present PM demodulator, has been shown previously in figure 11. The S-band rf level is -124.5 dBm, corresponding to the worst-case expected power level into the MSFN ground receiver. The crystal filters provide a better noise reduction when compared to the helical resonators (figs. 32 and 33). However, both configurations substantially reduce the backup-voice interference with the telemetry.

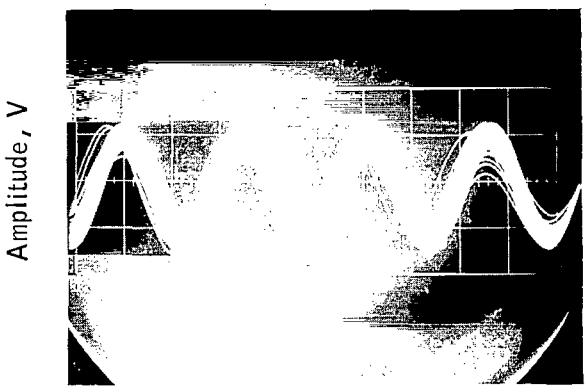

Figure 32. - Fundamental component of a 1.6-kbps PCM 101010 code, demodulated using the helical resonator filtering technique and the 50-megahertz PLL frequency-modulation demodulator (the backup-voice modulation index is 1.0-rad peak, and the radio-frequency level is -124.5 dBm).

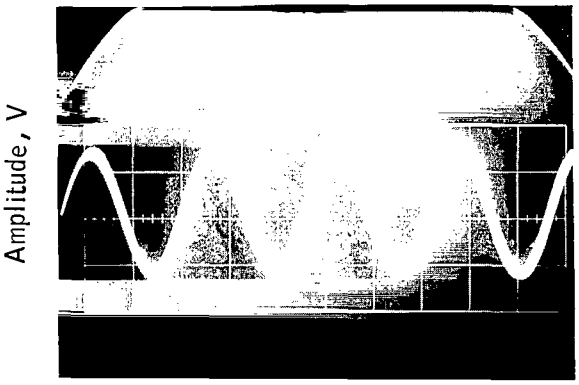

Figure 33. - Fundamental component of a 1.6-kbps PCM 101010 code, demodulated using the crystal filtering technique and the 50-megahertz PLL frequency-modulation demodulator (the backup-voice modulation index is 1.0-rad peak, and the radio-frequency level is -124.5 dBm).

Lunar module system tests. - This section presents the SNR and BER results for LM modes 4 and 8. The SNR measurements were made in the 6-kilohertz predetection bandwidth of the 1.024-megahertz subcarrier demodulator. These measurements were taken by using a wave analyzer to measure signal power with the noise present. A root-mean-square (rms) voltmeter measured noise when the 1.024-megahertz subcarrier was off. For all down-link tests, the up-link signal consisted of a carrier only, with a total-received power level at the LM receiver input of -70 dBm.

Lunar module mode 4 test results: The SNR data in the 1.024-megahertz subcarrier prefilter for LM mode 4, using FM detection with the helical resonators and with the crystal filters, are compared in figure 34. The helical resonator curve is degraded by 2 decibels because of a frequency misalinement in one of the resonators during the ESCL tests. This misalinement was not found until after the tests had been completed. The primary purpose of the resonator tests is to show that 51.2-kbps telemetry data can be processed through the composite band-pass filter. The crystal filter bandwidths are too narrow for 51.2-kbps telemetry.

The crystal filters provide an 8.0-decibel improvement in SNR over the helical resonators at the worst-case specified rf level of -124.5 dBm for the LM spacecraft at lunar distance. The FM threshold degradations are more pronounced with the helical resonators than with the crystals because of the difference in the ratio of the composite input filter bandwidths (252 kilohertz/23 kilohertz). However, by comparing the data taken with the MSFN wideband PM detector (curve C) with the data taken from the FM demodulation scheme using the crystal filters, the output SNR results were approximately the same at the -124.5 dBm rf level. But, the helical resonator curve is degraded by the FM threshold at the worst-case rf level.

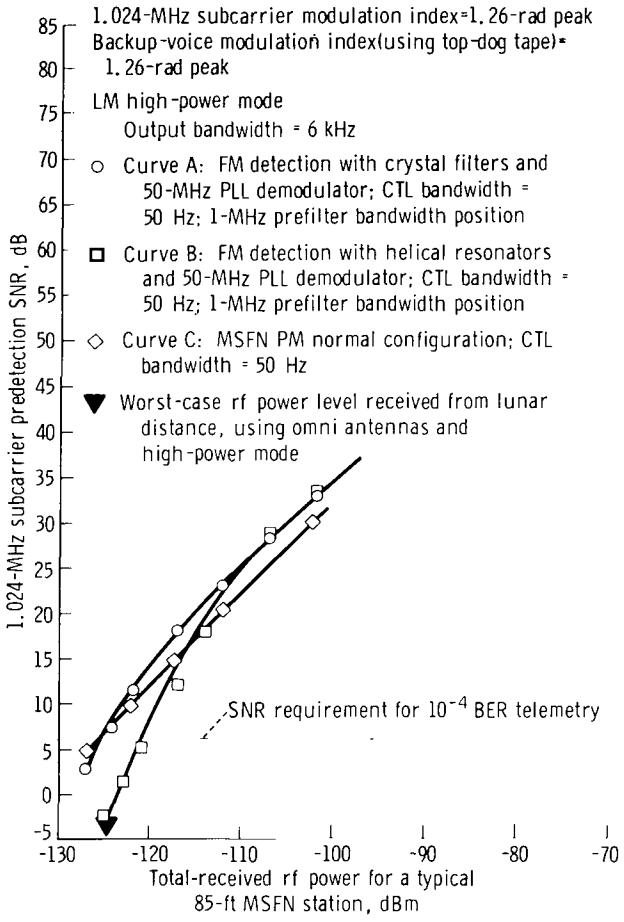

Figure 34. - Lunar module mode 4: 1.024-megahertz telemetry-subcarrier predetection SNR test results (test numbers TPET-021869-3 (curve A), TPET-021869-5 (curve B), and TPET-021069-1 (curve C)).

The LM mode 4 BER curves for 1.6-kbps telemetry are shown in figure 35 for the crystal filter and helical resonator configurations. The FM detection scheme with the narrowband prefilters produces significant improvement over the present MSFN PM detection system configured in the 700-hertz carrier loop position (curve F). Thus, the backup-voice interference with telemetry can be reduced greatly by linear detection using FM demodulation techniques. However, there is a 0.5-decibel degradation in telemetry

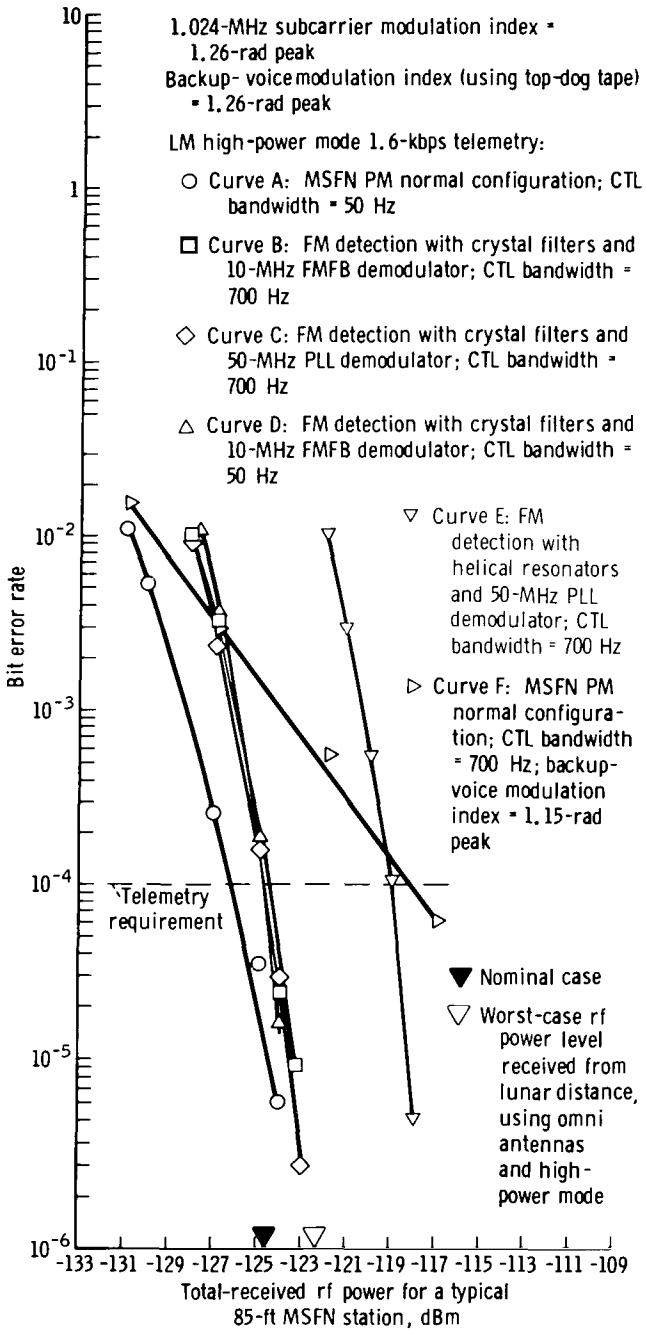

Figure 35. - Lunar module mode 4: bit error rate for 1.6-kbps telemetry (test numbers TPET-021369-2 (curve A), TPET-021769-9 (curve B), TPET-021869-4 (curve C), TPET-021769-8 (curve D), TPET 021869-7 (curve E), and TPET-021069-3 (curve F)).

performance at the -124.5 dBm rf level (using the FM demodulation technique) when compared to PM demodulation with the 50-hertz carrier loop configuration (curve A) for the modulation indices tested. Telemetry performance is not affected by the bandwidth switch positions (50 or 700 hertz) of the CTL when the FM demodulation technique is used. Curves B and D (fig. 35) represent data taken with the crystal filters and the FMFB demodulator when the CTL was in the 700- and 50-hertz bandwidth positions, respectively. Also, one test was made with the crystal filters preceding the MSFN FM demodulator. In this test (curve C), the 10-megahertz signal at the output of the crystal filters was heterodyned up to 50 megahertz and was inserted into the MSFN demodulator. By comparing the performance of the crystal filters used with the FMFB discriminator and with the MSFN demodulator, the BER curves for the two configurations are found to be identical (curves B and C). Henceforth, no distinction will be made as to which demodulator is used with the crystal filters. The helical resonator BER data (curve E) are degraded because of the aforementioned frequency misalinement in one of the resonators and because of the operation below FM threshold.

Lunar module mode 8 test results: The BER test results for 51.2-kbps telemetry for LM mode 8 are shown in figure 36. The FM detector with the helical resonators provides significant improvement over the unmodified MSFN PM demodulator for all rf power levels when using the 700-hertz carrier loop configuration. The resonator filtering technique shows improvement over the PM demodulator 50-hertz carrier loop configuration at the worst-case expected rf level of -102.3 dBm when using the LM steerable antenna. It should be noted that the 51.2-kbps biphase-modulated telemetry data pass through the 85-kilohertz predetection filters (helical resonators) of the 1.024-megahertz subcarrier ($f_{IF} \pm f_{TM}$) with little degradation. An optimization study on widening the predetection filter bandwidth to allow the telemetry data to pass with minimum degradation and reducing the predetection bandwidth to improve the FM threshold performance possibly could yield further BER improvements as a function of rf level.

Command and service module mode 8 test results. - The SNR tests for 1.6-kbps telemetry were performed, using the predetection 6-kilohertz filter bandwidth of the 1.024-megahertz subcarrier. By comparing the curves in figure 37 at the worst-case expected rf level of -123.1 dBm with the CSM omni antennas, the FM SNR data taken (using the crystal filters) are approximately the same as that for the PM data.

The BER curves for 1.6-kbps telemetry in CSM mode 8 are shown in figure 38. The BER data taken with the crystal filters are degraded by 1.0 to 1.5 decibels in comparison to the data taken with the unmodified MSFN PM detector with the 50-hertz carrier loop filter. However, the data with the unmodified MSFN detector in the 700-hertz loop-filter configuration are severely degraded. The amount of degradation for the unmodified 50-hertz loop-filter condition is negligible because the backup-voice modulation index (0.85-radian peak) is small. At the expected worst-case rf level of -123.1 dBm, using the CSM omni antennas at lunar distance, the 10^{-4} BER requirement is acheived easily by using FM demodulation with the crystal filters (700-hertz loop bandwidth) and by using PM demodulation with the unmodified MSFN phase detector (50-hertz loop bandwidth).

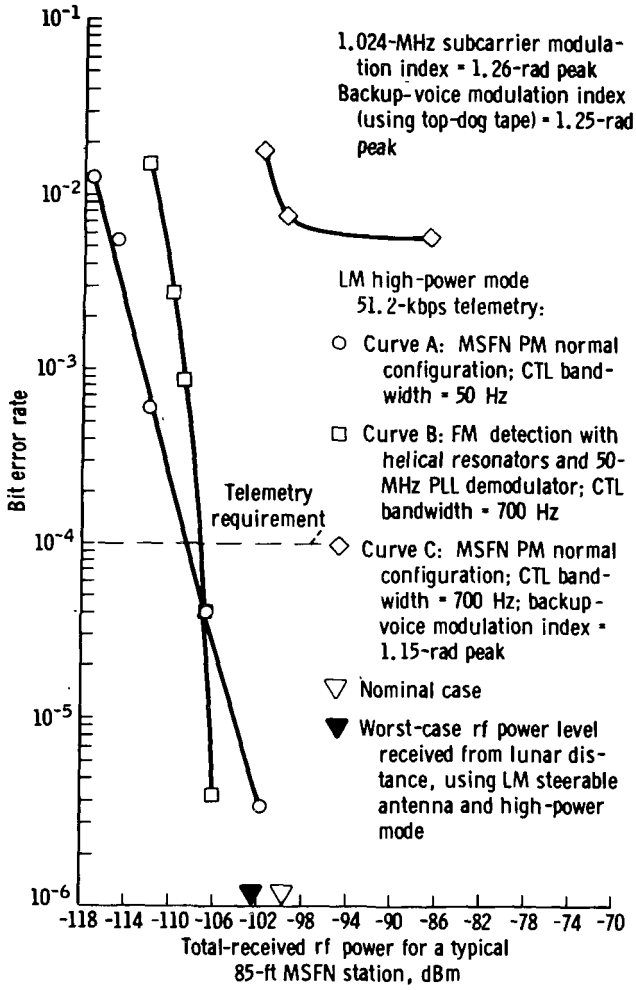

Figure 36.- Lunar module mode 8: bit error rate for 51.2-kbps telemetry (test numbers TPET-021369-4 (curve A), TPET-021869-8 (curve B), and TPET-021069-4 (curve C)).

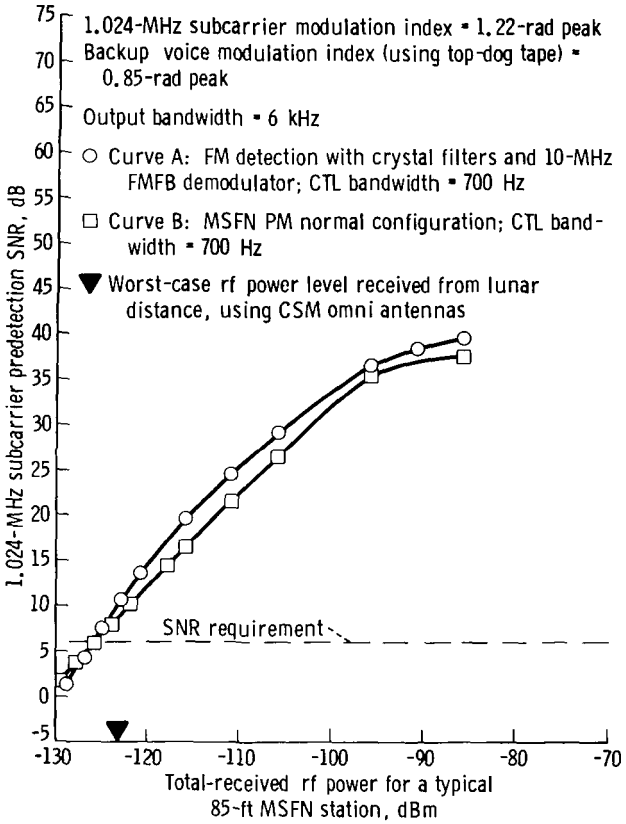

Figure 37.- Command and service module mode 8: 1.024-megahertz subcarrier predetection SNR in 6-kilohertz bandwidth (test numbers TPET-021969-5 (curve B) and TPET-022069-7 (curve A)).

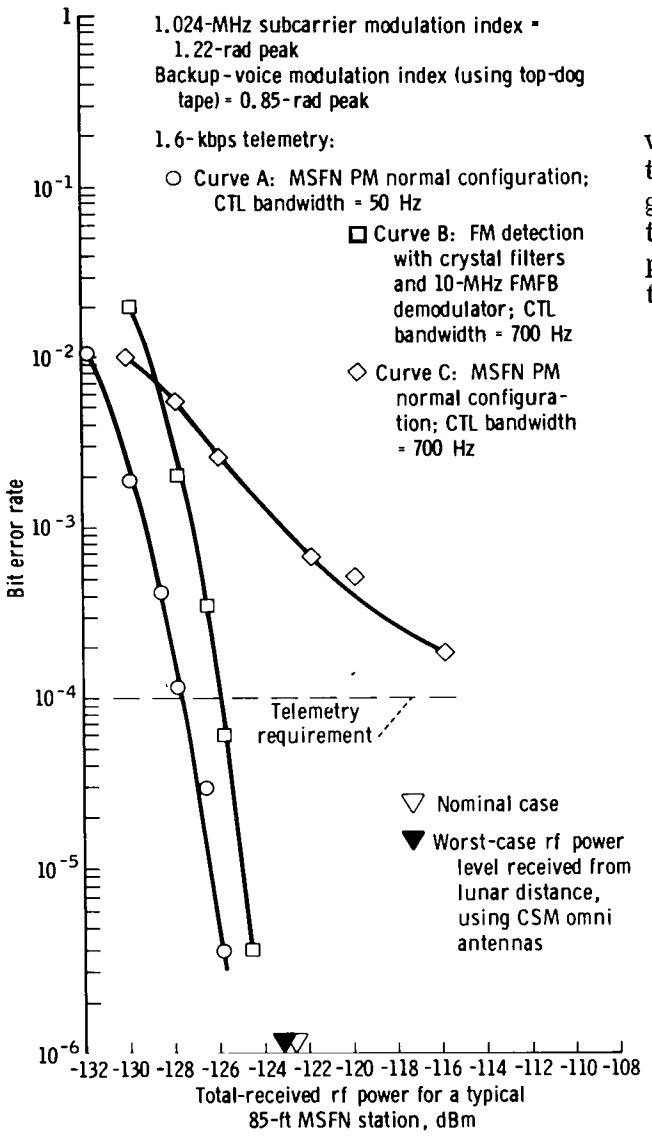

Figure 38. - Command and service module mode 8: bit error rate for 1.6-kbps telemetry (test numbers TPET-021969-7 (curve A), TPET-022069-8 (curve B), and TPET-021969-8 (curve C)).

Summary of Tests Conducted to Verify Telemetry Performance

A summary of the tests conducted to verify the telemetry performance, using the various demodulation techniques, is given in the following data. The tests show that the negative-feedback-loop technique provides better telemetry BER performance than does the FM detection method.

Spacecraft configuration (mode)	Modulation index, rad		CTL bandwidth, Hz	Telemetry bit rate, kbps	Demodulation technique	Total-received power required to achieve a 10^{-4} BER, dBm
	β_v	β_{TM}				
LM mode 4	1.15	1.26	50	1.6	Normal	-126.5
	1.15	1.26	50	1.6	Simplified phase cancellation	-126.7
	1.26	1.26	50	1.6	Normal	-126.0
	1.26	1.26	50	1.6	Crystal filter, FMFB demodulator	-124.5
	1.15	1.26	700	1.6	Normal	-118.2
	1.15	1.26	700	1.6	Simplified phase cancellation	-126.7
	1.26	1.26	700	1.6	Crystal filter, FMFB demodulator	-124.3
	1.26	1.26	700	1.6	Crystal filter, PLL demodulator	-124.5
	1.26	1.26	700	1.6	Helical resonators, PLL demodulator	-118.7
	1.3	1.26	700	1.6	Negative feedback	-125.0
	1.25	1.26	50	51.2	Normal	-108.5
	1.15	1.26	50	51.2	Negative feedback	-113
	1.15	1.26	700	51.2	Normal	Not possible to attain 10^{-4} BER
	1.15	1.26	700	51.2	Simplified phase cancellation	-113.5
LM mode 8	1.1	1.26	50	1.6	Normal	-126.8
	1.1	1.26	50	1.6	Negative feedback	-126.5
	1.1	1.26	700	1.6	Normal	-125.8
	1.1	1.26	700	1.6	Negative feedback	-126.5
	1.1	1.26	50	51.2	Normal	-112.6
	1.1	1.26	50	51.2	Negative feedback	-113.0
	1.25	1.26	50	51.2	Normal	-108.3
	1.25	1.26	50	51.2	Helical resonator, PLL demodulator	-107.3
	1.1	1.26	700	51.2	Normal	Not possible to attain 10^{-4} BER
	1.1	1.26	700	51.2	Negative feedback	-113.0
	1.25	1.26	700	51.2	Normal	Not possible to attain 10^{-4} BER
	1.25	1.26	700	51.2	Helical resonator, PLL demodulator	-107.3
CSM mode 8	.85	1.22	50	1.6	Normal	-127.7
	.85	1.22	50	1.6	Negative feedback	-127.7
	.85	1.22	700	1.6	Normal	-112.0
	.85	1.22	700	1.6	Negative feedback	-127.0
	.85	1.22	700	1.6	Crystal filter, FMFB demodulator	-125.7
	1.47	1.24	50	51.2	Normal	Not possible to attain 10^{-4} BER
	1.47	1.24	700	51.2	Negative feedback	-112.3

CONCLUSIONS AND RECOMMENDATIONS

Two different demodulation techniques have been analyzed as possible solutions to the modulation/demodulation compatibility problem in the Apollo communication system when voice (at baseband) and telemetry (modulated onto a subcarrier) are phase-modulated onto an S-band carrier. Both techniques provide a linear detection scheme without major modifications to the present Manned Space Flight Network demodulation system. One technique uses an external negative feedback loop which consists of a loop filter, an amplifier, a phase modulator, and the present phase-modulation phase detector. The other technique uses the present Manned Space Flight Network phase-lock-loop frequency-modulation demodulator preceded by a composite filter consisting of three high Q band-pass filters in parallel.

The experimental results indicate that both demodulation techniques will significantly reduce the backup-voice interference with telemetry. The voice signal, which is demodulated in the carrier tracking loop of the Manned Space Flight Network receiver, is not affected by either demodulation technique. The negative-feedback-loop technique provides better telemetry bit-error-rate performance than does the frequency-modulation detection method.

The simplified method of providing phase cancellation by using a voice-modulated quadrature reference to the wideband phase detector works satisfactorily for 1.6-kbps telemetry data rates. However, this method, which does not use a feedback loop, will not eliminate the voice interference with 51.2-kbps telemetry data. The demodulation techniques are summarized as follows.

Negative Feedback Loop

1. The negative-feedback-loop technique reduces backup-voice interference with 1.6- and 51.2-kbps telemetry data.

2. The technique reduces backup-voice interference with the 3.9-, 5.4-, 7.35-, 10.5-, and 14.5-kilohertz biomedical subcarriers.

3. The technique works with the present Manned Space Flight Network wideband phase detector. (No switching in the ground station is required at any time. The feedback loop would remain activated in the receiver for all modes, regardless of whether a baseband voice mode is transmitted.)

Frequency-Modulation Demodulation with Narrowband Predetection Filtering

1. This technique reduces the backup-voice interference with 1.6- and 51.2-kbps telemetry data. However, a frequency-modulation threshold problem exists when the demodulator prefilter bandwidth is enlarged to pass the 51.2-kbps data.

2. The technique works with the present Manned Space Flight Network carrier frequency demodulator. However, switching in and out of the prefilters would be

required to demodulate the normal command and service module and lunar module frequency-modulation modes unless additional Manned Space Flight Network frequency-modulation demodulators are provided. (Because the improved phase-lock-loop frequency-modulation demodulators are now being installed in the Manned Space Flight Network stations, the existing frequency-modulation demodulators could be available for use with the phase-modulation backup-voice modes.)

3. The composite filter should use crystal filters rather than helical resonators. The crystal filters have inherently narrow bandwidths (high Q) which may be varied, are simple to construct, and do not have the mechanical stability problems associated with the helical resonators.

4. It is not possible to detect the biomedical subcarriers of lunar module mode 8 with the frequency-modulation demodulators tested. The very small phase deviations associated with the biomedical subcarriers are not compatible with the existing Manned Space Flight Network frequency-modulation demodulators. Therefore, it is recommended that the negative feedback loop (consisting of a loop filter, amplifier, and phase modulator) be incorporated into the Manned Space Flight Network receivers to eliminate backup-voice interference with telemetry. The construction costs for the feedback loop should be minimal because no developmental work is required. It is recommended that efforts be made to incorporate these units into the Manned Space Flight Network receivers prior to the later Apollo lunar-landing missions.

Manned Spacecraft Center
National Aeronautics and Space Administration
Houston, Texas, December 24, 1969
914-50-40-06-72

REFERENCES

1. Webb, J. A.; and Downing, J. J.: A Study of Those USB Modulator and Demodulator Characteristics which Affect LM Modes PM 4 and PM 8. LEC Rept. No. 704002, July 1968.

2. Melton, R. E.: Design Specification MSFN Ground Equipment Unified S-Band RF Receiver/Exciter Subsystem. JPL DNR-1086-DSN-A, Feb. 1966.

3. Anon.: LM-MSFN S-Band System Signal Performance and Interface Specification. Grumman Aircraft Engineering Corporation, LSP-380-17A, Jan. 1969.

4. Gardner, Floyd M.: Phaselock Techniques. John Wiley & Sons, Inc., New York, 1966.

5. Haagen, G. V. Vander: The Electrical Tuning of Helical Resonators. The Microwave J., Aug. 1967, pp. 83-90.

6. Harton, Paul L.: A Comparison of Helical Resonator and Crystal Filters. LEC HASD 822226, Sept. 1968.

7. Zverev, A. I.; and Blinchikoff, H. J.: Realization of a Filter with Helical Components. IRE Transactions on Component Parts, Sept. 1961, pp. 99-110.

8. Macalpine, W. W.; and Schildknecht, R. O.: Coaxial Resonators with Helical Inner Conductors. Proceedings of IRE, Dec. 1959, pp. 2099-2105.

APPENDIX A

SYMBOLS

A	arbitrary value
$A(S)$	product of transfer functions, $K_2F_2(S)G_3H_3(S)$
$B(S)$	product of transfer functions, $G_2H_2(S)K_1F_1(S)G_1H_1(S)K_v$
B_{BR}	bit-rate bandwidth
B_{IF}	i.f. noise bandwidth
B_{IN}	input noise bandwidth
B_{PRED}	predetection filter noise bandwidth
C	crystal capacitance
C_0	junction capacitance for a reverse voltage of 1 volt
C_b	balance capacitance
C_h	holder capacitance
E_0	output voltage of MSFN phase detector
$E_{0_{TM}}$	output telemetry voltage
E_{RF}	rf voltage
E_r	maximum amplitude of quadrature reference voltage
e	output voltage
e_0	output voltage of filters
$\left(\frac{e_0}{\phi_i}\right)_{MOD}$	closed-loop transfer response for the modified MSFN carrier phase demodulator

$\left(\frac{e_0}{\phi_i}\right)_{UNMOD}$	closed-loop transfer response for the unmodified MSFN carrier phase demodulator
e_{D0}	output of phase detector
e_{IN}	input signal voltage
$e_r(t)$	instantaneous quadrature reference voltage
$F(S)$	loop-filter-response function
$F_1(S)$	feedback-loop-filter response
$F_2(S)$	phase-shift network response
$F_I(S)$	transfer function of an RC integrator
$F_L(S)$	CTL filter response
f_0	center frequency
f_c	carrier frequency
f_{c1}	center frequency of band-pass filter 1
f_{c2}	center frequency of band-pass filter 2
f_{c3}	center frequency of band-pass filter 3
f_{IF}	i.f. center frequency
f_{TM}	telemetry-subcarrier frequency
$f_v(t)$	voice signal time waveform
$f'_v(t)$	differentiated voice signal
G_1	feedback-loop amplifier gain
G_2	video amplifier gain

G_3	modification-module-output amplifier gain
$H_1(S)$	feedback-loop amplifier response
$H_2(S)$	video amplifier frequency response
$H_3(S)$	modification-module-output amplifier response
I_1, I_2	loop currents
$J_{0, 1, 2}$	Bessel functions
j	imaginary quantity
K	CTL gain, $K_0K_LK_d$
K_0	CTL VCO sensitivity
K_1	feedback-loop-filter constant
K_2	phase-shift network constant
K_d	CTL phase-detector sensitivity
K_L	CTL filter constant
K_m	wideband phase-detector sensitivity
K_v	phase-modulator sensitivity
k	Boltzmann's constant
L	inductance
L_D	assumed degradation of the decommutation equipment for a matched filter detector, dB
L_{LIM}	limiter degradation
m(t)	switching function, ± 1
P_N	noise power

P_r	total-received power
P_S	signal power
P_{tr}	total-received power at receiver input
Q_1	Q associated with band-pass filter 1
Q_2	Q associated with band-pass filter 2
Q_3	Q associated with band-pass filter 3
R	resistance
R_1, R_2	load resistances
S	differential operator
$(SNR)_{IF}$	i.f. SNR
$(SNR)_{PRED}$	telemetry predetection SNR
$(SNR)_T$	theoretical SNR in a bit rate bandwidth for a given BER, dB
T_D	time delay
T_{D1}	time delay associated with band-pass filter 1
T_{D2}	time delay associated with band-pass filter 2
T_{D3}	time delay associated with band-pass filter 3
T_S	system temperature
t	time variable
t_i	transition time
V	voltage
V_0	output voltage of phase shifter

V_a	lower input voltage to subtracter
V_b	upper input voltage to subtracter
V_d	phase-detector output voltage
V_{FO}	loop filter output voltage
V_I	integrated output voltage
V_i	input voltage of phase shifter
$V_I(S)$	integrated output voltage (frequency domain)
X	reactance
X_c	capacitive reactance
Z_b	impedance of balance capacitor
Z_c	impedance of crystal and holder
$\beta_{3.9}$	3.9-kilohertz biomedical-subcarrier modulation index
$\beta_{5.4}$	5.4-kilohertz biomedical-subcarrier modulation index
$\beta_{7.35}$	7.35-kilohertz biomedical-subcarrier modulation index
$\beta_{10.5}$	10.5-kilohertz biomedical-subcarrier modulation index
$\beta_{14.5}$	14.5-kilohertz biomedical-subcarrier modulation index
β_{TM}	telemetry-subcarrier modulation index
β_v	baseband voice modulation index
Δf_1	difference between instantaneous modulating frequency within the filter passband and the center frequency of band-pass filter 1, $\Delta f_1 = f_M - f_{c1}$
Δf_2	difference between instantaneous modulating frequency within the filter passband and the center frequency of band-pass filter 2, $\Delta f_2 = f_M - f_{c2}$

Δf_3	difference between instantaneous modulating frequency within the filter passband and the center frequency of band-pass filter 3, $\Delta f_3 = f_M - f_{c3}$
$\delta(t_i)$	impulse function occurring at each telemetry bit-transition time t_i
ζ	loop damping constant
θ	phase
$\theta_{0, 1, 2}$	VCO output signal phase
θ_{c1}	phase shift at center frequency of band-pass filter 1 caused by external phase delays
θ_{c2}	phase shift at center frequency of band-pass filter 2 caused by external phase delays
θ_{c3}	phase shift at center frequency of band-pass filter 3 caused by external phase delays
θ_{D1}	phase shift through path of band-pass filter 1
θ_{D2}	phase shift through path of band-pass filter 2
θ_{D3}	phase shift through path of band-pass filter 3
θ_{DIF}	difference in phase at upper and lower telemetry sidebands in a conventional wideband filter
θ_e	phase error
$\frac{\theta_e}{\theta_i}$	phase error response
θ_i	input signal phase
$\theta_i(t)$	input modulation time expression
ρ_v	peak/rms ratio for clipped voice signal
ϕ_0	crystal oscillator phase reference
ϕ_{CTL}	CTL VCO output phase

ϕ_i	received rf signal phase
ϕ'_i	wideband phase-detector i.f. input phase
ϕ_m	modification-module output phase
ϕ_r	carrier-phase-demodulator output phase
$\phi_{TM}(t)$	telemetry-subcarrier phase modulation
$\phi_v(t)$	baseband voice phase modulation
ω	frequency
ω_c	carrier radian frequency, rad/sec
ω_I	integrator cut-off frequency
ω_n	loop natural frequency, rad/sec
ω_{TM}	telemetry-subcarrier radian frequency, rad/sec
ω_v	baseband voice radian frequency, rad/sec

APPENDIX B

LINEAR MODEL ANALYSIS OF THE CARRIER PHASE DEMODULATOR WITH NEGATIVE FEEDBACK

Consideration of the linearized model for the carrier phase demodulator with the negative feedback loop (fig. 5) leads to the closed-loop transfer response for the system.

By using Laplace transform notation

$$e_0 = e\left[G_2H_2(S)\right] \tag{B1}$$

where

$$e = K_m\left[\phi_i' - K_2F_2(S)\phi_m\right] \tag{B2}$$

and

$$\phi_m = G_3H_3(S)\left[\phi_0 + e_0K_1F_1(S)G_1H_1(S)K_v\right] \tag{B3}$$

Substitute equation (B3) into equation (B2) to obtain

$$e = K_m\left\{\phi_i' - K_2F_2(S)G_3H_3(S)\cdot\left[\phi_0 + e_0K_1F_1(S)G_1H_1(S)K_v\right]\right\} \tag{B4}$$

Substitute equation (B1) into equation (B4) to obtain

$$e = K_m\left\{\phi_i' - K_2F_2(S)G_3H_3(S)\cdot\left[\phi_0 + eG_2H_2(S)K_1F_1(S)G_1H_1(S)K_v\right]\right\} \tag{B5}$$

For convenience of notation, let

$$A(S) = K_2 F_2(S) G_3 H_3(S) \tag{B6}$$

and

$$B(S) = G_2 H_2(S) K_1 F_1(S) G_1 H_1(S) K_v \tag{B7}$$

Then, by using the above notation in equation (B5)

$$\begin{aligned} e &= K_m \left\{ \phi_i' - A(S) \cdot \left[\phi_0 + eB(S) \right] \right\} \\ &= K_m \left\{ \phi_i' - A(S)\phi_0 - A(S)B(S)e \right\} \\ &= K_m \frac{\left[\phi_i' - A(S)\phi_0 \right]}{1 + K_m A(S)B(S)} \end{aligned} \tag{B8}$$

Rearranging equation (B1) yields

$$e = \frac{e_0}{G_2 H_2(S)} \tag{B9}$$

which, when equated to equation (B8), gives

$$\frac{e_0}{\phi_i' - A(S)\phi_0} = \frac{K_m G_2 H_2(S)}{1 + K_m A(S)B(S)} \tag{B10}$$

Divide the numerator and denominator of the left-hand side of equation (B10) by ϕ_i' to obtain

$$\frac{\frac{e_0}{\phi_i'}}{1 - A(S)\frac{\phi_0}{\phi_i'}} = \frac{K_m G_2 H_2(S)}{1 + K_m A(S)B(S)} \tag{B11}$$

or

$$\frac{e_0}{\phi_i'} = \frac{K_m G_2 H_2(S)}{1 + K_m A(S)B(S)} \left[1 - A(S)\frac{\phi_0}{\phi_i'}\right] \tag{B12}$$

Equation (B12) is the closed-loop transfer response for the system e_0/ϕ_i', in terms of ϕ_0/ϕ_i'.

The representation of the linear model of the CTL is shown in figure 5. From the linear model, a transfer response e_0/ϕ_i can be developed

Again, use Laplace transform notation to obtain

$$\phi_i' = \phi_i - \phi_{CTL} \tag{B13}$$

where

$$\phi_{CTL} = \frac{96K_0}{S} K_L F_L(S) V_d \tag{B14}$$

and

$$V_d = K_d\left(\phi_i' - \phi_0\right) \tag{B15}$$

After substituting equations (B14) and (B15) into equation (B13)

$$\phi_i' = \phi_i - \frac{96K_0}{S} K_L F_L(S) K_d (\phi_i' - \phi_0) \tag{B16}$$

By letting $K \equiv 96K_0K_LK_d$ (where K is the gain of the CTL), equation (B16) can be rewritten as follows.

$$\phi_i' \left[1 + \frac{KF_L(S)}{S}\right] = \phi_i + \frac{KF_L(S)}{S} \phi_0 \tag{B17}$$

By substituting equation (B17) into equation (B12) (closed-loop transfer function), the transfer characteristic for the modified system (fig. B-1) can be written as follows.

$$\frac{e_0}{\phi_i} = \frac{K_m G_2 H_2(S)}{1 + K_m A(S) B(S)} \left[\frac{S}{S + KF_L(S)} + \frac{KF_L(S)}{S + KF_L(S)} \frac{\phi_0}{\phi_i} - \frac{A(S)\phi_0}{\phi_i}\right] \tag{B18}$$

where $A(S) = K_2 F_2(S) G_3 H_3(S)$ and $B(S) = G_2 H_2(S) K_1 F_1(S) G_1 H_1(S) K_v$. Equation (B18) is the response of the carrier phase demodulator with the negative feedback loop.

When the negative feedback loop is not used around the wideband phase detector, then equation (B18) reduces to the response for the carrier phase demodulator without modification. This condition is satisfied mathematically by setting the loop-filter response $K_1 F_1(S)$ equal to zero and by setting the rf amplifier response $G_3 H_3(S)$ equal to unity. Then, the phase reference ϕ_0 is connected directly to the phase-shift network $K_2 F_2(S)$. Under these conditions, equation (B18) reduces to

$$\frac{e_0}{\phi_i} = K_m G_2 H_2(S) \left[\frac{S}{S + KF_L(S)} + \frac{KF_L(S)}{S + KF_L(S)} \frac{\phi_0}{\phi_i} - K_2 F_2(S) \frac{\phi_0}{\phi_i}\right] \tag{B19}$$

Equation (B19) is the transfer characteristic for the unmodified carrier phase demodulator.

Normalizing the modified demodulator response to the unmodified demodulator response and making the restriction that $G_3H_3(S) = 1$ yields

$$\frac{\left(\frac{e_0}{\phi_i}\right)_{MOD}}{\left(\frac{e_0}{\phi_i}\right)_{UNMOD}} = \frac{1}{1 + K_m K_2 F_2(S) B(S)} \tag{B20}$$

where $K_m K_2 F_2(S) B(S)$ is the feedback factor. The experimental curve resulting from normalizing the experimental modified demodulator response curve to the experimental unmodified demodulator response curve is shown in figure B-1. This experimentation

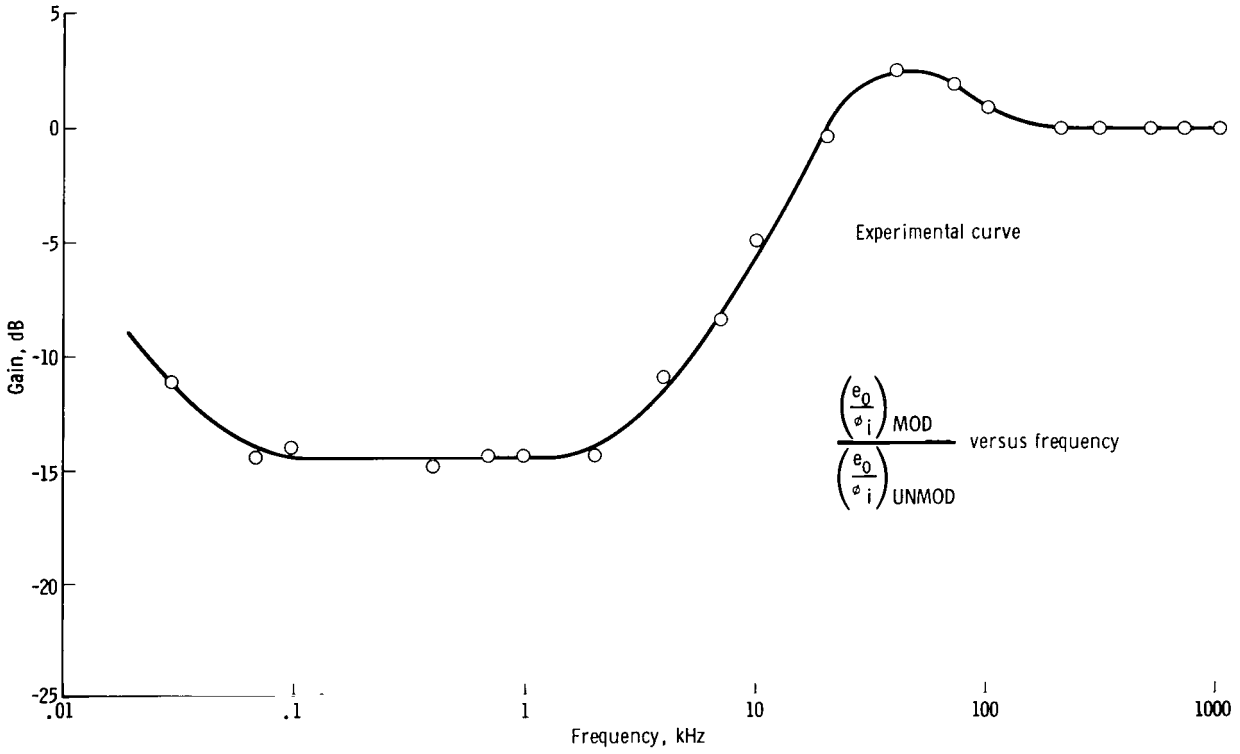

Figure B-1. - Frequency response curve for the carrier phase demodulator engineering model implemented with the modification module.

was performed on the carrier phase-demodulator engineering model when implemented with the modification module. Baseband voice frequencies will be attenuated by 14.5 decibels, but frequencies greater than 200 kilohertz will remain unaffected (fig. B-1). By assuming a voltage signal reduction of 14.5 decibels, the feedback factor is

$$1 + K_m K_2 F_2(S) B(S) = 5.31(14.5\ \text{dB}) \tag{B21}$$

and

$$K_m K_2 F_2(S) B(S) = 4.31(12.7\ \text{dB}) \tag{B22}$$

APPENDIX C

VOLTAGE-CONTROLLED PHASE SHIFTER

By W. B. Warren
TRW Systems Group
Houston, Texas

The following material describes various voltage-controlled phase-shifter circuit designs. The basic circuit of a voltage-controlled phase shifter is shown in figure C-1.

The lower input voltage to the subtracter is V_a, where

$$V_a = \left(\frac{R}{R + jX}\right)V_i \qquad \text{(C1)}$$

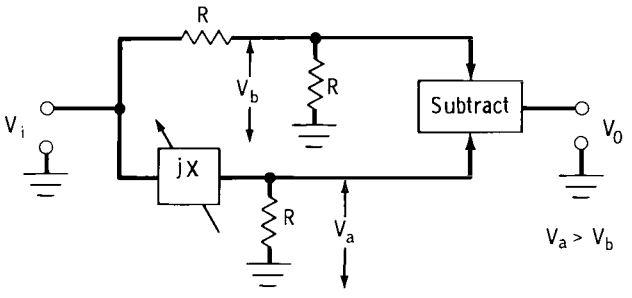

Figure C-1. - Basic circuit of a voltage-controlled phase shifter.

The upper input voltage to the subtracter is V_b, where

$$V_b = \frac{R}{2R}V_i = \frac{V_i}{2} \qquad \text{(C2)}$$

The output voltage from the subtracter is V_0, and

$$V_0 = V_a - V_b = \left(\frac{R}{R + jX} - \frac{1}{2}\right)V_i = \left[\frac{2R - R - jX}{2(R + jX)}\right]V_i$$

$$= \frac{R - jX}{2(R + jX)}V_i = \frac{V_i}{2}\frac{|R - jX|}{|R + jX|}\frac{\angle \tan^{-1}\left(\frac{-X}{R}\right)}{\angle \tan^{-1}\left(\frac{X}{R}\right)} \qquad \text{(C3)}$$

$$= \frac{V_i}{2}\angle 2 \tan^{-1}\left(\frac{-X}{R}\right)$$

because

$$-\tan^{-1}(X/R) = \tan^{-1}(-X/R)$$

The magnitude of the output voltage V_0 is independent of the value of X or R. The phase shift of V_0 with respect to V_i is

$$\theta = 2 \tan^{-1}\left(\frac{-X}{R}\right) \tag{C4}$$

Consequently, variation of the reactance X will produce a variation of θ but no variation in the output amplitude of V_0.

The variable X can be realized through the use of a voltage variable capacitance diode or varactor diode. The variation of capacitance with voltage for a typical varactor diode is

$$C = C_0 V^{-1/2} \tag{C5}$$

which, for X_c, gives

$$X_c = \frac{1}{\omega C} = \frac{1}{\omega C_0 V^{-1/2}} = \frac{V^{1/2}}{\omega C_0} \tag{C6}$$

Substitute X_c for X in equation (C4) to obtain

$$\theta = -2 \tan^{-1} \frac{\sqrt{V}}{\omega C_0 R} \tag{C7}$$

A differential amplifier can perform the necessary subtraction as well as supply the 6-decibel gain required to compensate for the loss through the phase shifter. A typical arrangement is shown in figure C-2.

An improvement in sensitivity can be gained by resonating the variable capacitor in the middle of its range at the operating frequency. A small change in capacitance will produce large changes in reactance as the resonant frequency of the circuit is varied on either side of resonance. The use of the resonant circuit to increase the slope of the phase shift versus control voltage curve is outlined in figure C-3.

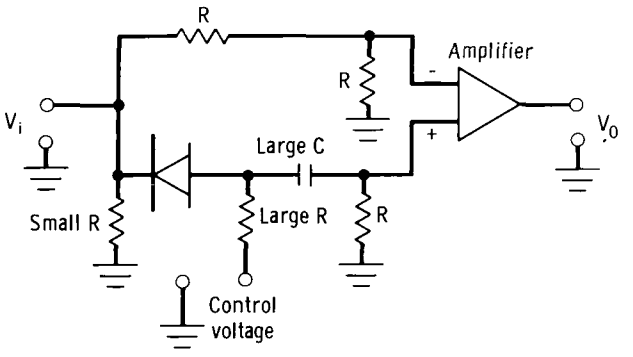

Figure C-2. - Voltage-controlled phase shifter with varactor and differential amplifier.

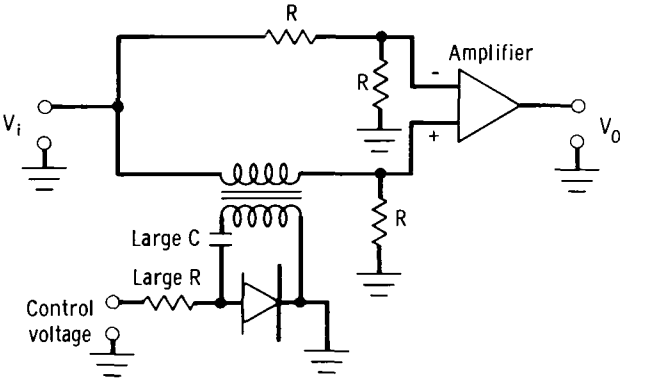

Figure C-3.- Transformer coupling to scale the reactance (primary inductance of the transformer resonates with the varactor at the operating frequency with nominal control voltage applied).

With circuits of the type shown in figure C-2, it is possible that the range of reactance variation may not be sufficient to give a wide range of phase shift. For example, to obtain a 180° phase-shift range, the reactance should vary from +R to -R. From equation (C4)

$$\left.\begin{aligned} \theta_1 &= 2\tan^{-1}\left(\frac{-X_1}{R}\right) = 2\tan^{-1}\left(\frac{+R}{R}\right) = +90^\circ \\ \theta_2 &= 2\tan^{-1}\left(\frac{-X_2}{R}\right) = 2\tan^{-1}\left(\frac{-R}{R}\right) = -90^\circ \\ \theta_1 - \theta_2 &= +90^\circ - (-90^\circ) = 180^\circ \end{aligned}\right\} \qquad \text{(C8)}$$

where $X_1 = -R$ and $X_2 = +R$. The proper range of X can be obtained by coupling to the tuned circuit with a transformer (fig. C-3). If a large range of $\Delta\theta$ is required, phase shifters can be used in cascade. For example, two shifters (each supplying a $\Delta\theta$ of 180°) could be used to give an overall 360° phase range.

The voltage-controlled phase shifter in the modification module uses a slight variation of the circuit shown in figure C-3. Two varactor diodes are used in place of the one varactor. The resulting phase modulator has the 10-megahertz phase characteristic given in figure C-4. The phase shifter has a symmetrical phase characteristic and provides a linear phase shift of ±40°. The modulator is capable of a ±140° total phase swing.

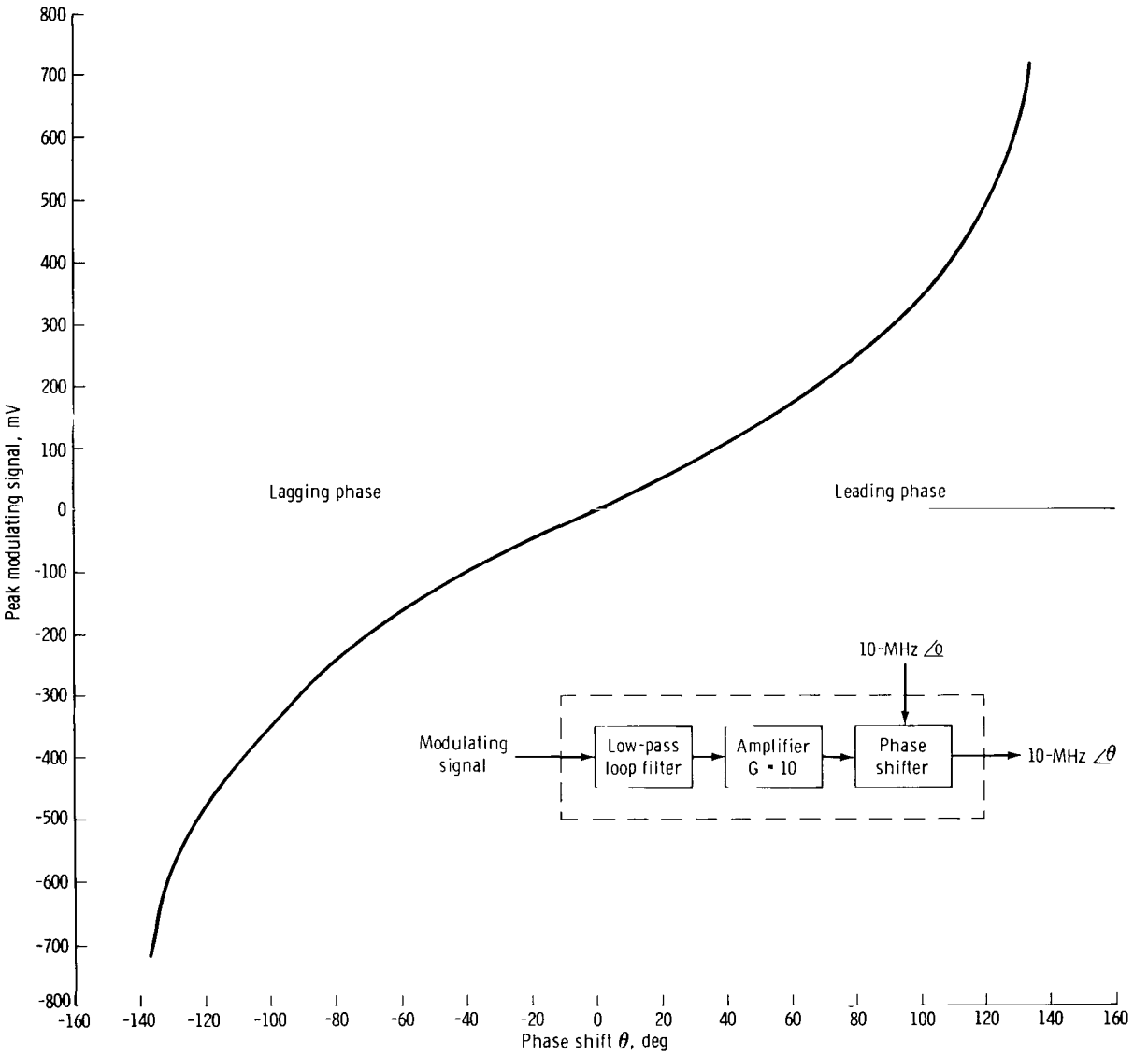

Figure C-4. - Ten-megahertz phase-modulator characteristic.

APPENDIX D

APOLLO TELEMETRY MATHEMATICAL MODELS

Theoretical performance of the PM telemetry channel in the MSFN receiver is determined by tne equations given in the following discussion for LM modes 4 and 8 and CSM mode 8. Telemetry performance is predicted in terms of the received telemetry subcarrier SNR at the output of a telemetry predetection filter and the probability of bit errors in the demodulated PCM wave train. Both telemetry SNR and BER predictions are calculated as a function of total-received power at the MSFN receiver input.

Telemetry Predetection SNR Mathematical Model

$$(SNR)_{PRED} = \frac{P_S}{P_N}$$

$$= \frac{P_r 2J_1^2(\beta_{TM}) \cos^2\left(\frac{\beta_v}{\rho_v}\right) J_0^2(\beta_{14.5}) J_0^2(\beta_{10.5}) J_0^2(\beta_{7.35}) J_0^2(\beta_{5.4}) J_0^2(\beta_{3.9}) L_{LIM}}{kT_S B_{PRED}} \qquad \text{(D1)}$$

where $(SNR)_{PRED}$ = telemetry predetection SNR, dB

P_S = signal power

P_N = noise power

P_r = total-received power

β_{TM} = telemetry-subcarrier modulation index

β_v = baseband voice modulation index

ρ_v = peak/rms ratio for clipped voice signal

$\beta_{14.5}$ = 14.5-kilohertz subcarrier modulation index

$\beta_{10.5}$ = 10.5-kilohertz subcarrier modulation index

$\beta_{7.35}$ = 7.35-kilohertz subcarrier modulation index

$\beta_{5.4}$ = 5.4-kilohertz subcarrier modulation index

$\beta_{3.9}$ = 3.9-kilohertz subcarrier modulation index

L_{LIM} = limiter degradation

k = Boltzmann's constant

T_S = receiver system temperature referenced to receiver input

B_{PRED} = predetection filter noise bandwidth, Hz

Telemetry BER Mathematical Model

The telemetry predetection SNR (in decibels) required for a given BER is computed from equation (D2).

$$(SNR)_{PRED} = (SNR)_T + 10 \log_{10}\left(\frac{B_{BR}}{B_{PRED}}\right) + L_D \qquad \text{(D2)}$$

where $(SNR)_T$ = theoretical SNR (in decibels) in a bit-rate bandwidth for a given BER

B_{BR} = bit-rate bandwidth, Hz

L_D = assumed degradation (in decibels) of the decommutation equipment for a matched filter detector

The values of $(SNR)_T$ for given BER are plotted in figure D-1. To obtain BER values as a function of total-received power, the calculated values of $(SNR)_{PRED}$ in equation (D2) are translated to values of P_r by using equation (D1).

Ground-Station Parameters

Ground-station parameters used to calculate theoretical telemetry performance for this report are listed as follows.

1. For the ESCL ground station, L_D is 2.0 decibels for 1.6- and 51.2-kbps telemetry.

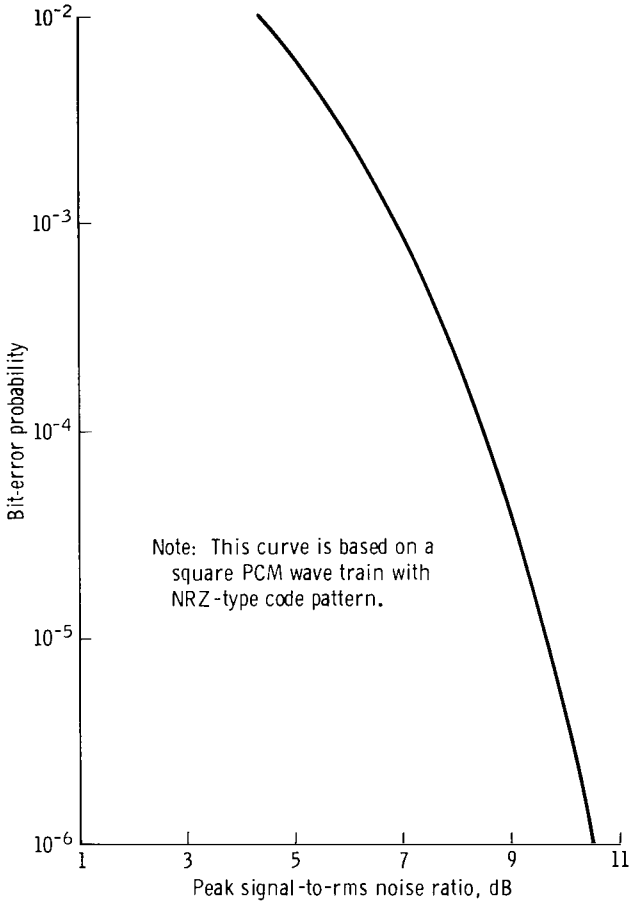

Figure D-1.- Theoretical bit-error probability versus peak signal-to-rms noise ratio in a bandwidth equal to bit rate.

2. B_{BR} is 1.6 kilohertz for 1.6-kbps telemetry and 51.2 kilohertz for 51.2-kbps telemetry.

3. B_{PRED} is 6.7 kilohertz for 1.6-kbps telemetry and 177 kilohertz for 51.2-kbps telemetry.

4. $(SNR)_T$ — See figure D-1.

5. T_S is 209° Kelvin for an MSFN ground station. (The ESCL experimental data have been transposed by 10 decibels in rf level to represent the system temperature T_S for an 85-foot station with a moon-at-zenith antenna viewing condition.)

6. k is $1.38 \times 10^{-23} \frac{W}{Hz \cdot {}^\circ Kelvin}$

7. L_{LIM} is calculated as a function of the 10-megahertz i.f. SNR. The 10-megahertz i.f. SNR is defined as $(SNR)_{IF} = P_r/kT_SB_{IF}$ where B_{IF} is the i.f. noise bandwidth, which is approximately 4 megahertz. The limiter degradation is $L_{LIM} = \pi/4$ for $(SNR)_{IF} < 0.035$, $L_{LIM} = 0.68(SNR)_{IF} + 0.76$ for $0.035 < (SNR)_{IF} < 0.35$, and $L_{LIM} = 1$ for $(SNR)_{IF} > 0.35$. The parameter values for the modulation indices are specified in the report text on the measured curves. Thus, $\rho_v = 1.77$ (empirically derived) for LM mode 4 and CSM mode 8 (20-decibel clipping) and $\rho_v = 5.3$ for LM mode 8 (0-decibel clipping).

APPENDIX E

TWO THEORETICAL ASPECTS OF FREQUENCY-MODULATION DETECTION OF THE PHASE-MODULATION TELEMETRY SIGNAL

Effects of Parallel Filtering on a Phase-Modulated Signal

The phasing effects of three parallel band-pass filters on an i.f. carrier phase-modulated with a baseband voice signal and a 1.024-megahertz telemetry subcarrier will be considered. The band-pass filters (fig. E-1) are centered at the carrier frequency f_c and the upper and lower subcarrier sideband frequencies $f_c \pm f_{TM}$. Each signal path has a high-Q narrowband filter with an associated time delay T_D. The outputs from each path are summed and routed to the input of the FM demodulator. The analysis in this section is based upon the following two assumptions.

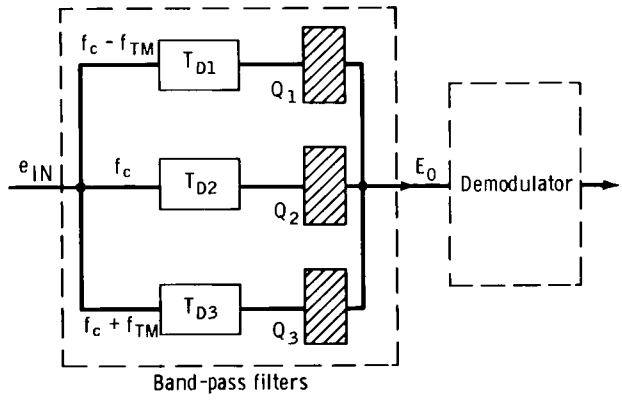

Figure E-1. - Band-pass filter configuration.

1. There is complete isolation between each path.

2. The output signal from each signal path has the same amplitude. Let the input signal e_{IN} be represented by

$$e_{IN} = A \sin \left[\omega_c t + \phi_v(t) + \phi_{TM}(t)\right] \tag{E1}$$

where

$$\phi_v(t) = \beta_v f_v(t) \tag{E2}$$

is the baseband voice signal and

$$\phi_{TM}(t) = \beta_{TM} \sin\left(\omega_{TM} t \pm \pi/2\right) \tag{E3}$$

is the telemetry signal. Equation (E1) can be expanded by using trigonometric identities as follows

$$e_{IN} = A \sin \omega_c t\left[\cos \phi_v(t)\cos \phi_{TM}(t) - \sin \phi_v(t)\sin \phi_{TM}(t)\right] + A \cos \omega_c t\left[\sin \phi_v(t)\cos \phi_{TM}(t) + \cos \phi_v(t)\sin \phi_{TM}(t)\right] \quad \text{(E4)}$$

By substituting equations (E2) and (E3) into equation (E4) and by rewriting in terms of Bessel functions, the input voltage is determined to be

$$e_{IN} = A \sin \omega_c t\left\{\cos\left[\beta_v f_v(t)\right]\left[J_0(\beta_{TM}) + 2\sum_{n=1}^{n=\infty} J_{2n}(\beta_{TM})\cos 2n\left(\omega_{TM}t \pm \frac{\pi}{2}\right)\right]\right.$$
$$\left. - \sin\left[\beta_v f_v(t)\right] 2\sum_{n=1}^{n=\infty} J_{2n-1}(\beta_{TM})\sin\left[(2n-1)\left(\omega_{TM}t \pm \frac{\pi}{2}\right)\right]\right\}$$
$$+ A \cos \omega_c t\left\{\sin\left[\beta_v f_v(t)\right]\left[J_0(\beta_{TM}) + 2\sum_{n=1}^{n=\infty} J_{2n}(\beta_{TM})\cos 2n\left(\omega_{TM}t \pm \frac{\pi}{2}\right)\right]\right.$$
$$\left. + \cos\left[\beta_v f_v(t)\right] 2\sum_{n=1}^{n=\infty} J_{2n-1}(\beta_{TM})\sin\left[(2n-1)\left(\omega_{TM}t \pm \frac{\pi}{2}\right)\right]\right\} \quad \text{(E5)}$$

Equation (E5) is the input voltage to the three band-pass filters. The input signal includes the carrier and the sum and difference frequencies of the baseband voice and telemetry subcarrier.

The effects of the phase characteristics of the band-pass filters on the input signal components now can be considered. The phase and amplitude characteristics of the high-Q band-pass filters are shown in figure E-2.

The 3-decibel bandwidth of a particular filter is related to the center frequency and the Q of the filter by the expression $BW_{3dB} = f_{center}/Q$.

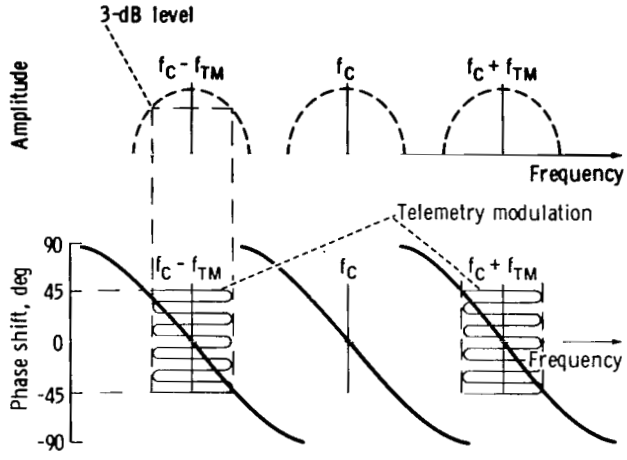

Figure E-2. - Amplitude and phase characteristics of three parallel band-pass filters.

If it is assumed that the phase slope through the band pass of the filter is linear, then the change in phase as a function of frequency is

$$\frac{\partial \theta}{\partial f} = \frac{-\frac{\pi}{2}}{BW_{3dB}} = -\frac{\pi}{2}\left(\frac{Q}{f_{center}}\right) \text{(rad/Hz)} \qquad \text{(E6)}$$

The relative phase shift between the upper and lower telemetry sideband frequencies ($f_{IF} + f_{TM}$ and $f_{IF} - f_{TM}$, respectively) and the i.f. center frequency f_{IF} is different for the case of the three band-pass filters, as compared to the single wideband filter which passes the entire signal spectrum. This is readily apparent when comparing the phase characteristics shown in figure E-2 with the phase characteristics of the normal wideband filter shown in figure E-3.

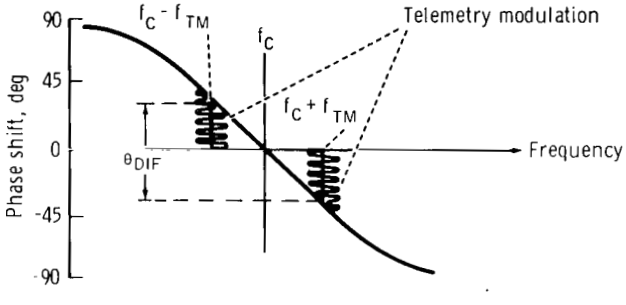

Figure E-3. - Phase-shift characteristics of a conventional wideband filter.

The phase difference between $f_{IF} - f_{TM}$ and $f_{IF} + f_{TM}$ is zero for the parallel filter configuration as compared to a value θ_{DIF} for the single wideband filter. The exact value of θ_{DIF} is dependent upon the phase slope of the wideband filter. However, it will be shown that as long as the phase characteristics of the paths for the upper and lower telemetry sidebands are the same, the relative phase shift between the paths is of no importance.

The output voltage of the filters e_0 is determined from the input signal (eq. (E5)) and the filter phase characteristics shown in figure E-2.

$$
\begin{aligned}
e_0 = {} & A \sin\left(\omega_c t + \theta_{D2}\right)\cos\left[\beta_v f_v(t)\right]J_0\left(\beta_{TM}\right) \\
& + A \cos\left(\omega_c t + \theta_{D2}\right)\sin\left[\beta_v f_v(t)\right]J_0\left(\beta_{TM}\right) \\
& + A \sin\left[\beta_v f_v(t)\right]J_1\left(\beta_{TM}\right)\left[\cos\left(\omega_c t + \omega_{TM} t \pm \frac{\pi}{2} + \theta_{D3}\right)\right. \\
& \left. - \cos\left(\omega_c t - \omega_{TM} t \mp \frac{\pi}{2} + \theta_{D1}\right)\right] \\
& + A \cos\left[\beta_v f_v(t)\right]J_1\left(\beta_{TM}\right)\left[\sin\left(\omega_c t + \omega_{TM} t \pm \frac{\pi}{2} + \theta_{D3}\right)\right. \\
& \left. - \sin\left(\omega_c t - \omega_{TM} t \mp \frac{\pi}{2} + \theta_{D1}\right)\right] \qquad \text{(E7)}
\end{aligned}
$$

where θ_{D1}, θ_{D2}, and θ_{D3} are the phase shifts through the three parallel paths shown in figure E-1. These phase shifts are caused by the modulation signals and/or external phase delays.

The phase shifts through the parallel paths can be written in terms of individual filter parameters, using the relationship from equation (E6). Specifically, the phase shift through the first path is

$$
\theta_{D1} = \theta_{c1} - \frac{\partial\theta}{\partial f}(\Delta f) = \theta_{c1} - \frac{\pi}{2}\frac{Q_1}{f_{c1}}\left(\Delta f_1\right) \qquad \text{(E8)}
$$

where θ_{c1} = phase shift at the center frequency of the band-pass filter caused by external phase delays

Q_1 = Q of the first filter

f_{c1} = center frequency of the first filter ($f_{c1} = f_c - f_{TM}$)

Δf_1 = difference between the instantaneous modulating frequency within the filter passband and the center frequency of filter 1 ($\Delta f_1 = f_M - f_{c1}$)

Similarly, the phase shifts for the other paths can be written as follows.

$$
\theta_{D2} = \theta_{c2} - \frac{\pi}{2}\frac{Q_2}{f_{c2}}\left(\Delta f_2\right) \qquad \text{(E9)}
$$

and

$$\theta_{D3} = \theta_{c3} - \frac{\pi}{2}\frac{Q_3}{f_{c3}}(\Delta f_3) \tag{E10}$$

By substituting equations (E8), (E9), and (E10) into equation (E7), the voltage at the output of the filters can be written as follows.

$$\begin{aligned} e_0 = {} & A \sin\left[\omega_c t + \theta_{c2} - \left(\frac{\pi}{2}\frac{Q_2}{f_{c2}}\right)\Delta f_2\right]\cos\left[\beta_v f_v(t)\right]J_0(\beta_{TM}) \\ & + A\cos\left[\omega_c t + \theta_{c2} - \left(\frac{\pi}{2}\frac{Q_2}{f_{c2}}\right)\Delta f_2\right]\sin\left[\beta_v f_v(t)\right]J_0(\beta_{TM}) \\ & + A\sin\left[\beta_v f_v(t)\right]J_1(\beta_{TM})\left\{\cos\left[\omega_c t + \omega_{TM} t \pm \frac{\pi}{2} + \theta_{c3} - \left(\frac{\pi}{2}\frac{Q_3}{f_{c3}}\right)\Delta f_3\right]\right. \\ & \left. - \cos\left[\omega_c t - \omega_{TM} t \mp \frac{\pi}{2} + \theta_{c1} - \left(\frac{\pi}{2}\frac{Q_1}{f_{c1}}\right)\Delta f_1\right]\right\} \\ & + A\cos\left[\beta_v f_v(t)\right]J_1(\beta_{TM})\left\{\sin\left[\omega_c t + \omega_{TM} t \pm \frac{\pi}{2} + \theta_{c3} - \left(\frac{\pi}{2}\frac{Q_3}{f_{c3}}\right)\Delta f_3\right]\right. \\ & \left. - \sin\left[\omega_c t - \omega_{TM} t \mp \frac{\pi}{2} + \theta_{c1} - \left(\frac{\pi}{2}\frac{Q_1}{f_{c1}}\right)\Delta f_1\right]\right\} \end{aligned} \tag{E11}$$

Equation (E11) indicates that the amplitude and phase characteristics of only the first and third band-pass filters ($f_c \pm f_{TM}$) affect the phase information on the first-order telemetry-subcarrier sidebands. The phase effects caused by the upper and lower sideband filters on the detected telemetry signal can be determined by passing the summed output filter voltage (eq. (E11)) through a quadrature product phase detector. The output of the phase detector e_{D0} can be determined by multiplying the summed output filter voltage by a quadrature reference voltage e_r where $e_r = E_R \cos \omega_c t$. After eliminating the double frequency terms, the phase detector output voltage can be written as follows.

$$e_{D0} = \frac{AE_r}{2} \sin\left[\theta_{c2} - \left(\frac{\pi}{2}\frac{Q_2}{f_{c2}}\right)\Delta f_2\right]\cos\left[\beta_v f_v(t)\right]J_0(\beta_{TM})$$

$$+ \frac{AE_r}{2} \cos\left[\theta_{c2} - \left(\frac{\pi}{2}\frac{Q_2}{f_{c2}}\right)\Delta f_2\right]\sin\left[\beta_v f_v(t)\right]J_0(\beta_{TM})$$

Out-of-phase telemetry components

$$\left\{ \begin{aligned} &+ \frac{AE_r}{2}\sin\left[\beta_v f_v(t)\right]J_1(\beta_{TM})\left\{\cos\left(\omega_{TM}t \pm \frac{\pi}{2}\right)\cos\left[\theta_{c3} - \left(\frac{\pi}{2}\frac{Q_3}{f_{c3}}\right)\Delta f_3\right]\right. \\ &- \sin\left(\omega_{TM}t \pm \frac{\pi}{2}\right)\sin\left[\theta_{c3} - \left(\frac{\pi}{2}\frac{Q_3}{f_{c3}}\right)\Delta f_3\right] \\ &- \cos\left(-\omega_{TM}t \mp \frac{\pi}{2}\right)\cos\left[\theta_{c1} - \left(\frac{\pi}{2}\frac{Q_1}{f_{c1}}\right)\Delta f_1\right] \\ &\left.+ \sin\left(-\omega_{TM}t \mp \frac{\pi}{2}\right)\sin\left[\theta_{c1} - \left(\frac{\pi}{2}\frac{Q_1}{f_{c1}}\right)\Delta f_1\right]\right\} \end{aligned} \right.$$

In-phase telemetry components

$$\left\{ \begin{aligned} &+ \frac{AE_r}{2}\cos\left[\beta_v f_v(t)\right]J_1(\beta_{TM})\left\{\sin\left(\omega_{TM}t \pm \frac{\pi}{2}\right)\cos\left[\theta_{c3} - \left(\frac{\pi}{2}\frac{Q_3}{f_{c3}}\right)\Delta f_3\right]\right. \\ &+ \cos\left(\omega_{TM}t \pm \frac{\pi}{2}\right)\sin\left[\theta_{c3} - \left(\frac{\pi}{2}\frac{Q_3}{f_{c3}}\right)\Delta f_3\right] \\ &+ \sin\left(\omega_{TM}t \pm \frac{\pi}{2}\right)\cos\left[-\theta_{c1} + \left(\frac{\pi}{2}\frac{Q_1}{f_{c1}}\right)\Delta f_1\right] \\ &\left.+ \cos\left(\omega_{TM}t \pm \frac{\pi}{2}\right)\sin\left[-\theta_{c1} + \left(\frac{\pi}{2}\frac{Q_1}{f_{c1}}\right)\Delta f_1\right]\right\} \end{aligned} \right.$$

(E12)

In order for the in-phase telemetry components to add and the out-of-phase components to cancel in equation (E12), it is necessary for the phase contributions from the upper and lower sideband filters ($f_c \pm f_{TM}$) to be equal. Therefore, when $\theta_{c1} = -\theta_{c3}$ and

$$\left(\frac{\pi}{2}\frac{Q_1}{f_{c1}}\right)\Delta f_1 = -\left(\frac{\pi}{2}\frac{Q_3}{f_{c3}}\right)\Delta f_3 \tag{E13}$$

the output telemetry voltage is

$$E_{0_{TM}} = \frac{AE_r}{2}\cos\left[\beta_v f_v(t)\right] 2J_1(\beta_{TM})\left[\sin\left(\omega_{TM}t \pm \frac{\pi}{2}\right)\cos\theta_{D3} + \cos\left(\omega_{TM}t \pm \frac{\pi}{2}\right)\sin\theta_{D3}\right] \tag{E14}$$

which is the same expression that would be obtained when using a single wideband predetection filter instead of the parallel composite filters. The phase conjugate conditions are satisfied in the paralleled filters because of the inherent negative sign between Δf_1 and Δf_3 (eqs. (E8) and (E10)). Thus, it has been shown that the telemetry signal is not affected adversely by the composite parallel filters. These filters pass only the first-order telemetry sidebands which then are inserted into an FM demodulator being used for linear phase detection. The voice interference terms are eliminated in the linear detection process of the FM demodulator (eq. (28)).

Use of Nonintegrated Frequency-Modulation Demodulator Output for a Special Phase-Modulation Input

The following discussion explains why an integrator was not used at the output of an FM demodulator when it was used to demodulate PM information of the type in LM modes 4 and 8 and CSM mode 8. This analysis is based on two premises which are unique to the MSFN demodulation scheme. One premise is that the baseband voice for these modes is demodulated in the MSFN narrowband CTL rather than in the wideband phase detector where the telemetry subcarrier is demodulated. (Baseband voice also may be demodulated in the wideband phase detector; however, this is not the operational method in use at the MSFN ground stations.) The second premise is that the phase transitions, caused by the NRZ telemetry bit stream biphase-modulating the telemetry subcarrier, occur at the zero crossings of the subcarrier waveform.

With these two features in mind, a comparison of the demodulated output of an FM demodulator with and without an integrator will illustrate that there is no need to use an integrator to recover the PM telemetry information. A comparison is made of the nonintegrated output V_{F0} to the integrated output V_I (fig. E-4). The notation used in figure E-4 is defined in the section entitled Linear Detection Using Frequency-Modulation Demodulation Techniques, except for $F_I(S)$ which is the transfer function of the simple RC integrator represented in figure E-5. Thus, $F_I(S)$ may be expressed as

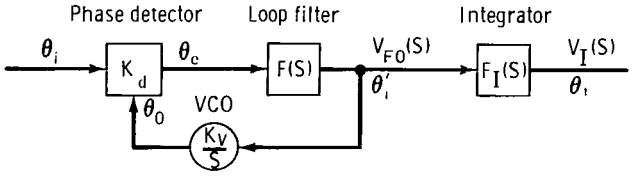

Figure E-4. - Linear representation of a PLL frequency-modulation demodulator followed by an integrator.

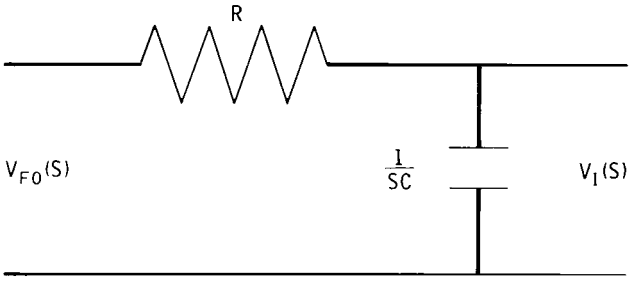

Figure E-5. - Simple resistive-capacitive integrator.

$$F_I(S) = \frac{V_I(S)}{V_{F0}(S)} = \frac{1}{RC}\left(\frac{1}{S + \frac{1}{RC}}\right) = \omega_I\left(\frac{1}{S + \omega_I}\right) \qquad \text{(E15)}$$

where ω_I is the radian cut-off frequency of the integrator. For $\omega_I << j\omega$

$$F_I(S) \cong \omega_I\left(\frac{1}{S}\right) \qquad \text{(E16)}$$

where $S \triangleq j\omega$. Now

$$V_I(S) = V_{F0}(S)F_I(S) \qquad \text{(E17)}$$

where $V_{F0}(S)$ is defined as

$$V_{F0}(S) = \left[S\theta_i(S)\right]\left(\frac{1}{K_v}\right)\left(\frac{\omega_n^2}{S^2 + 2\zeta\omega_n S + \omega_n^2}\right) \qquad \text{(E18)}$$

Therefore

$$V_I(S) = \left[\theta_i(S)\right]\left(\frac{1}{K_v}\right)\left(\frac{\omega_I \omega_n^2}{S^2 + 2\zeta\omega_n S + \omega_n^2}\right) \tag{E19}$$

A comparison of $V_{F0}(S)$ and $V_I(S)$ indicates that the only difference in the two expressions (besides the factor ω_I in the integrated expression) appears in the bracketed term, whereby the telemetry-signal phase-modulation term $\theta_i(S)$ is operated upon by the differential operator S in the nonintegrated expression. In the time domain, the two bracketed expressions are

$$\theta_i(t) = \beta_v f_v(t) + \beta_{TM} \sin\left[\omega_{TM} t + m(t)\left(\frac{\pi}{2}\right)\right] \tag{E20}$$

and

$$\theta_i'(t) = \beta_v f_v'(t) + \beta_{TM}\left[\frac{\pi}{2} m'(t) + \omega_{TM}\right] \cos\left[\omega_{TM} t + m(t)\left(\frac{\pi}{2}\right)\right] \tag{E21}$$

where the prime notation indicates differentiation, $m(t) = \pm 1$ (a switching function), and $m'(t) = \pm \delta(t)$ (the delta or impulse function). The other notations are defined in the section Linear Detection Using Frequency-Modulation Demodulation Techniques, where $\theta_i(t)$ is the input modulation expression consisting of a voice term $\beta_v f_v(t)$ and a telemetry term $\beta_{TM} \sin [\omega_{TM} t + m(t)(\pi/2)]$. From figure E-4, it can be seen that $\theta_i'(t)$ is the FM demodulator output expression for the demodulated phase angle containing voice and telemetry information. The desired expression at the output is $\theta_i(t)$, the original modulation, which is obtained by integrating $\theta_i'(t)$. However, by investigating equation (E21), it can be shown that $\theta_i'(t)$ is sufficient for demodulation of the telemetry wave train without integration. First, notice that the term $\beta_v f_v'(t)$ will be filtered out by a band-pass filter preceding the telemetry-subcarrier demodulator (fig. 1). Since one of the premises of this analysis disclosed that baseband voice is demodulated elsewhere in the MSFN ground-station receiver, the differentiated condition of this term is of no concern. The second term of $\theta_i'(t)$ can be shown to represent the original telemetry-modulation term $\beta_{TM} \sin [\omega_{TM} t + m(t)(\pi/2)]$, shifted 90° in phase. This phase shift is a result of the second unique premise, whereby the phase transitions caused by the bit-stream biphase modulation of the telemetry subcarrier occur only at the zero crossings of the subcarrier waveform. This result is

illustrated in figure E-6, in which the telemetry modulation term of $\theta'_i(t)$, that is, $\beta_{TM}[\,(\pi/2)m'(t) + \omega_{TM}]\cos[\,\omega_{TM}t + m(t)\,(\pi/2)]$, is developed to represent a composite waveform. The development of figure E-6 is seen more easily by rewriting the modulation term as

$$\left\{\beta_{TM}\cos\left[\omega_{TM}t + m(t)\,\frac{\pi}{2}\right]\right\}\left\{\left(\frac{\pi}{2}\right)m'(t)\right\} + \left\{\beta_{TM}\omega_{TM}\cos\left[\omega_{TM}t + m(t)\,\frac{\pi}{2}\right]\right\} \tag{E22}$$

where the terms within each set of braces, reading from left to right, correspond respectively to the waveforms designated as A, B, and D in figure E-6. The composite differentiated telemetry waveform E is constructed by multiplying waveforms A and B, thus resulting in waveform C. Waveform C is nonexistent since waveform B exists only at the phase transitions, and the phase transitions occur only when the telemetry waveform A is zero (that is, at zero crossings). Waveform C is added to waveform D, which results in waveform E (fig. E-6). According to the second premise, equation (E21) is accurately represented by

$$\beta_{TM}\left[\left(\frac{\pi}{2}\right)m'(t) + \omega_{TM}\right]\cos\left[\omega_{TM}t + m(t)\left(\frac{\pi}{2}\right)\right] \equiv \beta_{TM}\omega_{TM}\cos\left[\omega_{TM}t + m(t)\left(\frac{\pi}{2}\right)\right] \tag{E23}$$

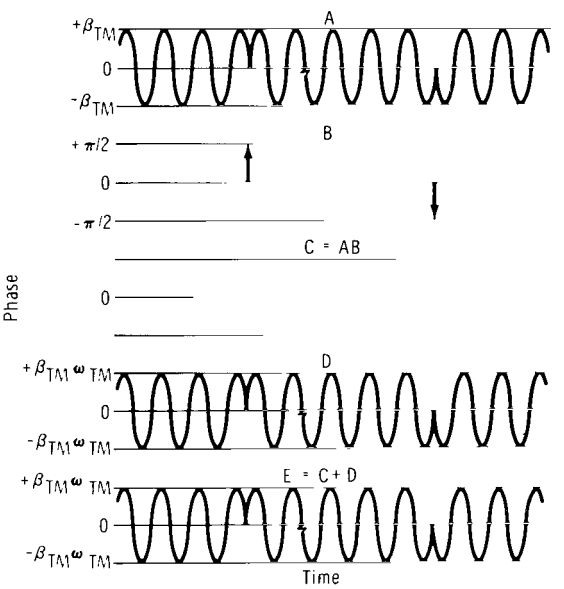

Figure E-6. - Demodulated telemetry waveform.

Thus, in regard to the telemetry terms of the expressions for $\theta_i(t)$ and $\theta'_i(t)$, the only difference (except in amplitude) between the integrated and nonintegrated expressions is a 90° phase shift of the entire nonintegrated expression. Such a shift is of no consequence to proper detection of the telemetry bit stream. Therefore, an integrated output is not necessary to demodulate properly PM telemetry information with an FM demodulator for the Apollo baseband voice modes (LM modes 4 and 8 and CSM mode 8). This analysis assumes ideal conditions, that is, a linear PLL FM demodulator and an instantaneous transition time. A noninstantaneous transition, even when the PLL is operating linearly, will cause waveform C (fig. E-6) to have some type of discrete waveform over each transition time, which will result in amplitude bursts of the composite waveform in E, for each respective transition time. However, experimental results have shown these to be negligible or nonexistent.

APPENDIX F

NARROWBAND FILTER CONSTRUCTION

Two sets of narrowband filters were constructed for this study. One set was designed for operation with the S-band receiver 50-megahertz i.f. channels; whereas, the other set was designed for operation with the receiver 10-megahertz i.f. channels. The 50-megahertz i.f. filters consisted of three helical resonators. The 10-megahertz i.f. filters consisted of three quartz crystals. These two types of filters were selected because of their wide usage as predetection (band pass) narrowband filters and because high-Q filters are not readily attainable with standard resistive-inductive-capacitive (RLC) circuit components.

Both sets of filters (crystals and resonators) consist of three separate filters in parallel, forming a composite filter with three passbands; one passband is centered at the i.f., one passband is centered at a frequency equal to the i.f. plus 1.024 megahertz (the telemetry-subcarrier frequency), and one passband is centered at a frequency equal to the i.f. minus 1.024 megahertz. Therefore, the composite crystal filter in the 10-megahertz i.f. contains passbands centered at 8.976, 10, and 11.024 megahertz. Likewise, the composite resonator filter contains passbands centered at 48.976, 50, and 51.024 megahertz. Both composite filters are illustrated in figure F-1.

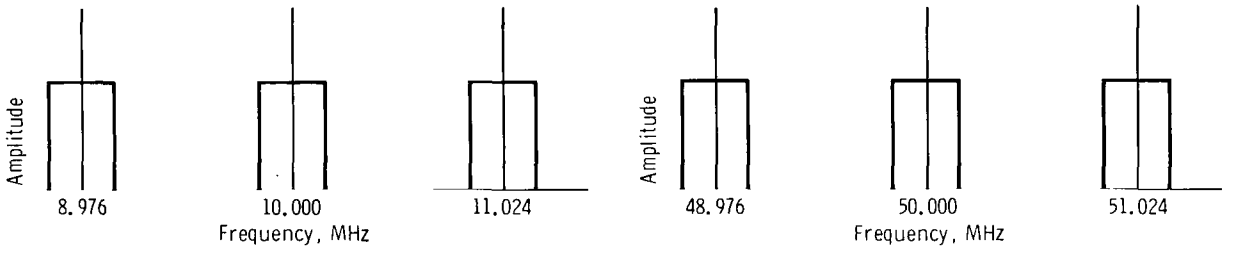

(a) Composite crystal filter, 10-megahertz intermediate frequency.

(b) Composite resonator filter, 50-megahertz intermediate frequency.

Figure F-1. - Amplitude characteristics of parallel band-pass filters.

Crystal Filter Construction

The basic circuit schematic diagram and the equivalent circuit for one of the crystal filters are illustrated in figure F-2.

The equivalent circuit of the crystal and its holder is represented by the inductor L, the capacitors C and C_h

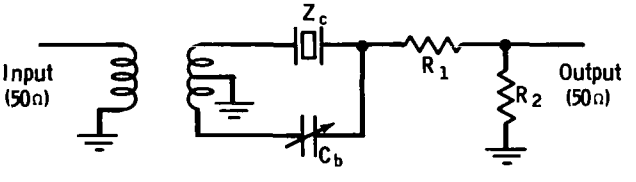

(a) Basic circuit.

Figure F-2. - Crystal filter configuration.

(representing the crystal capacitance and the holder capacitance, respectively), and the resistor R (fig. F-2(b)). The impedance of the crystal and holder (ref. 6) is determined to be

$$Z_c = \frac{\left(\frac{1}{SC_h}\right)\left(R + SL + \frac{1}{SC}\right)}{R + SL + \frac{1}{SC_h} + \frac{1}{SC}} \qquad \text{(F1)}$$

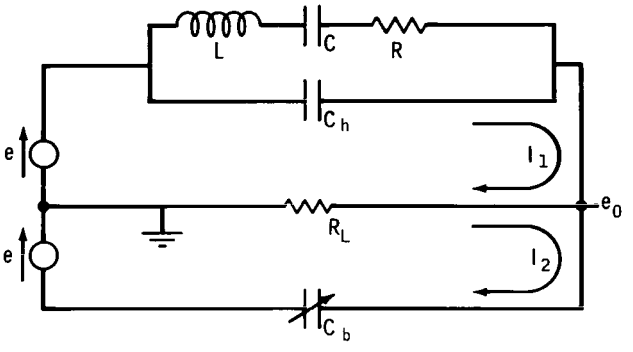

(b) Approximate equivalent circuit.

Figure F-2. - Concluded.

The voltage transfer function e_0/e for the entire filter circuit (fig. F-2(b)) is given by

$$\frac{e_0}{e} = \frac{\left(Z_b - Z_c\right) R_L}{\left(Z_b + Z_c\right) R_L + Z_b Z_c} \qquad \text{(F2)}$$

where $Z_b = \frac{1}{SC_b}$

$$Z_c = \frac{1}{SC_h}\left[\frac{S^2 + \left(\frac{R}{L}\right) S + \frac{1}{LC}}{S^2 + \left(\frac{R}{L}\right) S + \frac{1}{LC_e}}\right]$$

$$C_e = \frac{C + C_h}{CC_h}$$

$$R_L = \frac{R_2}{R_1 + R_2}$$

Equation (F2) is expanded further to give

$$\frac{e_0}{e} = \frac{SD\left(S^2 + \omega_1 S + \omega_q{}^2\right)}{S^3 + \omega_e S^2 + \omega_n{}^2 S + \omega_c{}^3} \qquad \text{(F3)}$$

where $\omega_1 = \frac{R}{L} = \frac{1}{T_1}$

$$\omega_q^2 = \frac{C + C_h - C_b}{LC(C_h - C_b)}$$

$$T_2 = R_L(C_b + C_h)$$

$$\omega_e = \frac{T_1 + T_2}{T_1 T_2}$$

$$\omega_p^2 = \frac{\frac{R}{R_L}}{L(C_b + C_h)}$$

$$\omega_0^2 = \frac{C + C_h + C_b}{LC(C_h + C_b)}$$

$$\omega_n^2 = \omega_0^2 + \omega_p^2$$

$$\omega_c^3 = \frac{1}{T_3 LC}$$

$$D = \frac{C_h - C_b}{C_h + C_b}$$

when the holder capacitance C_h equals the balance capacitance C_b, the transfer function becomes

$$\frac{e_0}{e} = \frac{S\omega_h^2}{S^3 + \omega_4 S^2 + \omega_m^2 S + \omega_g^3} \qquad \text{(F4)}$$

where $\omega_h^2 = \frac{1}{2LC_h}$

$$T_3 = 2R_L C_h$$

$$\omega_4 = \frac{1}{T_1} + \frac{1}{T_3}$$

$$\omega_m^2 = \omega_h^2 \left(1 + \frac{2C_h}{C} + \frac{R}{R_L}\right)$$

$$\omega_g^3 = \frac{\omega_h^2}{R_L C}$$

The denominator of equation (F4) will normally have a pair of complex conjugate poles near the $j\omega$ axis and a pole along the negative real axis. If the frequency is increased along the positive $j\omega$ axis, a maximum value of the function in equation (F4) occurs near the complex conjugate pole in this region. At higher frequencies, the function decreases monotonically; at lower frequencies, the function decreases toward the zero given by the numerator of equation (F4). Therefore, a suitable transfer characteristic for a band-pass filter is achieved by using a crystal when the balance capacitance C_b (fig. F-2) equals the crystal holder capacitance C_h.

Each of the three crystal filters was constructed according to figure F-2(a). The input transformer matches the filter input to a 50-ohm source and provides balanced voltage sources to the filter. The transformer is a carbonyl iron-powder-core toroid with an outer diameter of approximately 0.31 inch, an inner diameter of approximately 0.156 inch, and a height of approximately 0.125 inch. The balancing capacitor C_b ranges from 2 to 25 picofarads and was used to adjust the center frequency of each pass-band. Load resistors R_1 and R_2 were adjusted to provide a 50-ohm output impedance. By increasing or decreasing values of R_1, the 3-decibel bandwidth of the filter is correspondingly increased or decreased.

The composite crystal filter consists of three paralleled filters, as shown in figure F-3. The corresponding composite amplitude- and phase-response measurements presented in figure 29 indicate that each filter has a 3-decibel bandwidth of approximately 7.5 kilohertz, which corresponds to a Q that is greater than 1300.

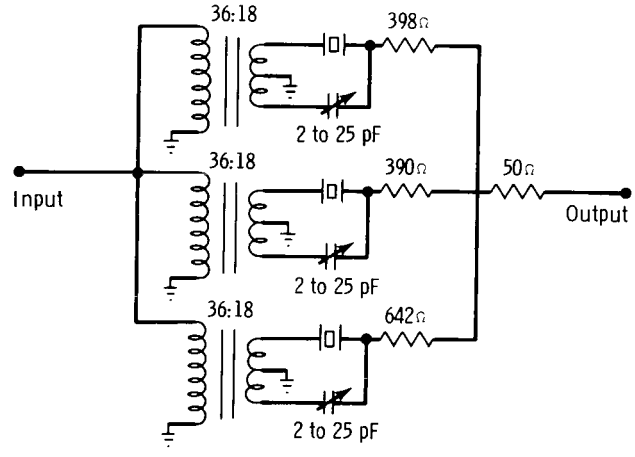

Figure F-3. - Composite crystal filter.

The insertion loss for the composite crystal filter is approximately 45 decibels as compared to an insertion loss of 27 decibels for the composite helical resonator filter.

Helical Resonator Construction

The helical resonator filters are constructed according to the design theory contained in references 7 and 8. Three resonators, centered at 48.976, 50, and 51.024 megahertz, are used to provide the composite filter passbands illustrated in figure F-1. The resonators are constructed of brass; each cavity has an inner diameter of 2.83 inches, an outer diameter of 3.0 inches, and a height of approximately 7.0 inches (fig. F-4). The brass helix for the 50-megahertz resonator consists of a 0.1875-inch-diameter brass stock wound into a 17-turn coil that is 4.88 inches in length, 1.575 inches outer diameter, and has a pitch of 0.287 inch (fig. F-5). The 48.976- and 51.024-megahertz helices are similar in that they have 17 turns and 16 turns, respectively. The bottom of the helix (fig. F-6) is threaded to be screwed into the resonator base. Because mechanical vibration of the helix is a serious problem, a Teflon form was fitted tightly within the helix to provide additional support.

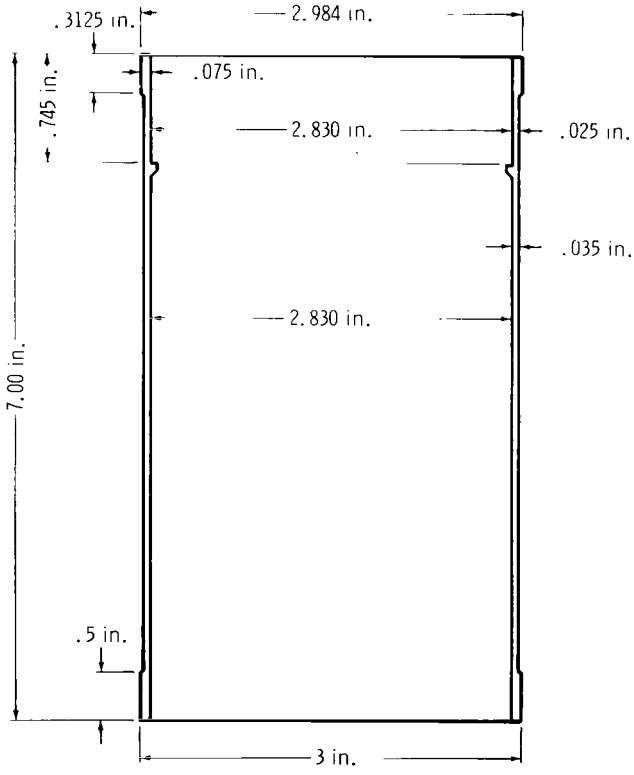

Figure F-4. - Circular resonator cavity (brass material).

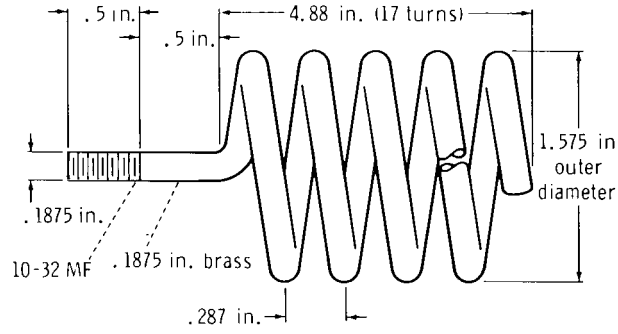

Figure F-5. - Helix 50-megahertz 17-turn coil.

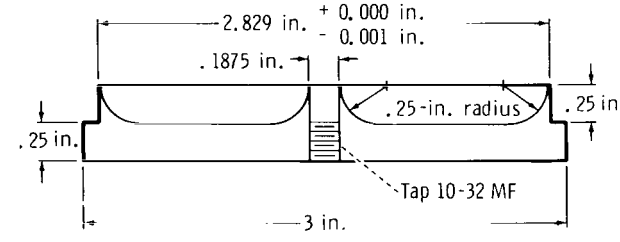

Figure F-6. - Bottom for cavity.

The top plate of the cavity is illustrated in figure F-7. A hollow brass tuning rod enters the cavity through the assembly in the center of the top plate. The center frequency of the cavity is adjusted by raising or lowering the tuning rod. The tuning rod (fig. F-8) provides a tunable frequency range from 0.5 to 1.5 megahertz for each resonator. There is a Teflon spacer between the threaded brass rod and the hollow brass rod which is the actual tuning device. The Teflon spacer provides electrical isolation for the hollow tuning rod within the cavity.

Electrical connections are made to the resonant cavity through two thin-walled coaxial stainless-steel transmission lines. These lines are designed to have a characteristic impedance of 50 ohms. The coupling to the cavity is varied by raising and lowering the input and output probes inside the cavity. These input and output probes are made of brass rods inserted inside Teflon-insulated, threaded brass tubes, with BNC connectors at the top for use with BNC connector coaxial cables (fig. F-9). The brass tubes screw into the threaded mountings on the top plate of the cavity (fig. F-8).

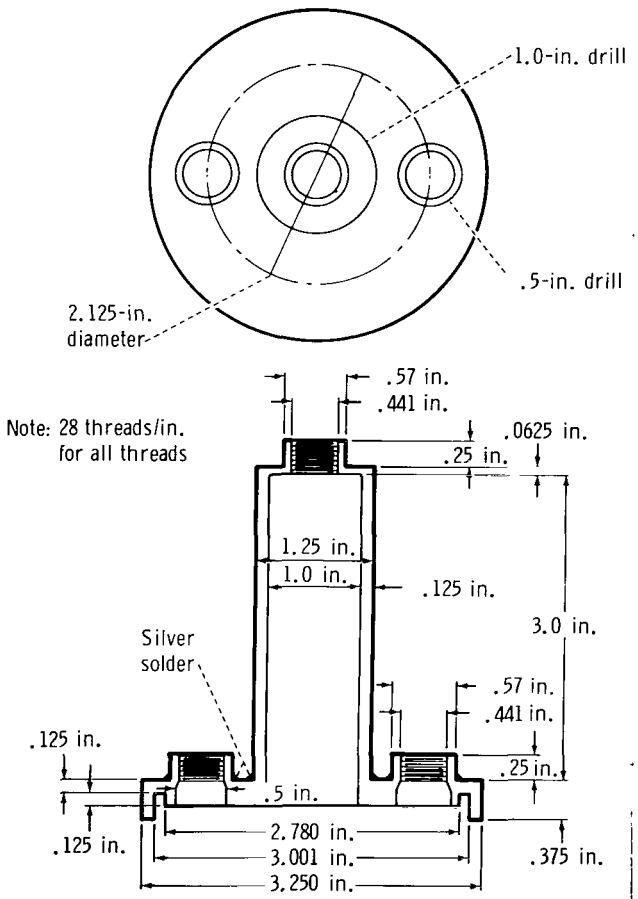

Figure F-7. - Fixed top plate of cavity (brass material).

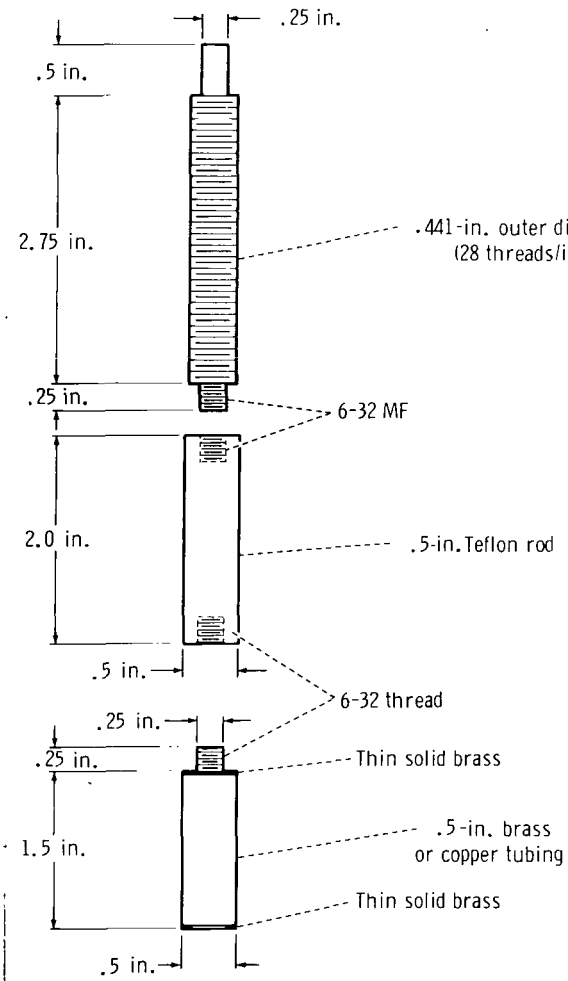

Figure F-8. - Tuning slug and isolation rod.

The studies of the effects of input and output probe lengths resulted in the information presented in figure F-10, which shows the effects on center frequency and bandwidth as a function of probe length. From these data, a probe length of 33 millimeters was chosen for each of the filters.

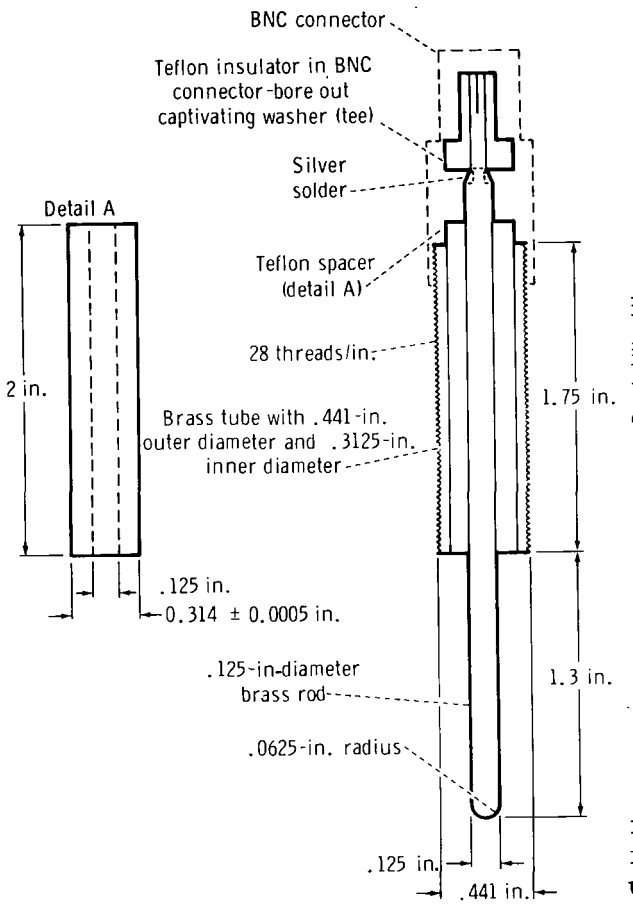

Figure F-9. - Resonator probe for cavity.

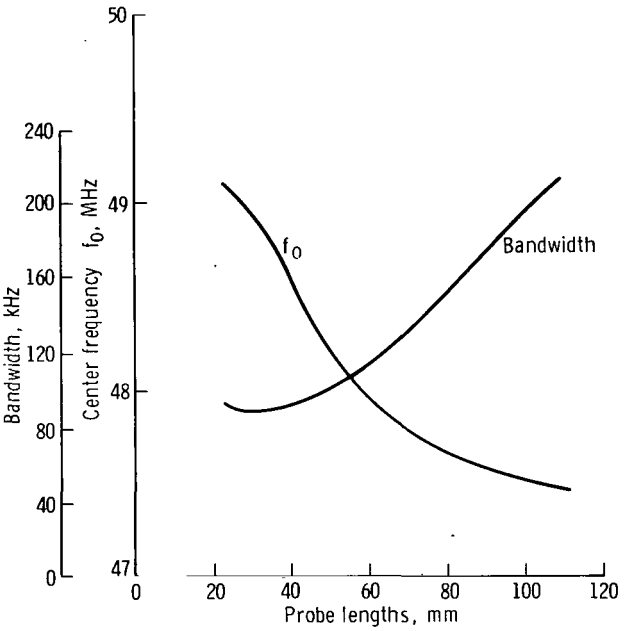

Figure F-10. - Effect of resonator probe lengths on frequency and bandwidth.

An operational helical resonator filter is shown in figure F-11. Then, the three resonators are connected in parallel by using isolation transformers at both the input and output terminals. The insertion loss for each of the three resonators is approximately 28 decibels, including the losses in the isolation transformers. The amplitude and phase responses of the composite filter are presented in figure F-12.

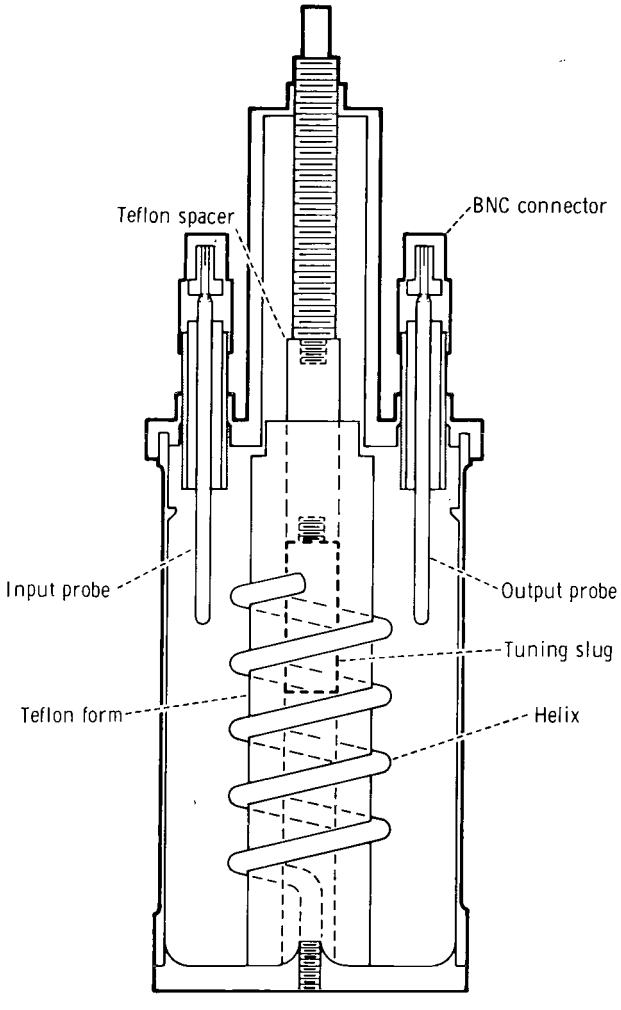

Figure F-11. - Diagram of composite helical resonator (not to scale).

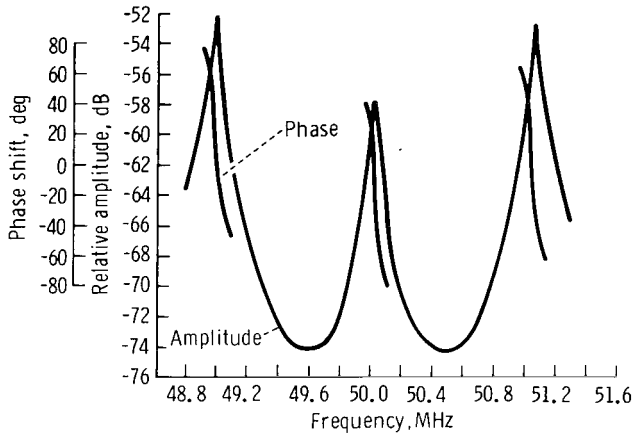

Figure F-12. - Amplitude and phase response (helical resonators).

NASA-Langley, 1970 —— 7 S-228